IRE
Transactions
on Microwave Theory and Techniques

VOLUME MTT-4 JANUARY, 1956 NUMBER 1

PUBLISHED BY THE
fessional Group on Microwave Theory and Techniques

IRE TRANSACTIONS

on Microwave Theory and Techniques

Published by the Institute of Radio Engineers, Inc., for the Professional Group on Microwave Theory and Techniques, at 1 East 79th Street, New York 21, New York. Responsibility for the contents rests upon the authors, and not upon the IRE, the Group, or its members. Prices per copy: IRE PGMTT members, $1.65; IRE members, $2.45; nonmembers, $4.95. Annual subscription price: IRE members, $8.50; colleges and public libraries, $12.75; nonmembers, $17.00.

Address all manuscripts to Theodore S. Saad, Sage Laboratories, 30 Guinan St., Waltham, Mass.

Message from the Editor

This month we are pleased to feature Mr. André G. Clavier as our eminent microwave personality. His many contributions are well known to most members. His editorial speaks for itself.

Included in this issue is a list of the members of the professional group. We hope that this will be an annual feature of the January issue.

Editorial Board

We would also like to announce a change in our editorial board. Mr. Wilbur L. Pritchard, who has recently been named Chairman of the Membership Committee, has been replaced by Mr. Ernest Wantuch of Raytheon Manufacturing Co., Bedford, Mass.

—The Editor

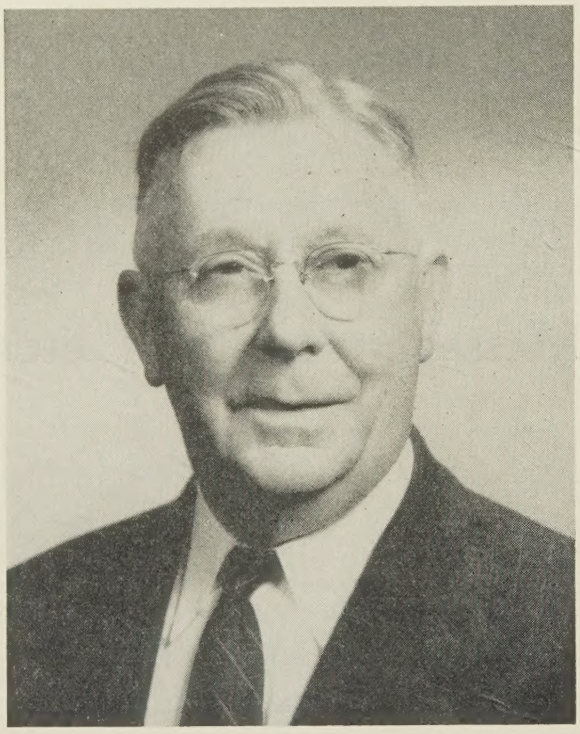

A. G. Clavier

A. G. Clavier was born in France in 1894. He graduated at the Sorbonne as "Licencie en Sciences Physiques et Mathématiques" and received the diploma of Electrical Engineer from the École Superieure d'Électricité (Paris) in 1920.

He started his career of radio research as the head of one of the Laboratories of the French Signal Corps, in charge of military developments in the higher part of the radio-frequency spectrum. He was a member of the French jury supervising the famous amateur contest in 1923 for short-wave transatlantic communication. He was Secretary of the Redaction of "Onde Électrique" during its first years of existence (1922–1925).

After a short stay with the International Western Electric in London (1925), and the Société Française Radioélectrique in Paris, he joined the International Telephone and Telegraph System in 1929 as a member of the staff of Laboratoire Standard, which later became Laboratoire Central de Télécommunications. He was Assistant Research Director in 1946 when he was transferred to Federal Telecommunication Laboratories. He was named a Technical Director of FTL in 1952 and a Vice President in 1955, acting as general coordinator for research and development activities.

Mr. Clavier is widely recognized as a pioneer in the development of microwave communication. He played a major role in the first successful demonstration of microwave transmission across the English Channel (Calais to Dover) in 1931, and directed the project which led to the opening of the world's first microwave radiotelephone and teleprinter link between England and France in 1934. He contributed to the theory and applications of waveguides and their relationship with coaxial cables (1937) and was among the first to recommend the use of electron transit times in microwave vacuum tubes (1939). In 1941 he conducted with V. Altovsky a series of beyond-the-horizon propagation over the Mediterranean between Toulon and the Spanish and Algerian coasts. This work remained unpublished on account of French Military classification. With the same co-worker, he established in 1945 a microwave transmission for 12 telephone channels using frequency division and frequency modulation at 3,000 megacycles per second between Paris and Montmorency.

Mr. Clavier taught field theory and applications of ultra-high frequencies at the École Superieure d'Électricité from 1942 to 1945. He has written extensively on hf, uhf and shf radio communication and on microwave vacuum tubes as well as electromagnetic theory. He is the author of some 70 patents in the field of telecommunications.

Mr. Clavier is a Member of the French Society of Radio Engineers, a Membre Laureat of the Société Française des Électriciens, a Member of the Institution of Electrical Engineers of Great Britain, and a Vice-President of the American Section of the Société des Ingenieurs Civils de France. He was made a Fellow of the American Institute of Electrical Engineers in 1953 for "pioneer work in research, development and engineering in the microwave field."

He has been a Fellow of the IRE since 1939.

"Wire" vs "Wireless" Communication

A. G. CLAVIER

Federal Telecommunication Laboratories

Though the integration of all modes of electrical communication is a practical *fait accompli* under the progress and aegis of the information theory, the fact remains that there is an undeniable and healthy competition between wire and wireless means in almost all communication fields. I would like to devote this editorial to some aspects of this technical feud, and to be allowed to present some personal technical *souvenirs* at this occasion.

I began my career on the radio side, and was at the start mainly concerned with military applications of the higher part of the radio frequency spectrum, which in 1920 we situated in a few hundreds of megacycles. We were quite enthused, of course, with the new technique, though at times we wondered whether General Ferrie, our boss, was not right when he would jokingly tell us that "had wireless communication come first, wire would have been considered a great improvement."

Yet, things were achieved with "wireless" that wire could not do. I remember how thrilling it was for me to hear on the radio transatlantic tests between Rocky Point and New Southgate (London) the voice of a Bell Telephone Laboratories engineer, who had participated in the tests in England and had just sailed back to the United States. Wire had achieved transatlantic telegraphy in 1857, but wireless had entered the field in 1901. and radio-telephone was opened to the public in 1927. This was the long-wave circuit, soon to be supplemented by the short-wave circuits in 1928.

Is it not, therefore, somewhat of a shock to the radio engineer to have to acknowledge in 1954[1] that "no way has been found to provide (with short waves) day-to-day continuity and reliability comparable to that of good wire lines!" The wire communication engineers have fought back successfully in this case. In spite of enormous difficulties, a transatlantic telephone cable is being laid to link the United Kingdom, Canada, and the United States, and is scheduled to be completed in 1956.

Radio, however, which seems to have lost this round in the never-ending battle, has, meanwhile, invaded a well-guarded bailiwick of wire communication: the toll network of public telephone networks. This is a conquest of microwaves in a field where equal reliability of operation is necessary to compete. The Bell System in June, 1954 was providing more than five million telephone circuit miles by microwave radio.

This line-of-sight microwave communication has had an added incentive due to the need for TV transmission. It had the drawback of requiring optical line-of-sight between successive repeater stations. However, recent experimental work has shown that, provided suitable power and antenna gain is utilized, microwaves can be sent over the horizon at 200 miles or more. At this distance radio would seem to compete favorably with an expensive submarine cable, and regain some of the ground lost on the longer transatlantic routes.

The guided propagation inside metallic pipes, the so-called waveguide, may change the picture in the future. Should the demand for more bandwidth increase, waveguides would give a means to obtain a tremendous capacity of radio and TV channels; and very high carrier frequencies would be used advantageously, because in one mode of propagation (TE 01) they are less attenuated than lower frequencies, a fact established by both theory and experiment which came to light as a big surprise just before the Second World War broke out.

Thus, wire and wireless are pushing each other along the route of progress. It is tempting to conclude, as an old professor of mine, who used to advocate the 1) thesis, 2) antithesis, and 3) synthesis theme for any lecture or discourse, would have done. The development of communication is going on at such a rate that both methods have ample possibilities. In its annual report for 1954, the Federal Communications Commission starts by saying that its 20th anniversary saw the nation studded with 700,000 radio transmitters, 50 million telephones, and nearly 3.5 million channel miles of telegraph circuitry! Should this state of things be generalized to the whole planet, there would be need for all known communication means to provide the required facilities. In some cases wire would seem to be the better solution, as is the case for the local areas of public telephone networks. In other cases, radio is a must, as for mobile communication, air-to-ground and plane-to-plane transmission. In many cases, however, the fight is open, along the toll routes for telephone or television for example. Who could also predict with certainty which will win over the long international routes for TV transmission? I would like to repeat here the concluding words I used in a lecture on "New Advances in Guided Propagation," which I gave last year at one of the Centennial Meetings of the Polytechnic Institute of Brooklyn: "Helped by a clearer understanding of the laws governing the transmission of information, it would seem safe to assume that wire and radio are henceforth indissolubly linked under a broader concept, which should lead some day to a rational organization of communications over our planet, as a prelude to more ambitious adventures outside of our earthly atmosphere." We microwave engineers have plenty of work on our hands, and higher frequencies may still hold new wonders in reserve and ample ground for imaginative and profitable enterprise.

[1] M. J. Kelly, Sir Gordon Radley, G. W. Gilman, and R. J. Halsey, "A Transatlantic Telephone Cable," *Proc. I.E.E.* (London), Part B, vol. 102, pp. 127–130; March, 1955.

The Characteristic Impedance of a Slotted Coaxial Line

R. E. COLLIN†

Summary—The propagation of a second type of TEM mode in a slotted coaxial line is analyzed. The characteristic impedance of the slotted line is evaluated by means of variational expressions giving upper and lower bounds to the true value. A two term approximation to the charge distribution and a one term approximation to potential distribution give results accurate to within ±2 per cent. Curves of characteristic impedance against angular slot width are presented.

Introduction

IN A SLOTTED coaxial line as illustrated in Fig. 1 two types of TEM modes may propagate. The first is a perturbed fundamental coaxial line mode. If the slots are narrow, then apart from a small amount of fringing of the field in the region of the slots, the field is confined entirely to the region between the inner and outer conductors. The second type is a mode with the electric field lines of force crossing the symmetry plane everywhere at right angles. Unlike the first type of

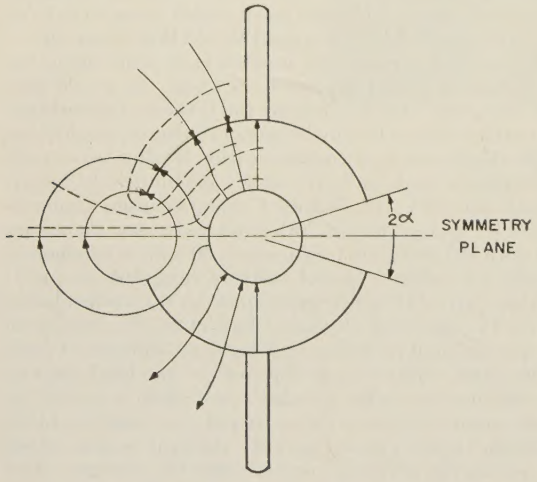

Fig. 1—Field distribution of second type of TEM mode illustrating excitation of dipole wings. —— electric field. ------ magnetic field.

TEM mode, the field of this second mode extends into all of the space surrounding the coaxial line. The existence of this mode is of fundamental importance in the slotted coaxial line dipole antenna feed.[1] It is this mode that excites currents on the dipole wings and causes the dipole to radiate. This mode should not be confused with a perturbed second order coaxial line mode and in practice is usually excited by short circuiting inner conductor to outer conductor by a short circuiting post located in plane perpendicular to symmetry plane.

This paper is primarily concerned with the evaluation of the characteristic impedance of the slotted coaxial line for this second type of transmission line mode. A rigorous solution in closed form has not been found. However by a variational method similar to that used in waveguide problems[2] upper and lower bounds to the characteristic impedance have been obtained. The procedure used is capable of giving a result of as high a degree of accuracy as desired. The upper bound to the characteristic impedance is found from a variational expression involving the charge on the outer conductor while the lower bound is obtained from a variational expression involving the potential distribution in the slotted regions. Due to the symmetry of the problem it is only necessary to consider the solution to the reduced problem illustrated in Fig. 2 and consisting of the two half coaxial cylinders above the symmetry plane and an infinite conducting plane placed coincident with the symmetry plane. The field distribution below the symmetry plane is the mirror image of that above. For this reason the current flowing on the lower half coaxial cylinders will be directed oppositely to that flowing on the upper half cylinders. There will be no net current flow on the center conductor; the current flowing down the line on one outer half cylinder and back on the other. It is seen that the slotted coaxial line is thus a balanced three wire line as far as this second type of TEM mode is concerned.

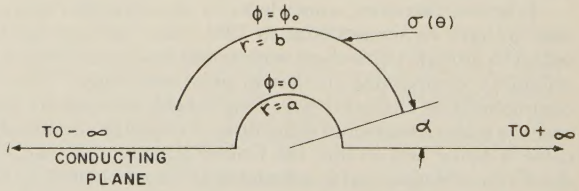

Fig. 2—Reduced problem obtained by image theory.

Upper Bound to Characteristic Impedance

For a TEM mode the field distribution in the transverse plane is a solution of Laplace's equation and may therefore be derived from an appropriate potential or stream function. In the cylindrical coordinate system r, θ, z the transverse electric and magnetic field components are related as follows:[3]

$$-j\omega\mu H_r = kE_\theta, \qquad j\omega\mu H_\theta = kE_r,$$

† Canadian Armament Research and Development Establishment, Valcartier, Quebec.

[1] S. Silver, "Microwave antenna theory and design," McGraw-Hill Bk. Co., New York, 1949. Chapter 8, Sec. 4.

[2] J. W. Miles, "The equivalent circuit for a plane discontinuity in a cylindrical waveguide," Proc. IRE, Vol. 34, p. 728; October, 1946.

[3] MKS units are used and the time factor $e^{j\omega t}$ is dropped for convenience.

where

$$k = j\omega\sqrt{\mu\epsilon} = \frac{j2\pi}{\lambda}$$

The inner and outer radii of the coaxial cylinder are taken as "a" and "b" respectively and the angular slot width as 2α. If $\phi(r, \theta)$ is the potential distribution in the space surrounding the half cylinders when the outer half cylinder is held at a potential ϕ_0 with respect to the inner half cylinder and ground plane, then the electric field may be found from the following relation:

$$E = -\operatorname{grad}\phi$$

In order that the outer half cylinder shall be at a potential ϕ_0 there must be a distribution of charge $\sigma(\theta)$ on the half cylinder. This charge distribution is proportional to the discontinuity of the normal electric field at $r=b$ and hence is proportional to the discontinuity in the tangential magnetic field at $r=b$ and thus proportional to current flowing on line. Explicitly one has:

$$I = \sqrt{\frac{\epsilon}{\mu}}\left[\int_\alpha^{\pi-\alpha}\left(\frac{\partial\phi}{\partial r}\bigg|_{r=b-} - \frac{\partial\phi}{\partial r}\bigg|_{r=b+}\right)d\theta\right]$$
$$= \frac{1}{\sqrt{\mu\epsilon}}\int_\alpha^{\pi-\alpha}\sigma(\theta)d\theta = \frac{Q}{\sqrt{\mu\epsilon}}$$

where I is the total current flowing and Q is the total charge on the upper half cylinder.

The characteristic impedance Z_0 measured between the two outer half cylinders is $2\phi_0/I$ and is equal to

$$\frac{2\phi_0}{Q}\sqrt{\mu\epsilon} = \frac{1}{Cv}$$

where C is the total capacity of the slotted coaxial line per unit length and v is the velocity of light in the surrounding medium. Thus it suffices to determine the capacity C in order to evaluate Z_0.

Consider first of all solution of following equation:

$$\nabla^2 G(r, \theta, \theta') = -\frac{1}{\epsilon}\delta(r-b)\delta(\theta-\theta') \qquad (1)$$

which defines the Green's function G for the above problem. The delta functions have the property that $\int\delta(r-b)dr$ equals unity if the interval of integration includes the point b and equals zero otherwise. The Green's function is subject to the boundary conditions that it vanishes on the inner half cylinder and ground plane, is continuous with a discontinuous normal derivative at $r=b$, and is regular at infinity. The Green's function is thus seen to be the potential due to unit charge located at b, θ'. A suitable form for Green's function is readily found by standard methods,[4] giving

$$G(r, \theta, \theta') = \frac{2}{\epsilon\pi}\begin{cases}\displaystyle\sum_{n=1}^{\infty}\frac{\sinh n\ln\frac{r}{a}\sin n\theta\sin n\theta'}{n\left(\sinh n\ln\frac{b}{a}+\cosh n\ln\frac{b}{a}\right)}, & r\le b\\ \displaystyle\sum_{n=1}^{\infty}\frac{\sinh n\ln\frac{b}{a}\,e^{-n\ln r/b}\sin n\theta\sin n\theta'}{n\left(\sinh n\ln\frac{b}{a}+\cosh n\ln\frac{b}{a}\right)}, & r\ge b\end{cases} \qquad (2)$$

By the superposition theorem the potential due to a charge distribution $\sigma(\theta)$ at $r=b$ is:

$$\phi(r, \theta) = \int_\alpha^{\pi-\alpha}\sigma(\theta')G(r, \theta, \theta')d\theta' \qquad (3)$$

Imposing the boundary condition that $\phi=\phi_0$ on the outer half cylinder gives the following integral equation whose solution determines the charge distribution $\sigma(\theta)$:

$$\phi_0 = \int_\alpha^{\pi-\alpha}\sigma(\theta')G(b, \theta, \theta')d\theta'. \qquad (4)$$

To obtain a variational expression for Z_0 multiply the above integral equation by $\sigma(\theta)$ and integrate over $\alpha\le\theta\le\pi-\alpha$. Introducing the value of Z_0 given by

$$\frac{2\phi_0}{v\int_\alpha^{\pi-\alpha}\sigma(\theta)d\theta}$$

and dividing both sides by $\left[\int_\alpha^{\pi-\alpha}\sigma(\theta)d\theta\right]^2$ gives:

$$Z_0 = \frac{\frac{2}{v}\int\int_\alpha^{\pi-\alpha}G(b, \theta, \theta')\sigma(\theta)\sigma(\theta')d\theta d\theta'}{\left[\int_\alpha^{\pi-\alpha}\sigma(\theta)d\theta\right]^2} \qquad (5)$$

The value of Z_0 as given by this expression is easily shown to be stationary with respect to arbitrary first order variations in the charge distribution $\sigma(\theta)$ and hence is the required variational expression. Furthermore this expression is a positive definite quadratic form so the stationary value is an absolute minimum for the correct form of $\sigma(\theta)$ and will therefore give an upper bound for the impedance Z_0. A suitable set of functions in which to expand $\sigma(\theta)$ that will converge to the rigorously correct solution are the following cosine functions:

$$\sum_{s=0}^{S} c_s\cos\frac{2\pi s(\theta-\alpha)}{\pi-2\alpha}.$$

The stationary value of Z_0 is obtained by substituting a finite number of terms of the above series into the variational expression, setting all the partial derivatives $\partial/\partial c_s$ equal to zero, solving the resultant equations for the c_s and finally substituting back into the variational expression and evaluating Z_0. There is no loss in gener-

[4] P. M. Morse and H. Feshback, *Methods of theoretical physics*, McGraw-Hill Book Co., New York, 1953.

ality by taking c_0 equal to unity since Z_0 depends only on the functional form of $\sigma(\theta)$. Using constant term and one cosine term following result is obtained for Z_0:

$$Z_0 = \frac{1920}{(\pi - 2\alpha)^2} \sum_{n=1,3\cdots}^{\infty} \frac{\cos^2 n\alpha \left[1 + c_1 \dfrac{n^2(\pi - 2\alpha)^2}{n^2(\pi - 2\alpha)^2 - 4\pi^2}\right]^2}{n^3 \left[1 + \coth n \ln \dfrac{b}{a}\right]} \text{ ohms} \tag{6}$$

where

$$c_1 = -\frac{\displaystyle\sum_{n=1,3\cdots}^{\infty} \frac{\cos^2 n\alpha}{n\left(1 + \coth n \ln \dfrac{b}{a}\right)[n^2(\pi - 2\alpha)^2 - 4\pi^2]}}{\displaystyle\sum_{n=1,3\cdots}^{\infty} \frac{[n \cos^2 n\alpha][\pi - 2\alpha]^2}{\left(1 + \coth n \ln \dfrac{b}{a}\right)[n^2(\pi - 2\alpha)^2 - 4\pi^2]^2}}$$

The above series are quite suitable for numerical computation as the terms decrease as n^3 and the summations are over odd integers only.

Lower Bound to the Characteristic Impedance

In order to obtain an estimate of the error involved in calculating Z_0 *from the* previous expression it is necessary to develop an alternative expression that will give a lower bound to Z_0. This may be done by solving the original problem in terms of the potential distribution in the slots. A suitable expansion of the potential function is the following:

$$\phi(r, \theta) = \begin{cases} \displaystyle\sum_{n=1,3\cdots}^{\infty} a_n \sin n\theta \sinh n \ln \frac{r}{a}, & r \leq b \\ \displaystyle\sum_{n=1,3\cdots}^{\infty} a_n \sinh n \ln \frac{b}{a} \sin n\theta e^{-n \ln r/b}, & r \geq b \end{cases} \tag{7}$$

If the potential in the region $0 \leqq \theta \leqq \alpha$, $r = b$ were known, then the coefficients a_n could be uniquely determined by Fourier analysis. However since the capacity C is required it will be sufficient to obtain a variational expression involving this unknown potential distribution $\phi(\theta)$ and which gives C as a stationary quantity. Since the electrostatic energy stored in the field is known to be a minimum and also proportional to ϕ_0^2 C it is clear that a variational expression for C can be developed by calculating the electrostatic energy in the field. The electric energy is given by:

$$W_e = \frac{\epsilon}{2} \int E^2 dv = \frac{\epsilon}{2} \int (\text{grad } \phi)^2 dv$$

Substituting for ϕ from (7), taking the gradient and integrating over the whole r, θ plane gives:

$$\frac{\pi\epsilon}{2} \sum_{n=1,3}^{\infty} a_n^2 n \sinh n \ln \frac{b}{a} \left(\cosh n \ln \frac{b}{a} + \sinh n \ln \frac{b}{a}\right) \tag{8}$$

for the total energy stored in the field per unit length of line. Now $2C\phi_0^2 = W_e$ and hence $Z_0 = \phi_0^2 / v W_e$. The coefficients a_n are given by Fourier analysis as follows:

$$a_n \frac{\pi}{2} \sinh n \ln \frac{b}{a} = \int_0^{\pi} \phi \sin n\theta d\theta = 2\left[\int_0^{\alpha} \phi \sin n\theta d\theta + \int_{\alpha}^{\pi/2} \phi_0 \sin n\theta d\theta\right]$$

since the potential reduces to ϕ_0 on the outer cylinder. Substituting into the expression for W_e gives:

$$Z_0^{-1} = \frac{4v\epsilon}{\pi\phi_0^2} \sum_{n=1,3\cdots}^{\infty} n\left(1 + \coth n \ln \frac{b}{a}\right) \cdot \left(\int_0^{\pi/2} \phi \sin n\theta d\theta\right)^2. \tag{9}$$

To show that $1/Z_0$ is stationary with respect to arbitrary first order variations in the functional form of ϕ, consider the variation in W_e due to a variation $\delta\phi$ in ϕ, thus:

$$\delta W_e = \frac{8\epsilon}{\pi} \int_0^{\pi/2} \delta\phi \left[\sum_{n=1,3\cdots}^{\infty} n\left(1 + \coth n \ln \frac{b}{a}\right) \sin n\theta \int_0^{\pi/2} \phi \sin n\theta d\theta\right] d\theta.$$

Since $\phi = \phi_0$ for $\alpha \leqq \theta \leqq \pi - \alpha$ the above result reduces to:

$$\delta W_e = \frac{8\epsilon}{\pi} \int_0^{\alpha} \delta\phi \left[\sum_{n=1,3\cdots}^{\infty} n\left(1 + \coth n \ln \frac{b}{a}\right) \sin n\theta \int_0^{\pi/2} \phi \sin n\theta d\theta\right] d\theta.$$

For the first variation in δW_e to vanish

$$\sum_{n=1,3\cdots}^{\infty} n\left(1 + \coth n \ln \frac{b}{a}\right) \sin n\theta \int_0^{\pi/2} \phi \sin n\theta d\theta$$

must equal zero over the region of the slots. This equation is also the condition that must be imposed on ϕ in order that the normal electric field in the slots be continuous and hence δW_e is identically zero. The expres-

sion for W_e is a positive definite quadratic form and therefore yields a lower bound to the characteristic impedance Z_0. A suitable form for the potential distribution that will result in a closed form for Z_0 is

$$\phi(\theta, b) = \begin{cases} \phi_0 \dfrac{\theta}{\alpha}, & 0 \leqq \theta \leqq \alpha. \\ \phi_0, & \alpha \leqq \theta \leqq \dfrac{\pi}{2}. \end{cases} \tag{10}$$

Substituting in the expression for Z_0 and performing the integration gives

$$\frac{1}{Z_0} = \frac{.00338}{\alpha^2} \sum_{1,3\cdots}^{\infty} \left(1 + \coth n \ln \frac{b}{a}\right) \frac{\sin^2 n\alpha}{n^3} \text{ ohms.} \tag{11}$$

The summation of the above series is carried out in the Appendix and gives finally

$$Z_0 = \frac{296 \text{ ohms}}{1.5 - \ln \alpha + \sum_{1,3\cdots}^{\infty} \left(\coth n \ln \frac{b}{a} - 1\right) \frac{\sin^2 n\alpha}{n^3\alpha^2}}. \tag{12}$$

The series converges rapidly since coth n ln b/a approaches unity rapidly. Higher order approximations to Z_0 may be obtained with the following series expansion for $\phi(\theta)$,

$$\phi(\theta) = \phi_0 \left[\frac{\theta}{\alpha} + \sum_{s=1}^{\infty} c_s \sin \frac{s\pi\theta}{\alpha}\right] \text{ for } 0 \leqq \theta \leqq \alpha.$$

Numerical Example

Upper and lower bounds to the characteristic impedance Z_0 as obtained from (6) and (12) have been evaluated for the particular case of $b/a = 2.6$. Curves of Z_0 vs slot angle 2α are plotted in Fig. 3 for a range of 2α from 0° to 30°. The average values of Z_0 as obtained from (6) and (12) are also given. The value of Z_0 for $2\alpha = 20°$ was also evaluated by using a three term approximation to the upper bound and a two term approximation to the lower bound. This shows that the average value of Z_0 given in Fig. 3 is probably accurate to within ± 2 per cent for most of the range of α considered. Characteristic impedance is relatively independent of ratio of b/a, provided ratio is greater than 3. In Fig. 4 average value of characteristic impedance is plotted as a function of slot angle for the case when ratio of outer to inner radii is large; i.e., $(b/a) > 6$. This value of Z_0 is average value obtained from (6) and (12) with coth n ln b/a replaced by unity.

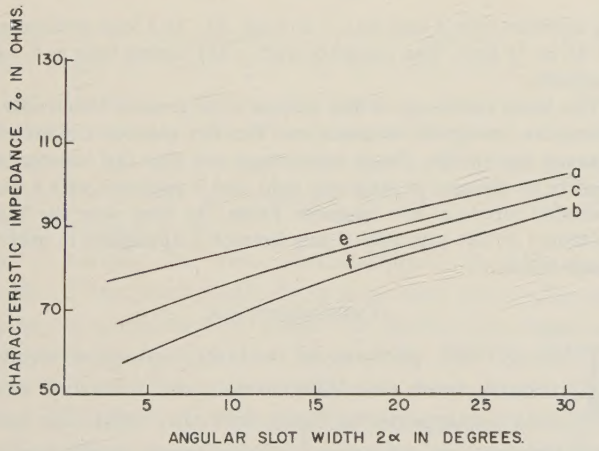

Fig. 3—Variation of characteristic impedance with slot angle for $b/a = 2.6$. (a) Two term approximation to upper bound. (b) One term approximation to lower bound. (c) Average of (a) and (b). (e) Three term approximation to upper bound. (f) Two term approximation to lower bound.

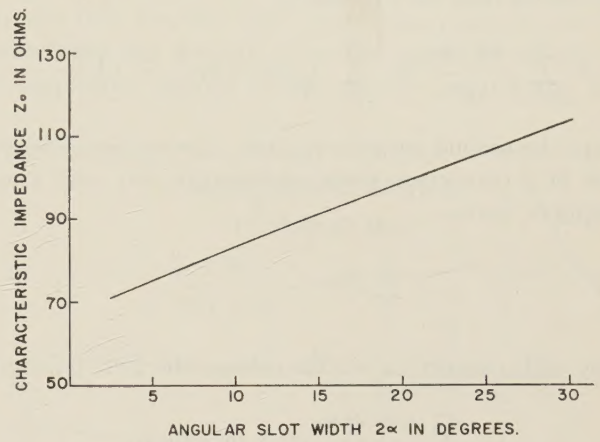

Fig. 4—Variation of characteristic impedance with slot angle for $b/a > 6$.

A plot of the charge distribution obtained for the three term approximation to the upper bound for Z_0 shows that the charge, and hence the current, is very heavily concentrated in the region of the slots.

Conclusions

The propagation of a second type of TEM mode on a slotted coaxial line has been discussed. In particular variational expressions giving upper and lower bounds to the characteristic impedance of the slotted line have been derived. The procedure developed is applicable generally and may be used to evaluate characteristic impedance of other structures occurring in practice.

For a generalized cylindrical transmission line the equivalent electrostatic problem is two dimensional. Let C_0 and C_1 be two open or closed curves coincident with the conducting surfaces of the line. Let $G(r, r')$ be the Green's function for the space surrounding C_0 in the absence of C_1 and such that G vanishes on C_0; i.e., G is the potential due to a unit charge at r' and such that the potential vanishes on C_0. The upper bound to the characteristic impedance of the line is then given by

$$Z_0 = \frac{\int\int_{c_1} G(r, r')\sigma(r)\sigma(r')dr dr'}{v\left(\int_{c_1} \sigma(r)dr\right)^2}$$

where $\sigma(r)$ is the charge distribution on C_1. The lower bound to Z_0 may be found by minimizing the volume integral of the electrostatic energy density of the field.

Appendix

The series to be summed is

$$\sum_{n=1,3\cdots}^{\infty}\left(1+\coth n\ln\frac{b}{a}\right)\frac{\sin^2 n\alpha}{n^3}.$$

This series may be written as:

$$2\sum_{1,3\cdots}^{\infty}\frac{\sin^2 n\alpha}{n^3}+\sum_{1,3\cdots}^{\infty}\left(\coth n\ln\frac{b}{a}-1\right)\frac{\sin^2 n\alpha}{n^3}$$

where the second series is rapidly converging and in the form of a correction term. Integrating the well known geometric series

$$\sum_{1}^{\infty}e^{2jn\alpha}=\frac{e^{2j\alpha}}{1-e^{2j\alpha}}$$

once with respect to α and taking the real part gives

$$\sum_{1}^{\infty}\frac{\cos 2n\alpha}{n}=-\ln 2\sin\alpha.$$

Replacing 2α by $\pi-2\alpha$ and adding and subtracting series, it is readily deduced that

$$2\sum_{1,3\cdots}^{\infty}\frac{\cos 2n\alpha}{n}=-\ln\tan\alpha.$$

Integrating this series twice with respect to α gives

$$\sum_{1,3}^{\infty}\frac{\sin^2 n\alpha}{n^3}=\int_0^{\alpha}\int_0^{x}\ln\tan y\,dy\,dx.$$

For a limited range of α, $\ln\tan y$ may be replaced by the first few terms of its Maclaurin's expansion and the integration may then be performed. One has

$$\ln\tan y=\ln y+\frac{y^2}{3}+\frac{7y^4}{90}+\cdots.$$

The integration gives

$$\sum_{1,3\cdots}^{\infty}\frac{\sin^2 n\alpha}{n^3}=(1.5-\ln\alpha)\frac{\alpha^2}{2}-\frac{\alpha^4}{36}-\cdots.$$

For $\alpha\leqq.5$ the following result is obtained:

$$\sum_{1,3\cdots}^{\infty}\left(1+\coth n\ln\frac{b}{a}\right)\frac{\sin^2 n\alpha}{n^3}$$
$$=(1.5-\ln\alpha)\alpha^2+\sum_{1,3}^{\infty}\left(\coth n\ln\frac{b}{a}-1\right)\frac{\sin^2 n\alpha}{n^3}.$$

Broadband Ferrite Microwave Isolator*

P. H. VARTANIAN†, J. L. MELCHOR†, and W. P. AYRES†

Summary—A new type broadband unidirectional transmission line has been built utilizing the difference in energy distribution between two counter-rotating circularly polarized waves in a circular waveguide containing a ferrite. This principle of isolation is different from those which have been used previously.

A large difference is observed in the energy distribution of two counter-rotating TE_{11} modes in a ferrite loaded circular waveguide. A ferrite rod magnetized along its axis presents an effective rf permeability of approximately two for the mode rotating in a negative screw sense with respect to the direction of magnetization. For the positive sense of rotation the effective rf permeability becomes very small and negligible energy is transmitted through the ferrite rod.

Unidirectional transmission characteristics were achieved by adding quarter wave plates before and after the ferrite rod and inserting an absorber into the ferrite. For the direction of propagation for which the quarter wave plate converts from a linear input to a positive circular rotation the positive wave tends to go around the ferrite with small loss. For the other direction of propagation the quarter wave plate converts the linear input wave to a negative wave which tends to concentrate in the ferrite and is absorbed.

Based on the principles described, an isolator was constructed which gives better than 30 db isolation over the range 8 to 11 kmc. The insertion loss is less than 2 db from 8 to 10.5 kmc and increases to 3 db at 11 kmc. The complete unit is $10\frac{1}{2}$ inches long and weighs $2\frac{1}{4}$ pounds.

The main advantage of this isolator over present transverse field rectangular waveguide isolators and Faraday rotation isolators is its improved bandwidth. Other advantages are that the isolator is not sensitive to changes in magnetic field and it operates with a readily obtainable ferrite at low magnetic fields. Its vswr over the band is less than 1.2. The principle of this isolator is applicable to other frequency bands.

* This work was performed under Signal Corps Contract No. DA-36-039-sc-31435.

† Electronic Defense Lab. of Sylvania Electric Products Inc., P.O. Box 205, Mountain View, Calif.

Introduction

TO KEEP abreast of current systems developments, both manufacturers and users of microwave components have felt the need for broadband microwave isolators. In attempts to make practical microwave isolators, ferrites have been heavily exploited in both circular and rectangular waveguide geometries. Effects of differential phase shift and differential resonance absorption for two directions of wave propagation are widely used as the basis for isolation in both waveguide geometries. In most reported cases, however, the bandwidth of these devices does not exceed ten per cent.

A new approach to microwave isolation in circular waveguide is reported here which does not not employ either Faraday rotation or magnetic resonance absorption. Instead, energy distribution differences for the two counter-rotating TE_{11} modes in a ferrite loaded circular waveguide are utilized as a basis for isolation. Energy distribution in a rectangular waveguide loaded with a transversely magnetized ferrite slab has been discussed by Lax *et al*;[1] but due to its added complexity the problem has not been solved in circular waveguide. Consequently the boundary value solution will not be discussed, but analogy will be made with waves propagating in infinite magnetic media and with waves propagating along an isotropic dielectric waveguide. With these analogies an attempt is made to give the reader a qualitative feeling for the energy distribution in ferrite loaded circular waveguide and to explain its applications in microwave isolators and other devices.

Theory of Operation

Experimental evidence has been found by the authors[2] in agreement with the Fox and Weiss[3] theory that the microwave energy distribution in a waveguide containing a magnetized ferrite is different for the two senses of circular polarization. The reason for this can be discussed qualitatively by examining the effective permeability seen by each of the rotating waves. Rotating waves are the normal modes of the problem in that the permeability is a scalar only for the case of circular polarization. For circularly polarized plane waves in a lossless infinite ferrite medium the scalar permeabilities are given by

$$\mu_{\pm} = 1 + \frac{\gamma 4\pi M_s}{\gamma H \pm \omega} \qquad (1)$$

where $4\pi M_s$ is the saturation magnetization, H is the applied magnetic field, γ is the gyromagnetic ratio, a negative number, and ω is the angular frequency. The symbol μ_+ denotes effective permeability for a wave rotating in the right hand direction looking along the magnetic field and μ_- denotes permeability for the counter-rotating wave.

Fig. 1 shows the two permeabilities of (1) as a function of magnetic field. It is seen that over a broad range of frequencies and magnetic fields, the negative polarization permeability is essentially two while the positive polarization permeability is very small. The μ_+ may actually in certain regions become zero or negative. For these regions it is necessary to include also the imaginary part of the permeability and the propagation constant is now more complicated but never less than zero.

[1] B. Lax, K. J. Button, and L. M. Roth, "Ferrite phase shifters in rectangular waveguide," *J. Appl. Phys.*, vol. 26, pp. 1413–1421; November, 1954.

[2] J. L. Melchor, W. P. Ayres, and P. H. Vartanian, "Energy concentration effects in ferrite loaded waveguides," *J. Appl. Phys.*, vol. 27; January, 1956.

[3] A. G. Fox and M. T. Weiss, "Discussion on ferromagnetic Faraday effect," *Rev. Mod. Phys.*, vol. 25, pp. 262–263; Janaury, 1955.

Since the dielectric constant of most ferrites is in the range of 10–15 the negative circular polarization sees a large $\mu\epsilon$ product and the ferrite rod acts essentially as a dielectric waveguide. Consequently, if a ferrite rod is placed in a circular or square waveguide, the energy of a negatively rotating wave will be concentrated in or near the rod. On the other hand, the positive circular polarization sees a small $\mu\epsilon$ in the region of the ferrite and hence the energy passes mainly around the rod.

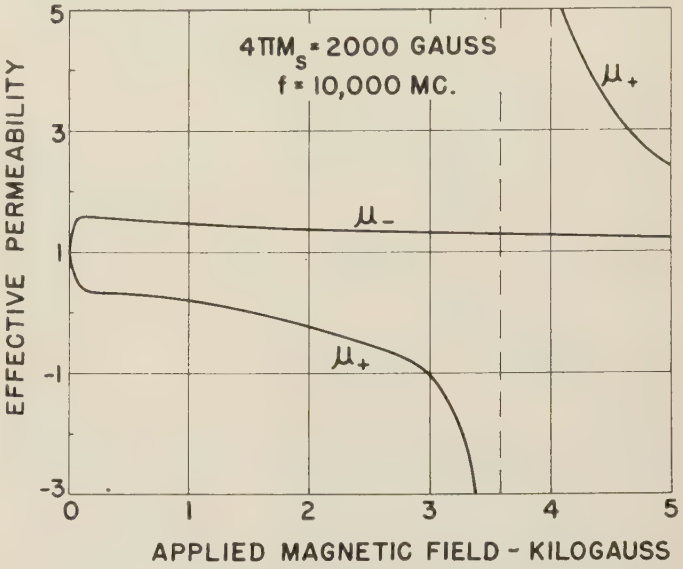

Fig. 1—Effective permeabilities for positive and negative circular waves in infinite lossless medium as a function of applied magnetic field.

There are several ways in which one of the two circular components may be selectively absorbed. A lossy material may be placed around the ferrite to fill the waveguide and absorb the positive wave; or an absorber may be introduced on the surface or inside the ferrite to absorb the negative wave.

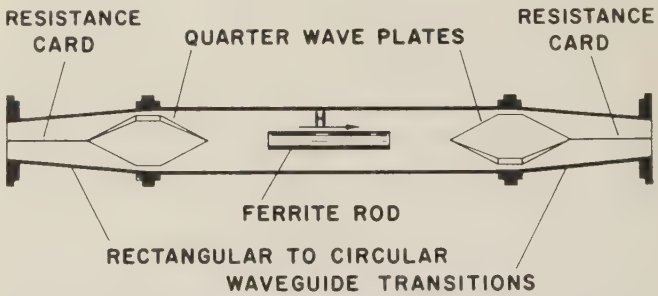

Fig. 2—Waveguide geometry used for loss measurements and used in construction of isolator.

Description of Isolator

An isolator was made by placing an Aquadag coated ferrite rod of the optimum diameter for the frequency band of interest between two quarter wave plates in a cylindrical waveguide as shown in Fig. 2. Ferrite, General Ceramics *R*-1, is magnetized to a low value with a longitudinal field produced by a permanent magnet.

The energy from the generator being isolated is converted by the first quarter wave plate into positive circular polarization which is transmitted essentially unattenuated and reconverted to linear polarization by the second quarter wave plate. Reflected energy from the load on the other hand is converted into negative circular polarization relative to the applied magnetic field and is attenuated in the absorber on the ferrite surface. Alternately the absorber may be put outside the ferrite to interact with the negative polarization. This has not performed as well since it requires a good match into the ferrite rod. The matches for the case of the absorber in the ferrite are not as important. This is because the discontinuity for the forward wave is very small since the permeability is small. The coated ferrite rod looks simply like an absorbing needle in the center of the guide which does not interact with the TE_{11} mode. For the backward wave there is a large discontinuity however, and reflections are absorbed in an H plane resistance card on the load side of the quarter wave plate. The quarter wave plate converts energy reflected from the ferrite into the H plane.

The quarter wave plates are of tapered polystyrene and are designed to give wide bandwidth. They have an ellipticity (ratio of space quadrature fields) of less than 2 db over the 8–11 kmc band. It can be shown that the forward loss caused by the quarter wave plate not converting all the energy into the proper polarization is

$$\frac{P_{\text{loss}}}{P_{\text{inc}}} = 1 - \frac{1}{4}\,\frac{(e+1)^4}{(e^2+1)^2}$$

where e is the ellipticity voltage ratio. Thus a 2 db ellipticity causes a loss of only 0.11 db in the forward direction for the two quarter wave plates.

The rectangular to circular waveguide transitions are approximately $2\frac{1}{4}$ inches long and have a vswr of less than 1.2 from 8 to 11 kmc. Tapered resistance cards are placed in the H plane of the transitions.

Isolation Characteristics

There are many modifications possible in the device shown in Fig. 2. It was found that the characteristics are sensitive to absorber position, rod diameter, absorber resistance, magnetic field, and ferrite used.

Absorber Position

As stated above, there are three possible places to locate the absorber: in the ferrite, on the ferrite, and outside of the ferrite. The absorber was placed inside of the ferrite by slicing a $\frac{1}{4}$-inch ferrite rod longitudinally and coating an absorbing material on the interfaces. The isolation is seen in Fig. 3 to be better than 15 db from 8 to 11 kmc with an insertion loss of less than 1.5 db. From 9 to 10 kmc the isolation exceeds 25 db while the insertion loss is less than 1 db. These data were taken with a solenoid adjusted for 375 gauss.

Isolators constructed with the absorbing material located between the ferrite and the waveguide wall were found to be unsatisfactory. Suitable isolation was achieved with this configuration but the insertion loss was found to be much too large. This can be attributed to losses due to a poor match between the waveguide and the ferrite rod which must act as a dielectric waveguide for the forward wave. These poor matches can also set up cavity resonances within the ferrite. Isolators constructed with the absorber outside the ferrite were compared extensively with those constructed with the absorber inside the ferrite. Rods with diameters as large as $\frac{1}{2}$ inch were used with the absorber outside. For all diameters between $\frac{1}{8}$ inch and $\frac{1}{2}$ inch the insertion loss was high except at discrete frequencies for larger diameter rods where the ferrite acted as a transmission cavity.[2]

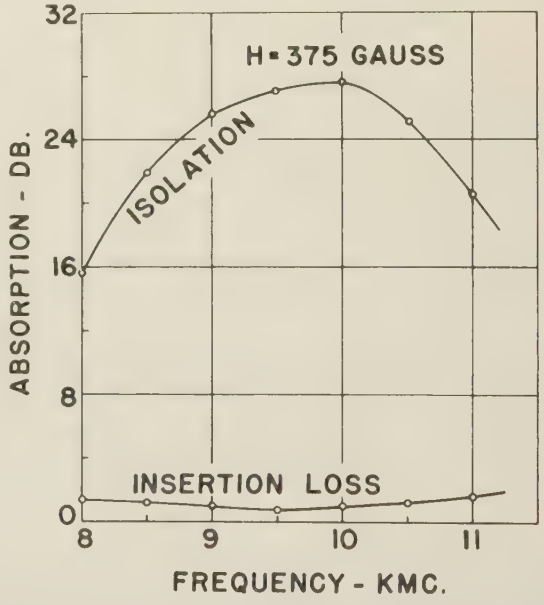

Fig. 3—Isolation and insertion loss versus frequency for isolator constructed with 0.250-inch diameter ferrite rod 2 inches long. Rod sawed in half longitudinally and absorber applied to interfaces.

The simplest and most convenient form of applying the absorber was to coat Aquadag on the ferrite surface. With this absorber configuration the insertion loss is still fairly low and the rod shape is preserved. The saw cut required with the absorber inside distorts the rod shape and decreases its effective diameter. As will be shown later in a discussion of the effects of diameter this can be important. In the remaining data to be discussed the absorber was coated on the ferrite surface.

Ferrite Rod Diameter Effects

As pointed out in the Theory of Operation, the ferrite rod begins to act as a dielectric waveguide for the negative rotating wave. Consequently we should expect operation of the isolator to be sensitive to rod diameter.

Curve *A* in Fig. 4 illustrates a 0.125-inch diameter rod beginning to act as a dielectric waveguide as frequency increases. The rod is 4 inches long, magnetized longitudinally, and coated with an absorber. The absorption of the negative wave increases with increasing frequency indicating that as frequency increases the ferrite begins to act more and more as a dielectric waveguide. This diameter rod would be useful in an isolator operating above 12 kmc but operation below 12 kmc requires larger diameter ferrite rods.

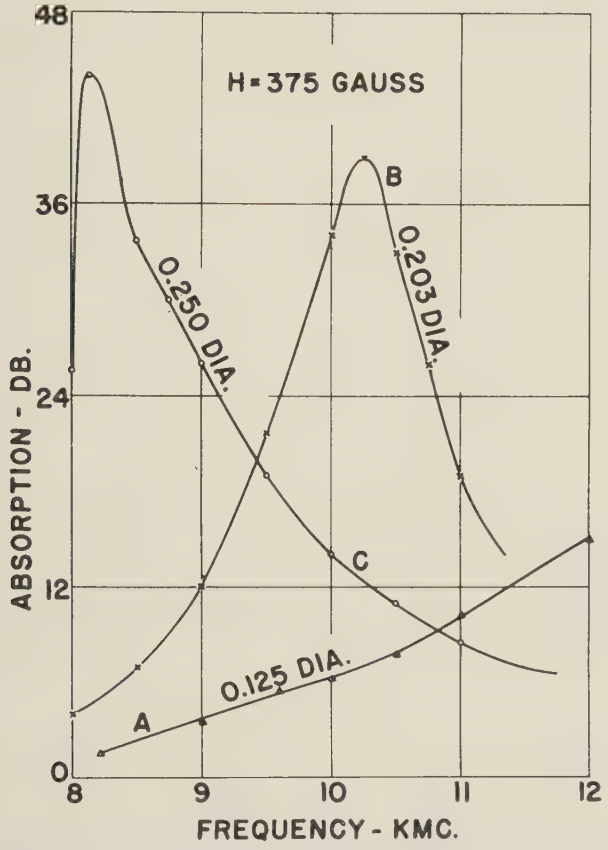

Fig. 4—Absorption losses versus frequency of negative wave for three different diameter rods with absorber coated on surface.

Curves *B* and *C* for rods of 0.203- and 0.250-inch diameters exhibit peaks in *X* band as shown in Fig. 4. Thus there is an optimum band of frequencies for dielectric waveguide effects for each ferrite diameter. The frequencies at which maximum isolations occur for a series of different diameter coated rods are shown in Fig. 5. Here it is seen that as diameter increases the frequency of the peak decreases. Fig. 5 indicates that rod diameters ranging from 0.155 to 0.250 inch will give isolation peaks distributed across the 8.2 to 12.4 kmc band. In practice three different diameter rods, each two inches long, are required to give better than 25 db isolation across this frequency band. However, with this arrangement the forward or insertion loss increases rapidly at the high frequency end of the band.

Surface Resistivity Effects

The isolation characteristics were found to depend strongly on the ferrite surface coating resistivity. A low surface resistivity resulted in less isolation, higher insertion loss, and a broader isolation curve as a function of frequency. Increased resistivity yielded lower insertion loss and a sharper isolation curve which reduced to isolation peaks due to reflection from the ferrite rod for very thin absorber films. An optimum resistance of roughly 2,000 ohms was found when measured from one end to the other on the periphery of a $\frac{1}{4}$-inch diameter rod, 2 inches long.

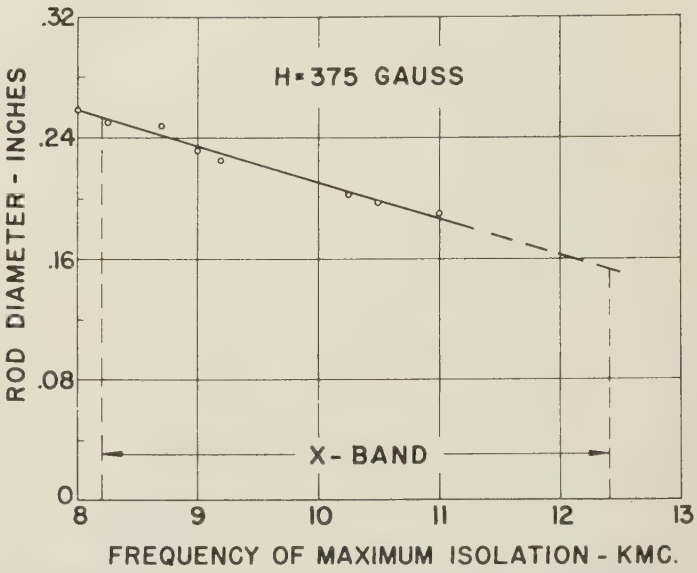

Fig. 5—Frequency of maximum isolation as a function of diameter of ferrite rods with absorber coated on the surface. Waveguide diameter is 0.93 inch.

Typical Isolator and Characteristics

An isolator was constructed with two ferrite rods of 0.250- and 0.190-inch diameters and 2 inches long placed end to end. Characteristics of this isolator are shown in Fig. 6. An isolation of greater than 30 db was achieved from 8 to 11 kmc with an insertion loss of less than 2 db from 8 to 10.5 kmc and increasing to 3 db at 11 kmc. The unit consists of two rectangular to circular waveguide transitions $2\frac{1}{4}$ inches long, two quarter wave plates, 6 ring magnets of the type Indiana Steel R-142, two pieces of resistance card, a circular waveguide section 6 inches long, and two absorber coated ferrite rods of 0.250- and 0.190-inch diameters. A photograph of the unit is shown in Fig. 7. It weighs $2\frac{1}{4}$ pounds and has an over-all length of $10\frac{1}{2}$ inches.

Merits of Isolator

An isolator based on differences in energy distribution for the rotating waves appears to be more broadband than a Faraday rotation isolator in the same geometry.

In addition the material requirements for this type of isolator are less stringent. Since the transmitted wave tends to pass around the ferrite there are less dielectric losses than for a Faraday rotator where half the energy

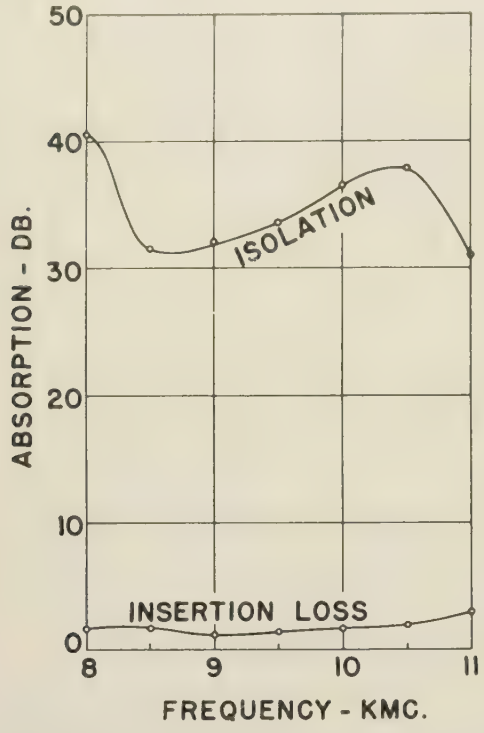

Fig. 6—Absorption characteristics of isolator constructed with 0.250-inch and 0.190-inch diameter rods.

is in the opposite sense of circular polarization and goes into the rod. In fact a ferrite with higher dielectric losses would be useful for this application.

The isolator is quite insensitive to magnetic field as expected from the effective permeability curves of Fig. 1. This makes it more practical for use with perma-

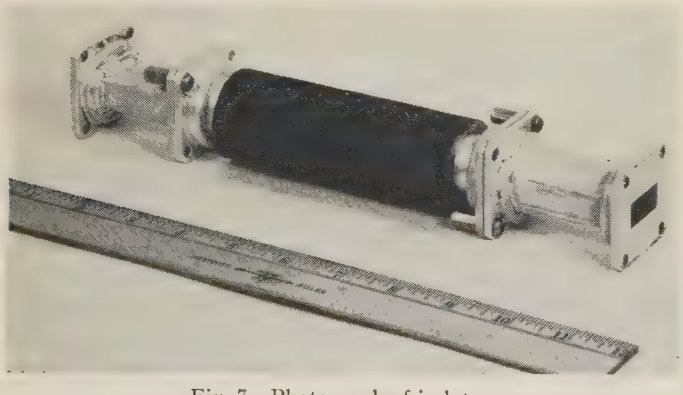

Fig. 7—Photograph of isolator.

nent magnets for which the magnetization changes with time. The magnetic field required is much smaller than that required with the resonance type isolator where fields of 2,000 to 3,000 gauss are commonly employed.

Since the loss occurs at the ferrite surface the problem of heat dissipation is less severe than for the other cases. With a metalized resistive coating and forced air cooling the potential high power applications are promising. A ferrite is a poor thermal conductor, making it difficult to extract energy absorbed within it by electric or magnetic losses. This type of isolator tends to reduce the losses which occur within the ferrite and reduces the problem of heat dissipation.

The isolator, which weighs $2\frac{1}{4}$ pounds, is considerably lighter than resonance absorption isolators, but comparable to Faraday rotation isolators. It has an advantage over the Faraday rotator in that any desired isolation, or reverse attenuation, can be achieved simply by making the ferrite element longer. Isolation was found to be directly proportional to the length of the element.

Limitations of Isolator

The principal limitation is the increase in insertion loss at higher frequencies. As seen from Figs. 3 or 6 the insertion loss begins to increase rather rapidly between 10 and 11 kmc. Upon examining individual isolation and insertion loss curves for different coated rod diameters it was found that the frequency for peak isolation is roughly 2 kmc below the frequency for which the sharp increase in insertion loss begins. In Fig. 6 the insertion loss at 11 kmc is due primarily to the $\frac{1}{4}$-inch rod. It increases continuously through 12.4 kmc which was the upper limit of the measurements. The increase is attributed to the fact that the effective permeability for the positive wave does not go to a sufficiently low value to exclude that wave from the ferrite at higher frequencies. To substantiate this hypothesis the applied magnetic field was increased in several steps to 1,500 gauss. At each successively higher field value the increased insertion loss occurred at a higher frequency. This indicates a reduction of the effective permeability for the positive wave which makes the rod's electrical size smaller, requiring higher frequencies for dielectric waveguide effects.

To avoid the problem of increasing insertion loss a material with lower μ_+ at magnetic saturation is desired. The field value for saturation is chosen because μ_- is a maximum there and it is an easily achievable magnetic field. At that point (1) becomes

$$\mu_\pm = \frac{\gamma B_s \pm \omega}{\gamma H_s \pm \omega} \tag{2}$$

where H_s is the magnetic field required to saturate the ferrite and B_s is the saturation flux density, $H_s + 4\pi M_s$. From this expression it is seen that μ_+ approaches zero as $|\gamma| B_s$ approaches ω. For X band operation a saturation moment greater than 3,000 gauss will give a more favorable ratio of propagation constants. Ferramic $R-1$ has a saturation moment of only 2,000 gauss.

Conclusion

Using the difference in energy distribution for circular waves transmitted through ferrite loaded circular waveguide, an isolator was constructed with 30 db isolation from 8 to 11 kmc. Its insertion loss is less than 3 db and it does not appear to be unduly critical with respect to any of the operating parameters. By providing means for varying the applied field the isolator becomes an amplitude modulator or electronic switch.

Since the energy transmitted in the forward direction tends to go around the ferrite, low magnetic and dielectric losses occur in it. This approach to isolation is promising for higher powers. A more suitable choice of material will reduce the insertion loss presently observed.

The frequency of maximum isolation for a single ferrite rod is inversely proportional to the ferrite diameter. Various diameter rods can be added in series to increase the isolation bandwidth. However, with the ferrite used an increase in insertion loss on the high frequency side discourages this beyond a 3 kmc bandwidth. The increase in insertion loss which occurs at higher frequencies is attributable to dielectric waveguide effects for the positive wave. With a dielectric constant of 13 the $\mu\epsilon$ product is large even if μ is as low as 0.3. In such a case, dielectric waveguide type transmission is expected to become noticeable at 11 kmc.

The use of differential energy distribution for nonreciprocal and magnetically controllable circuit elements is promising from the standpoint of stability, bandwidth, and power handling capacity.

Acknowledgment

The authors wish to thank Dr. A. L. Aden for his assistance in planning the project which led to this work, and for his helpful suggestions during the course of the work. We also wish to thank Mr. M. Medina for making many of the microwave measurements.

An Approximate Analysis of Coaxial Line with a Helical Dielectric Support*

J. W. E. GRIEMSMANN†

SHOWN in Fig. 1 is a cutaway section of coaxial cable with a helical dielectric support. The particular cable depicted bears the trade name of Styroflex[1] derived from the fact that the dielectric helix is built up in a winding operation from nonplasticized polystyrene tapes giving to the final assembly a tight grip on the center conductor and a good degree of allowable bending capability. The outer conductor in the original design of the cable consists of an aluminum sheath extruded over the dielectric. Other forms of cable with helical dielectric support are also available.

This type of cable is of interest as an alternative to broadband bead supported line, particularly for applications requiring long lengths of line or small diameter cable where multiplicity of bead supports can lead to high wave reflection characteristics in frequency bands of interest.

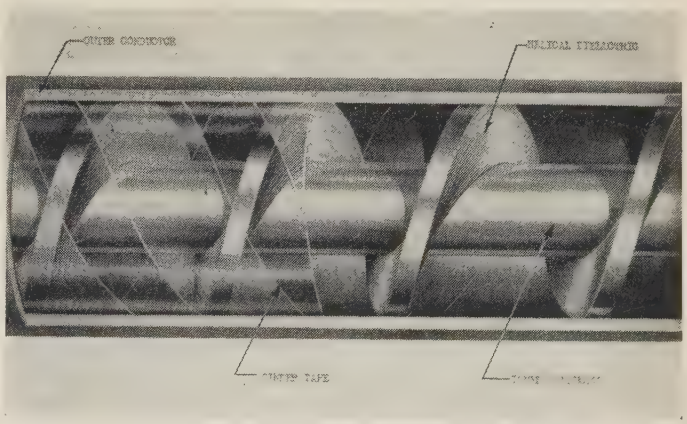

Fig. 1—Cut-away section of Styroflex cable.

The analysis given below shows that the total propagation in the helical line can be considered to be made up of two component propagations, one following the dielectric helix down the transmission line and the other following a helical path perpendicular to the dielectric. The latter type of propagation is that of an iterative transmission line and introduces for the overall propa-

* This analysis was conducted as part of the work under Signal Corps Contract DA-36-039 sc-42500 with the Polytechnic Institute of Brooklyn and was presented at the P.I.B. Symposium on Modern Advances in Microwave Techniques, November 8–10, 1954.

† Microwave Res. Inst., Polytechnic Inst. of Brooklyn, Bklyn., N. Y.

[1] Phelps Dodge Copper Products Corp.

gation characteristics of the line bands of propagation and attenuation. For practical purposes, operation is limited to frequencies approaching the first critical frequency which occurs approximately when the helical distance at the mean internal periphery measures an electrical half-wavelength between centers of the dielectric. The low frequency approximation which neglects the helical distribution of the dielectric and assumes the air and dielectric of the line to act in parallel is a satisfactory one for a major portion of the lowest propagating frequency region. The analysis given here shows a sharp rise in attenuation as the cutoff frequency is approached. This action is quantitatively confirmed by attenuation measurements on the transmission line.

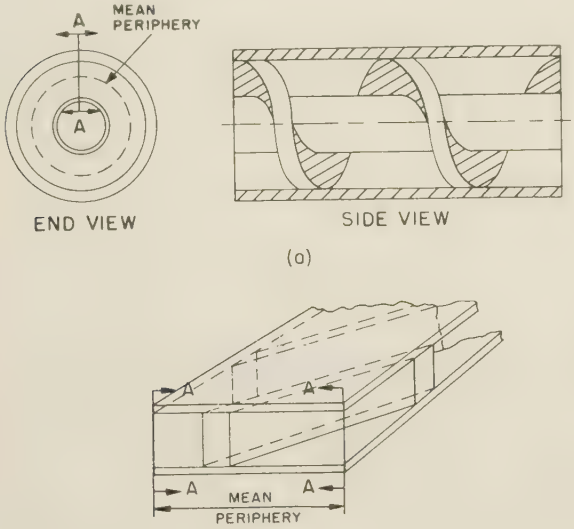

Fig. 2

Parallel Plate Approximation

The following analysis is based on the transformation of the problem in coaxial geometry to one in parallel plate geometry. Consider that the coaxial line shown in Fig. 2(a) is split radially from the outer conductor into the inner conductor along the line AA and for the entire length of coaxial line. Opening the line along this cut and continuously deforming it the parallel plate structure of Fig. 2(b) can be attained where the radial cut plane of the coaxial line splits into the two side planes through AA for the parallel plate line. It must now be understood, of course, that a condition for the parallel plate propagation is that the fields are identical in the side planes in order that the parallel plate line can again be reformed back into the original coaxial line. The parallel plate structure of Fig. 2(b) is considered to be part of a larger parallel plate system, the top view of which is shown in Fig. 3, since it would be inappropriate to consider edge effects for the parallel plate. The region of interest from the propagation standpoint is that between the two side planes through A-A. The mode and nature of propagation in the parallel plate line will now be very similar to that in the original coaxial line although any numerical values obtained represent an approximation to the values existing in the coaxial line. The rigorous solution in suitable radial or helical coordinates is required for exact values for the propagation characteristics and fields of lines with helical supports.

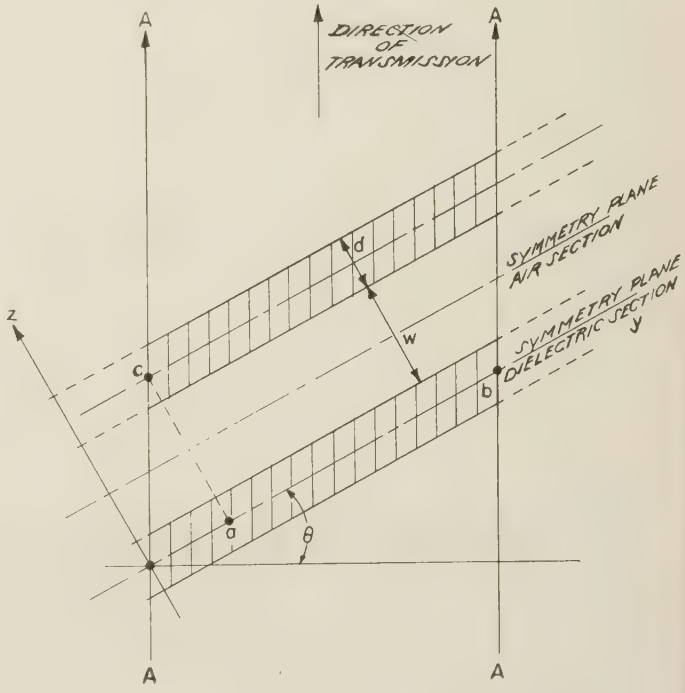

Fig. 3—Top view of extended parallel plate system.

Field Components

In any fundamental mode type of propagation in the parallel plate system there must be assumed to exist an electrical field perpendicular to the plates. This corresponds to a radial electric field in the coaxial line. The existence of this electric field component E_x which is noted to be directed parallel to the dielectric surface would require in general the two components H_y and H_z to exist in order to satisfy the boundary conditions corresponding to refraction at the air-dielectric interface. By trial the simplest mode which would satisfy the Maxwell's equations and boundary conditions was found to be the following set:

In Air Sections

$$H_{yo} = \frac{k_{zo}}{\omega\mu} A_o[1 - \Gamma_o\epsilon^{+2jk_{zo}z'}]\epsilon^{-jk_{zo}z'}\epsilon^{-jk_y y} \tag{1}$$

$$H_{zo} = -\frac{k_y}{\omega\mu} A_o[1 + \Gamma_o\epsilon^{+2jk_{zo}z'}]\epsilon^{-jk_{zo}z'}\epsilon^{-jk_y y} \tag{2}$$

$$E_{xo} = A_o[1 + \Gamma_o\epsilon^{+2jk_{zo}z'}]\epsilon^{-jk_{zo}z'}\epsilon^{-jk_y y} \tag{3}$$

where z' is measured from the symmetry planes of the air sections.

In Dielectric Sections

$$H_{y\epsilon} = \frac{k_{z\epsilon}}{\omega\mu} A_\epsilon [1 - \Gamma_\epsilon \epsilon^{+2jk_{z\epsilon}z''}] \epsilon^{-jk_{z\epsilon}z''} \epsilon^{-jk_y y} \quad (4)$$

$$H_{z\epsilon} = -\frac{k_y}{\omega\mu} A_\epsilon [1 + \Gamma_\epsilon \epsilon^{+2jk_{z\epsilon}z''}] \epsilon^{-jk_{z\epsilon}z''} \epsilon^{-jk_y y} \quad (5)$$

$$E_{x\epsilon} = A_\epsilon [1 + \Gamma_\epsilon \epsilon^{+2jk_{z\epsilon}z''}] \epsilon^{-jk_{z\epsilon}z''} \epsilon^{-jk_y y} \quad (6)$$

where z'' is measured from the symmetry planes of the dielectric sections.

With low losses a suitable approximation is that k_{zo}, $k_{z\epsilon}$ and k_y are respectively the phase constants in the z direction in air, in the z direction in the dielectric and in the y direction. The same phase constant k_y in the air and dielectric is necessary to satisfy the boundary condition along the air-dielectric interface. A_o and A_ϵ are complex constants indicating the relative magnitudes and phase of the field. The field distribution in the cross section is determined by the reflection coefficient Γ_o in the air sections and Γ_ϵ that in the dielectric sections. It is implicitly assumed that the field is periodic in the z direction and that the values of the complex constants A_o, A_ϵ, Γ_o and Γ_ϵ are determined by boundary conditions at the air-dielectric interface, transmission conditions and the power being transmitted.

For convenience in the understanding of the propagation characteristics of the line, it is desirable to consider that the total propagation is made up of two partial propagations in parallel, one in the y direction associated with the components E_x and H_z, and the other in the z direction associated with E_x and H_y. The propagation in the y direction or in the direction parallel to the dielectric has associated with it a constant cross section and only one forward traveling wave is needed to describe this propagation. The propagation in the z direction must be considered as an iterative transmission line having successive sections of air and dielectric. In order to satisfy the boundary conditions (or impedance conditions) at the air-dielectric boundaries, it is necessary to postulate forward and backward traveling waves (or to include the reflection coefficients) in each medium just as one would for an ordinary iterative transmission line structure. As seen later, reflection coefficients are real at lines of symmetry in the air and dielectric sections making them convenient reference points for extensions Z' and Z'' in z direction.

Phase Constant Relationships

The propagation constants in the y direction and z direction must be consistent with the over-all propagation constant in each of the media. Thus, in the dielectric sections,

$$k_{z\epsilon}^2 + k_y^2 = k_\epsilon k^2 \quad (7)$$

where k is free space phase constant and k_ϵ is relative dielectric constant of medium. In air section

$$k_{zo}^2 + k_y^2 = k^2 \quad (8)$$

where k for the air is assumed equal to that of free space.

In order to satisfy the condition that for the section of the parallel plate line the fields in the side planes must be identical, it is required that the phase of the field at the points, b and c, shown in Fig. 3 must be identical. This gives rise to another condition on the phase constants which may be derived by requiring that the change in phase of field experienced in going from the point a to b in Fig. 3 is the same as the change in phase in going from the point a to the point c. The resulting equation for this condition must be derived from iterative line considerations.

Propagation Characteristics in the z Direction

In the z direction, the transmission line structure is periodic and symmetrical with respect to propagation in the forward or backward z direction. The description for arbitrary terminating impedance is then conveniently given in terms of iterative impedances. Shown in Fig. 4(a) is the equivalent transmission line (for wave impedances) in the z direction for the extended parallel plate structure. Also shown in this figure, plotted on an admittance diagram, is a typical admittance cycle representing the locus of impedances of the transmission line matched in its iterative impedance. In general, of course, for this type of operation there will be standing waves in both the air sections and dielectric sections of the line but the iterative impedance matching implies that the magnitude of electric and magnetic field is repeated at successive corresponding structural points along the transmission line. Since for any transverse plane the points at the special AA side planes, described before in Fig. 3, are corresponding structural points in the iterative transmission, the boundary condition that the fields be identical at corresponding transverse side plane points is in part satisfied. The requirement of the boundary condition then remaining is that the phase be identical at the corresponding transverse side points. Determination of the phase constant for the iterative type transmission line in the y direction is then required. This solution will also yield the values of Γ_o and Γ_ϵ necessary for a quantitative knowledge of the field structure and the determination of attenuation constant for this line.

For further analytical work, one of the two most convenient sets of reference planes in the iterative structure is the centers of the air sections corresponding to the real admittance points Y_{co} on the admittance cycle. Shown in Fig. 4(b) is the structure between two successive reference planes terminated in the iterative impedances Y_{co}. Since the section is symmetrical, the value Y_{co} can be determined from

$$Y_{oc} = \sqrt{Y_{op(1/2)} \, Y_{sh(1/2)}} \quad (9)$$

where $Y_{op(1/2)}$ is the admittance measured at the input, a, with an open circuit at the center reference plane, d, and $Y_{sh(1/2)}$ is the admittance measured at the input with a short circuit at the center reference plane d.

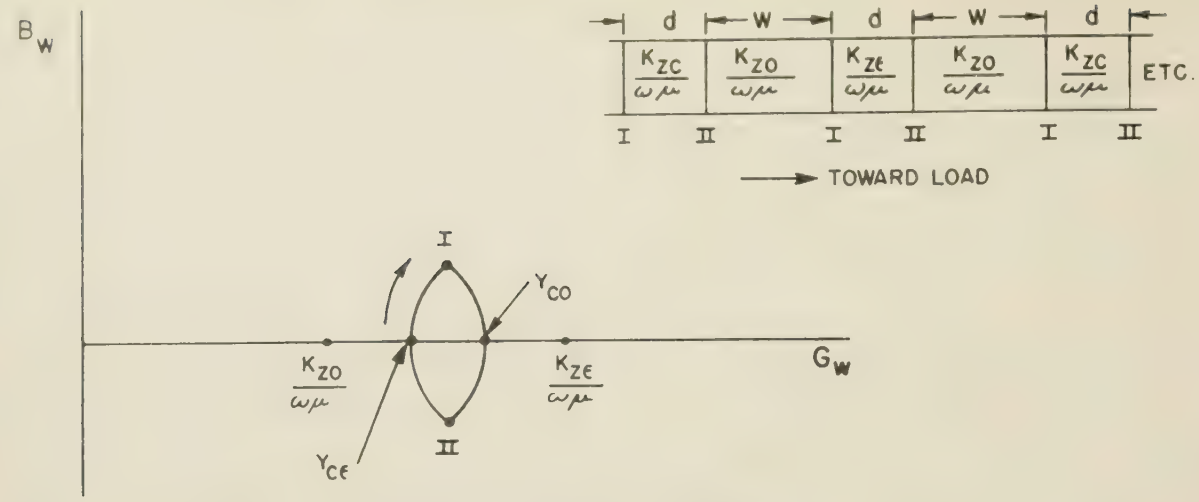

(a) SCHEMATIC ADMITTANCE CYCLE DIAGRAM

ITERATIVE TRANSMISSION LINE
(Z - DIRECTION)

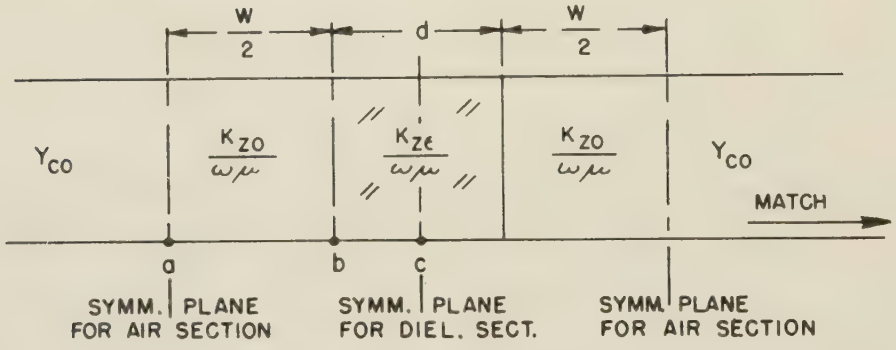

(b) COMPOSITE SYMMETRICAL SECTION

Fig. 4.

From transmission line calculations, the values of these admittances are determined to be the following:

$$Y_{op(1/2)} = j\frac{k_{zo}}{\omega\mu}\tan\left[k_{zo}\frac{w}{2} + \tan^{-1}\left(\frac{k_{z\epsilon}}{k_{zo}}\tan k_{z\epsilon}\frac{d}{2}\right)\right] \quad (10)$$

$$Y_{sh(1/2)} = -j\frac{k_{zo}}{\omega\mu}\cot\left[k_{zo}\frac{w}{2} + \tan^{-1}\left(\frac{k_{zo}}{k_{z\epsilon}}\tan k_{z\epsilon}\frac{d}{2}\right)\right] \quad (11)$$

whence

$$Y_{co}^2 = \left(\frac{k_{zo}}{\omega\mu}\right)^2 \frac{\tan\left[k_{zo}\frac{w}{2} + \tan^{-1}\left(\frac{k_{z\epsilon}}{k_{zo}}\tan k_{z\epsilon}\frac{d}{2}\right)\right]}{\tan\left[k_{zo}\frac{w}{2} + \tan^{-1}\left(\frac{k_{zo}}{k_{z\epsilon}}\tan k_{z\epsilon}\frac{d}{2}\right)\right]}; \quad (12)$$

the value of the reflection coefficient Γ_o at the center plane of the air section is then

$$\Gamma_o = \frac{1 - \left(\frac{\omega\mu Y_{co}}{k_{zo}}\right)}{1 + \left(\frac{\omega\mu Y_{co}}{k_{zo}}\right)}. \quad (13)$$

Alternatively, the reference planes for the start and finish of the composite line could have been selected as the center or symmetry planes for the dielectric sections which would correspond to the admittance $Y_{c\epsilon}$ on the schematic admittance cycle diagram of Fig. 4. By appropriate substitution of variables the value of the characteristic admittance would be found to be given by

$$Y_{c\epsilon}^2 = \left(\frac{k_{z\epsilon}}{\omega\mu}\right)^2 \frac{\tan\left[k_{z\epsilon}\frac{d}{2} + \tan^{-1}\left(\frac{k_{zo}}{k_{z\epsilon}}\tan k_{zo}\frac{w}{2}\right)\right]}{\tan\left[k_{z\epsilon}\frac{d}{2} + \tan^{-1}\left(\frac{k_{z\epsilon}}{k_{zo}}\tan k_{zo}\frac{w}{2}\right)\right]} \quad (14)$$

giving for

$$\Gamma_\epsilon = \frac{1 - \left(\frac{\omega\mu Y_{c\epsilon}}{k_{z\epsilon}}\right)}{1 + \left(\frac{\omega\mu Y_{c\epsilon}}{k_{z\epsilon}}\right)}. \quad (15)$$

For the structure shown in Fig. 4(b) the change in phase from input to output, Φ_I, is determined from iterative line considerations, being given by

$$\cos \Phi_I = \cos k_{z\epsilon} d \cos k_{zo} w - \frac{1}{2}\left(\frac{k_{z\epsilon}}{k_{zo}} + \frac{k_{zo}}{k_{z\epsilon}}\right) \sin k_{z\epsilon} d \sin k_{zo} w. \quad (16)$$

In order to satisfy the boundary condition, corresponding transverse points at the side planes must have the same phase as previously discussed under PHASE CONSTANT RELATIONSHIPS. Then, with reference to points b and c of Fig. 3, it is evident that

$$\Phi_I = k_y \frac{w + d}{\tan \theta} \pm n(2\pi) \quad (17)$$

whence

$$\cos k_y \frac{w + d}{\tan \theta} = \cos k_{z\epsilon} d \cos k_{zo} w - \frac{1}{2}\left(\frac{k_{z\epsilon}}{k_{zo}} + \frac{k_{zo}}{k_{z\epsilon}}\right) \sin k_{z\epsilon} d \sin k_{zo} w. \quad (16a)$$

The phase constants k_y, $k_{z\epsilon}$ and k_{zo} are now specified in terms of the dimensions, w, d, and θ, and the frequency or free space phase constant, k, through (7), (8), and (16a). The form of the field can then be specified at any frequency from an evaluation of Γ_o and Γ_ϵ, using (12) through (15). In the expression relating Φ_I and k_y above $n = 0$ corresponds to the lowest practical range of operation with a cutoff frequency of zero. Integer values of n correspond to higher mode operation having finite cutoff frequencies. The wavelength in the transmission direction (λ_g) may be determined from

$$k_y = \frac{2\pi}{\lambda_g} = \frac{k_y}{\sin \theta}. \quad (18)$$

Low Frequency Approximation

The low frequency approximation can be deduced directly from the consideration that dielectric and air sections act in parallel. The solution above reduces to this solution under the assumption of sufficiently low frequencies. For low frequencies, (16a) becomes under the assumption that typically $\sin \alpha = \alpha$ and $\cos \alpha = 1 - (\alpha^2/2)$

$$\left(k_y \frac{w + d}{\tan \theta}\right)^2 = (k_{z\epsilon}{}^2 d + k_{zo}{}^2 w)(w + d). \quad (16b)$$

Using (7) and (8), the phase constants become

$$k_y = k\left(\frac{k_\epsilon d + w}{w + d}\right)^{1/2} \sin \theta = k\, k_{eff}{}^{1/2} \sin \theta \quad (16c)$$

$$k_{z\epsilon} = k(k_\epsilon - k_{eff} \sin^2 \theta)^{1/2} \quad (7a)$$

$$k_{zo} = k(1 - k_{eff} \sin^2 \theta)^{1/2}. \quad (8a)$$

As indicated the expression

$$\left(\frac{k_\epsilon d + w}{w + d}\right)$$

is recognized to be the effective relative dielectric constant under the assumption that the dielectric sections and air sections are acting in parallel. For the iterative line in the z direction, the admittance cycle diagram of Fig. 4(a) reduces at low frequencies to a point for the values of iterative wave admittances from (12) and (14)

$$Y_{co} = Y_{c\epsilon} = \frac{k}{\omega\mu}\left[\frac{k_{z\epsilon}{}^2 d + k_{zo}{}^2 w}{k^2(w + d)}\right]^{1/2} = \frac{k}{\omega\mu} k_{eff}{}^{1/2} \cos \theta.$$

The expressions for the fields in the air sections become from (1), (2), and (3),

$$E_{zo} = A_o \frac{2(1 - k_{eff} \sin^2 \theta)^{1/2}}{(1 - k_{eff} \sin^2 \theta)^{1/2} + k_{eff}{}^{1/2} \cos \theta} \quad (3a)$$

$$H_{yo} = \frac{k}{\omega\mu} E_{zo} k_{eff}{}^{1/2} \cos \theta \quad (1a)$$

$$H_{zo} = \frac{k}{\omega\mu} E_{zo} k_{eff}{}^{1/2} \sin \theta. \quad (2a)$$

For fields in dielectric sections from (4), (5), and (6)

$$E_{x\epsilon} = A_\epsilon \frac{2(k_\epsilon - k_{eff} \sin^2 \theta)^{1/2}}{(k_\epsilon - k_{eff} \sin^2 \theta) + k_{eff}{}^{1/2} \cos \theta} \quad (6a)$$

$$H_{y\epsilon} = \frac{k}{\omega\mu} E_{x\epsilon} k_{eff}{}^{1/2} \cos \theta \quad (4a)$$

$$H_{z\epsilon} = \frac{k}{\omega\mu} E_{x\epsilon} k_{eff}{}^{1/2} \sin \theta. \quad (5a)$$

The total magnetic field in both the air and dielectric sections is noted to be transverse to the direction of propagation and to have the value

$$H_T = E_{zo} \frac{k}{\omega\mu} k_{eff}{}^{1/2} = E_{x\epsilon} \frac{k}{\omega\mu} k_{eff}{}^{1/2}.$$

The wave impedance is noted to be the same for both the air and dielectric sections supporting the low frequency assumption of TEM propagation in a homogeneous dielectric material, having a dielectric constant equal to the effective value given above. The propagation constant is that for a material with the effective dielectric constant, k_{eff}.

Modes of Operation

In general, the field pattern and the consequent performance characteristics of this type of transmission line are dependent on two factors. The first of these is, of course, the requirement that the phase is identical at corresponding transverse side points as indicated in Fig. 3 and covered by (16) and (17). The second factor is the type of propagation in the z direction which, because of its iterative nature, will have pass and stop bands as indicated by either (12) or (14). The influence of the second factor is dependent on the construction of the cable, being greater for smaller pitch angle, θ, and greater influence of the dielectric. As the pitch angle approaches $\pi/2$, the line is seen to approach a line with a longitudinal dielectric support. In this case the propagation in the z direction is not a significant part of the

over-all propagation, but serves rather to determine the cutoff frequencies of the higher modes and the variation with frequency of the guide wavelengths for these higher modes.

While the foregoing analysis is applicable for any type of cable construction, consideration here will be limited to the case where the component propagation in the z direction is a significant part of the total propagation. Of chief concern will be the possible frequency limitations on the lowest mode of operation. The higher modes associated with a periodic variation of field with the coordinate x (perpendicular to plates) are not considered since, for the usual coaxial lines dimensions, the variation with y and z (parallel to plate) will impose greater limitations.

The critical frequencies for propagation in the z direction are those for which the iterative admittances, as given by (12) and (14), become infinite or zero and are the boundaries between purely propagating and purely attenuating bands. Shown in Table I are the

TABLE I
CRITICAL FREQUENCY RELATIONSHIPS

Desig	Determinental Equation	Value of[2] $\cos \Phi_I$	z Direction Wave Impedance	
			At center of Air Sections	At center of Dielectric Sections
A	$k_{z\epsilon} \tan \frac{k_{z\epsilon} d}{2} - k_{zo} \cot \frac{k_{zo} w}{2}$	-1	Short	Open
B	$k_{z\epsilon} \cot \frac{k_{z\epsilon} d}{2} = k_{zo} \tan \frac{k_{zo} w}{2}$	-1	Open	Short
C	$k_{z\epsilon} \tan \frac{k_{z\epsilon} d}{2} = -k_{zo} \tan \frac{k_{zo} w}{2}$	$+1$	Open	Open
D	$k_{z\epsilon} \cot \frac{k_{z\epsilon} d}{2} = -k_{zo} \cot \frac{k_{zo} w}{2}$	$+1$	Short	Short

[2] See (16).

formulas which define these critical frequencies listed in order of increasing frequency for a given value of n in (17). These values could also have been obtained by letting $\cos \Phi_I = \pm 1$ in (16), as indicated in Table I, or that Φ_I is an appropriate multiple of π. For any given critical frequency condition of Table I and any given value n, the critical frequency is determined using (17), (7), and (8). Operation down to zero frequency can occur only for the case $n = 0$. In this case, the infinite sequence of alternating pass and stop bands, defined by the conditions A, B, C, and D, have a propagating region between zero frequency and that of condition A. For other values of n, there will be non-zero cutoff frequencies and the sequence of pass and stop bands can be of opposite character to that for $n = 0$. The value of $k_y(w+d)/\tan \theta$ assumes values equal to multiples of π and the value zero for critical frequencies of A, B, C, and D. The value of k_y will, however, vary with frequency making the main direction of propagation a function of frequency. Total propagation in the z direction, for example, is obtained only at cutoff frequencies for which k_y can be zero, as can be noted from (2) and (5). Increasing frequency above these cutoff values will cause propagation to start in the y direction. The modes of operation then can only be characterized by n which can assume positive or negative values. Since there is a wide variation of the positioning of critical frequencies with respect to cable construction, it appears best to reserve further discussion of the modes of operation to specific cable constructions.

Power Flow

From (1), (2), and (3), the Poynting vector for the air sections of the line is found to be

$$\begin{aligned} |P_o &= R_e\{|E \times |H^*\} \\ &= R_e\{x_o E_x \times [y_o H_y + z_o H_z]\} \\ &= \frac{|A_o|^2}{\omega\mu} [z_o k_{zo}(1 - |\Gamma_o|^2) \\ &\quad + y_o k_y |1 + \Gamma_o \epsilon^{jk_{zo}z'}|^2] \end{aligned} \tag{19}$$

where x_o, y_o, and z_o are respectively the unit vectors in the x, y, and z directions. The power in the z direction is noted to be independent of position in the line, but to be a function of frequency through the dependence of $|\Gamma_o|^2$ on frequency. When the line is propagating in its lowest mode Γ_o is a minimum, $\Gamma_o = -|\Gamma_o|$, at the center reference plane making the y component of Poynting vector a minimum at the center of the air section.

From (4), (5), and (6), the Poynting vector for the dielectric section of the line is found to be

$$\begin{aligned} |P_\epsilon &= \frac{|A_\epsilon|^2}{\omega\mu} [z_o k_{z\epsilon}(1 - |\Gamma_\epsilon|^2) \\ &\quad + y_o k_y |1 + \Gamma_\epsilon \epsilon^{+j2k_{z\epsilon}z''}|^2]. \end{aligned} \tag{20}$$

The total power flow crossing a given cross section of the transmission line may be obtained by appropriately summing the amounts of power flowing in the two directions and for both air and dielectric, as shown schematically in Fig. 5.

The power in the air section in the z direction crossing any given transverse cross section is

$$P_{zo} = \frac{k_{zo}}{\omega\mu} |A_o|^2 [1 - |\Gamma_o|^2] \frac{wh}{\tan \theta}$$

where h is the height of the line and using the projected area of the air portion of cross sectional area on a z = constant plane as shown in Fig. 5.

The power in the dielectric section in the z direction crossing any given transverse cross section is

$$P_{z\epsilon} = \frac{k_{z\epsilon}}{\omega\mu} |A_\epsilon|^2[1 - |\Gamma_\epsilon|^2] \frac{dh}{\tan\theta}.$$

The power in the air section in the y direction crossing any given cross section is

$$P_{yo} = \frac{k_y}{\omega\mu} |A_o|^2 h \int_{-w/2}^{+w/2} (1 + |\Gamma_o|^2 - 2|\Gamma_o| \cos 2k_{zo}z')\, dz'$$

where propagation conditions are considered which make $\Gamma_o = -|\Gamma_o|$ at $z' = 0$; *i.e.*, for image terminated transmission conditions in the z direction. The integration yields

$$P_{yo} = \frac{k_y}{\omega\mu} |A_o|^2 h \left[(1 + |\Gamma_o|^2)w - 2|\Gamma_o| \frac{\sin k_{zo}w}{k_{zo}}\right].$$

The power in the dielectric section in the y direction crossing any given cross section is similarly

$$P_{y\epsilon} = \frac{k_y}{\omega\mu} |A_\epsilon|^2 h \left[(1 + |\Gamma_\epsilon|^2)d + 2|\Gamma_\epsilon| \frac{\sin k_{z\epsilon}d}{k_{z\epsilon}}\right].$$

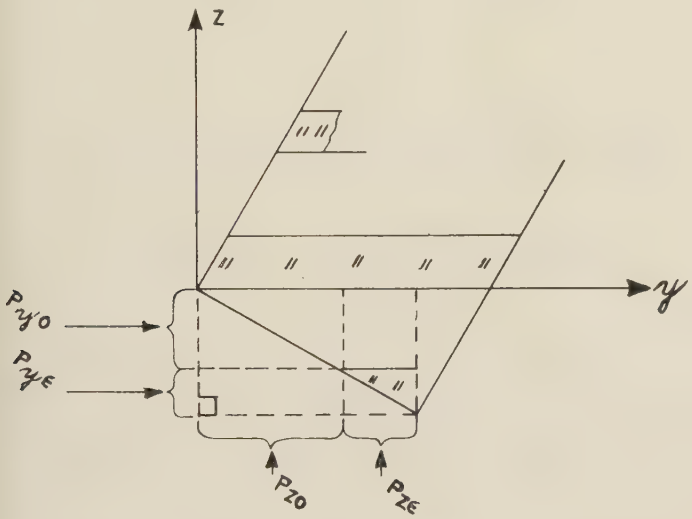

Fig. 5—Components of power flow across any given transverse cross section.

The total power is then the sum

$$P_T = P_{zo} + P_{z\epsilon} + P_{yo} + P_{y\epsilon}. \quad (21)$$

The continuity of the z components of the Poynting vector at the interface between the air section and dielectric section requires that

$$k_{zo}|A_o|^2[1 - |\Gamma_o|^2] = k_{z\epsilon}|A_\epsilon|^2[1 - |\Gamma_\epsilon|^2]. \quad (22)$$

A knowledge of the dimensions of the line and frequency then allows a determination of the magnitude of $|A_o|$ in terms of $|A_\epsilon|$. Quantitative values for the field quantities of (1) through (6) can then be obtained by expressing $|A_o|^2$ in terms of the total power transmitted by the line. The constant A_o for a given air section will lead in phase that of the next air section by angle Φ_I. This is true also for A_ϵ of dielectric sections.

Under the low frequency approximation previously considered, (32) reduces to

$$P_T \cong \left[|A_o|^2 \frac{4(1 - k_{eff}\sin^2\theta)}{[(1 - k_{eff}\sin^2\theta)^{1/2} + k_{eff}^{1/2}\cos\theta]^2}\right] \cdot \frac{kk_{eff}^{1/2}}{\omega\mu} h \frac{w + d}{\sin\theta} \quad (21a)$$

which agrees directly with that obtained directly from the fields using low frequency approximation; the bracketed term is $|E_{xo}|^2 \equiv |E_{x\epsilon}|^2$. In terms of the voltage, $V = |E_{xo}|h$, the total power is

$$P_T \cong \frac{V^2}{\frac{\omega\mu}{kk_{eff}^{1/2}} \frac{h}{(w + d)/\sin\theta}} = \frac{V^2}{Z_{opp}}$$

where Z_{opp} is recognized to be the characteristic impedance of the parallel plate line having a dielectric material with the dielectric constant k_{eff}.

Attenuation

The loss per unit length is the same at any given cross section and the same is true for the attenuation. For greater clarity, however, the loss per section will be calculated and the attenuation computed in this way.

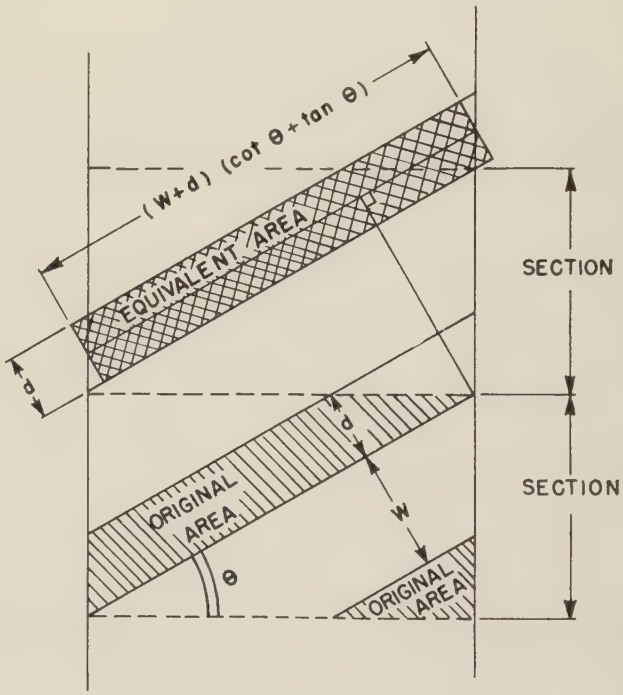

Fig. 6—Equivalent dissapative area under dielectric.

Conductor Losses

The component of field H_y gives rise to surface currents in the conductor planes in the z direction and the field H_z to currents in the y direction. Consider first the currents in the z direction for that portion of metal surface in contact with the dielectric. Shown in Fig. 6 is the original area per section in contact with one metal plane conductor and the equivalent area in terms of both the total original area and also the magnitude of the magnetic fields to which the surface is subjected.

The equivalent area can be seen to be built up of an equivalent piece taken from the original area and the substitution of equivalent areas above and below the field symmetry line. The power dissipated per section in the conductor walls under the dielectric by currents in the z direction is then, assuming negligible reaction on the modal character,

$$D_{\epsilon z} = 2(w + d)(\cot\theta + \tan\theta)R_s \int_{-d/2}^{+d/2} |H_y|^2 dz''$$

where R_s is the surface resistivity of the conductor.

Upon integration, this expression becomes

$$D_{\epsilon z} = 2\left(\frac{k_{z\epsilon}}{\omega\mu}\right)^2 |A_\epsilon|^2 R_s d(w + d)(\cot\theta + \tan\theta) \cdot \left[1 + |\Gamma_\epsilon|^2 - 2|\Gamma_\epsilon| \frac{\sin k_{z\epsilon} d}{k_{z\epsilon} d}\right].$$

A similar integration yields for the power dissipated per section by currents in the y direction,

$$D_{\epsilon y} = 2\left(\frac{k_y}{\omega\mu}\right)^2 |A_\epsilon|^2 R_s d(w + d)(\cot\theta + \tan\theta) \cdot \left[1 + |\Gamma_\epsilon|^2 + 2|\Gamma_\epsilon| \frac{\sin k_{z\epsilon} d}{k_{z\epsilon} d}\right].$$

By a similar determination of the equivalent area per section for the walls enclosing the air dielectric section, the power dissipated per section by currents in the z direction may be determined to be

$$D_{oz} = 2\left(\frac{k_{zo}}{\omega\mu}\right)^2 |A_o|^2 R_s w(w + d)(\cot\theta + \tan\theta) \cdot \left[1 + |\Gamma_o|^2 + 2|\Gamma_o| \frac{\sin k_{zo} w}{k_{zo} w}\right]$$

and the power dissipated per section in the y direction is

$$D_{oy} = 2\left(\frac{k_y}{\omega\mu}\right)^2 |A_o|^2 R_s w(w + d)(\cot\theta + \tan\theta) \cdot \left[1 + |\Gamma_o|^2 - 2|\Gamma_o| \frac{\sin k_{zo} w}{k_{zo} w}\right].$$

The total dissipation per section in the conductors is then

$$D_c = D_{\epsilon z} + D_{ey} + D_{oz} + D_{oy}. \tag{23}$$

The attenuation constant arising from attenuation in the walls is then

$$\alpha_c = \frac{1}{2} \frac{D_c}{P_T} \frac{\cos\theta}{w + d} \tag{24}$$

where P_T is given by (21) and the factor $\cos\theta/w+d$ converts the dissipation per section to that per unit length.

Again, the low frequency assumption reduces (23) such that when combined with (21) the expression for attenuation becomes identical to that calculated directly from the low frequency field equations, namely,

$$\alpha_{c\,LF} \cong \frac{R_s}{\left(\frac{\omega\mu}{k k_{eff}^{1/2}}\right)} \frac{1}{h} \frac{\frac{R_s}{Z_{opp}} \frac{\sin\theta}{w + d}}{}. \tag{24a}$$

Dielectric Losses

Power dissipated per section in dielectric is given by

$$D_\epsilon = (w + d)(\cot\theta + \tan\theta)h\omega\epsilon \tan\delta \int_{-d/2}^{d/2} |E_x|^2 dZ''$$

where $\tan\delta$ is the loss tangent of the dielectric and ϵ is the absolute dielectric constant. Upon integration, the dissipated power becomes

$$D_\epsilon = \omega\epsilon \tan\delta |A_\epsilon|^2 h(w + d)d(\cot\theta + \tan\theta) \cdot \left[1 + |\Gamma_\epsilon|^2 + 2\Gamma_\epsilon \frac{\sin k_{z\epsilon} d}{k_{z\epsilon} d}\right] \tag{25}$$

That portion of the attenuation resulting from dielectric losses is then

$$\alpha_\epsilon = \frac{1}{2} \frac{D_\epsilon}{P_T} \frac{\cos\theta}{W + d}. \tag{26}$$

The low frequency approximation for the attenuation resulting from dielectric losses is given by

$$\alpha_{\epsilon LF} = \frac{\omega\epsilon \tan\delta \frac{d}{w + d}}{2\left(\frac{k k_{eff}^{1/2}}{\omega\mu}\right)} = \frac{1}{2}\left(\frac{k_\epsilon}{k_{eff}^{1/2}}\right)\left(\frac{d}{w + d}\right) k \tan\delta. \tag{26a}$$

Application of Analysis to Coaxial Line with Helical Support

The phase constants, guide wavelength, and critical frequencies calculated for the equivalent parallel plate structure are assumed to be identical to those for the corresponding coaxial line, where, as initially indicated, the mean periphery of the coaxial line corresponds to the width of equivalent parallel plate. This same equivalence has been used to calculate the cutoff frequencies of coaxial line with good accuracy.[3]

To determine the attenuation of the coaxial line, the ratio of actual attenuation to that of the low frequency approximation is assumed to be the same for that of the coaxial line as for the equivalent parallel plate structure. Thus, for a coaxial line with helical dielectric support, attenuation resulting from conductor losses becomes

$$\alpha_{cc} = \frac{1}{2} \frac{\left(\frac{R_{si}}{\pi d} + \frac{R_{so}}{\pi D}\right)}{Z_o} \frac{\alpha_c}{\alpha_{cLF}} \tag{27}$$

[3] S. A. Schelkunoff, "Electromagnetic Waves," N. Y., D. Van Nostrand Co., Inc., 1951, p. 327, Fig. 8.51.

where Z_o is the characteristic impedance of the cable, R_{si} and d are respectively the surface resistivity and diameter of the inner conductor, R_{so} and D are respectively the surface resistivity and diameter of the outer conductor, α_{cLF} is the low frequency approximation for the parallel plate conductor attenuation obtained from (24a) and α_c is the actual value for the parallel plate conductor attenuation from (24). The attenuation resulting from dielectric losses is given by

$$\alpha_{\epsilon c} = \frac{k_\epsilon d}{w+d}\,\frac{Z_o}{Z_{oo}}\,\frac{\pi}{\lambda}\,\tan\delta\cdot\left(\frac{\alpha_\epsilon}{\alpha_{\epsilon LF}}\right) \tag{28}$$

where Z_o is the usual low frequency value of characteristic impedance of the cable, such as would be obtained from capacitance measurements, Z_{oo} is the characteristic impedance of the cable with dielectric removed, $\alpha_{\epsilon LF}$ is the low frequency approximation for the attenuation of the parallel plate which is due to dielectric losses as given in (26a) and α_ϵ is the actual attenuation of the parallel plate line caused by dielectric losses as given in (26). The total attenuation for the coaxial line is

$$\alpha_{Tc} = \alpha_{cc} + \alpha_{\epsilon c}. \tag{29}$$

The impedance of the cable and its possible variation with frequency requires further investigation.

Calculated Performance of ½ Inch 50 ohm Styroflex Line and Comparison with Measurements

Using the foregoing analysis, the propagation constants, some cutoff frequencies, and the attenuation in the dominant mode were calculated using the following dimensions for ½ inch Styroflex line:

Conductor	.165″
Helix-Width	.0985″
Helix-Lay	.564″
Helix-O.D.	.380″
Binder-Tape 3 Tapes	.907″ × .00473″
Binder-O.D.	.408″
Aluminum Sheath I.D.	.421″
Aluminum Sheath O.D.	.500″

The dimensions for the equivalent parallel plate line and other constant used were the following values:

$$h = \frac{.421 - .165}{2} = .128''$$

$$d = .0985''$$

$$\tan\theta = \frac{\pi(.421 + .165)}{2 \times .564} \quad (\theta = 32°)$$

$w = .564\cos\theta - .0985'' = .380''$
Polystyrene $k_\epsilon = 2.56$; $\tan\delta = .0002$
Surface Resistivity of Copper $= R_s = 2.61 \times 10^{-7}\sqrt{f}$
Surface Resistivity of Aluminum $= R_{sA} = 3.26 \times 10^{-7}\sqrt{f}$.

The effect of the binder tapes is neglected, the helix tape being assumed to extend to the outer conductor.

The critical frequencies calculated are tabulated as follows:

$n=0$	Condition	$n=1$	Condition
11.31 kmc/sec	(A)	20.44 kmc/sec	(C)
14.41 kmc/sec	(B)	23.56 kmc/sec	(D)
24.59 kmc/sec	(C)		

The chief band of interest is that between the frequencies zero and 11.31 kmc/sec. An attenuation band for propagation in the z direction exists between 11.31 and 14.41 kmc/sec with a second pass band appearing between 14.41 and 24.59 kmc/sec. The corresponding conditions of Table I are listed along with the frequencies. For $n=1$ in (17), and the conditions indicated in Table I, two other critical frequencies are calculated. An attenuation band exists between (C) and (D). From the above computations, there appears to be no higher mode interference in the chief band of interest.

TABLE II
Analysis of Operation
Dominant Mode

Frequency	$\frac{k_y}{k}$	$\frac{k_{zo}}{k}$	$\frac{k_{z\epsilon}}{k}$	$\left(\frac{\lambda}{\lambda_g}\right)$	Γ_o	Γ_ϵ	P_z	P_{yo}	$P_{y\epsilon}$	$\frac{f}{f_c}$
kmc/sec							%	%	%	
0	.610	.793	1.480	1.150	− .103	.206	71.9	22.3	5.8	0
6.28	.615	.789	1.478	1.160	− .154	.263	71.8	21.7	6.5	.55
8.24	.620	.784	1.476	1.169	− .219	.333	71.2	21.3	7.5	.729
9.90	.630	.777	1.472	1.189	− .363	.440	69.2	21.3	9.5	.875
10.48	.640	.768	1.468	1.207	− .480	.583	64.6	22.3	13.1	.927
11.03	.660	.751	1.459	1.244	− .698	.869	42.7	23.8	33.5	.975
11.31	.685	.728	1.447	1.292	−1.0	1.0	0	44.6	55.4	1.0

Shown in Table II above, for the parallel plate equivalent corresponding to ½ inch Styroflex, are values of phase constants divided by the free space phase constant; the square of the ratio of free space wavelength divided by the guide wavelength, $(\lambda/\lambda_g)^2$; the reflection coefficients associated with propagation in the z direction; and the percentages of power in given directions in air and dielectric all tabulated as a function of fre-

quency. As indicated in the relative frequency scale of the table, significant changes in the data are confined to the frequencies beyond $\frac{1}{2}$ the critical frequency for dominant mode operation. This is for the most part beyond the range at present considered for commerical use of the cable.

The over-all change in (k_y/k) is $+12.4$ per cent, that for (k_{zo}/k) is -8.2 per cent and that for $(k_{z\epsilon}/k)$ is -2.3 per cent. These changes in themselves are nominal and do not reflect the strong changes in the direction of power flow which takes place as the critical frequency is approached. The quantity, (λ/λ_g), shows that the guide wavelength decreases with frequency at a greater rate than the free space wavelength. For the low frequency approximation (λ/λ_g) is equivalent to the square root of the relative dielectric constant. Continuing this concept, it would be expected that there is a factor which reduces the characteristic impedance by the percentage change in the values of (λ/λ_g) over its zero frequency value. Further investigation is required before a useful value of impedance can be proposed since the influence of changes in field pattern has not as yet been considered.

The values of reflection coefficient Γ_o and Γ_ϵ are noted to have finite values at zero frequency. The electric field is uniform at low frequencies primarily because there is insufficient phase variation for the reflection coefficients to exert their effect. At the critical frequency, however, the variation acts like a complete standing wave in the z direction. This variation is depicted in Fig. 7 where the relative magnitude of electric field is

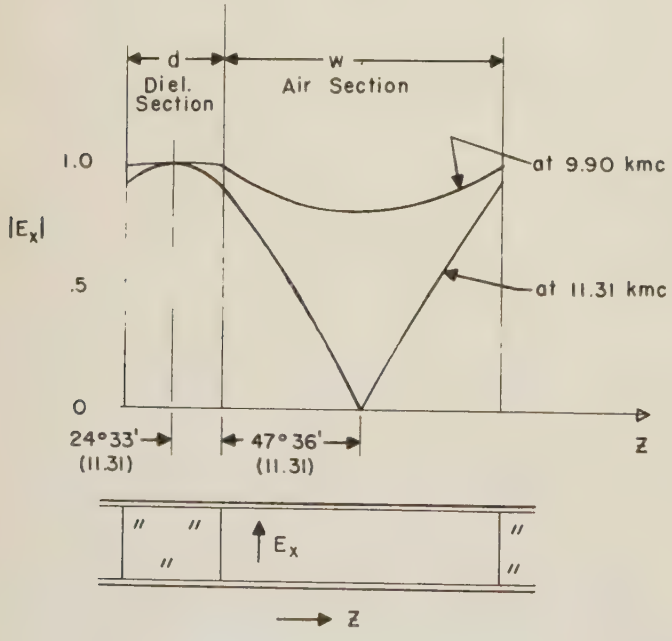

Fig. 7—Variation of electric field in cross section.

plotted as a function of distance in the z direction for 11.31 kmc/sec. This variation has a discontinuous derivative at the interface between air and dielectric as noted from the indicated angles. The variation would be of identical character in the transverse cross section of the line. In the coaxial line with helical support the corresponding cross sectional field pattern would have one zero and one maximum in the variation with angle. The distribution for lower frequencies lacks the zero value but has minimum and maximum fields at the same locations as illustrated in Fig. 7 by a plot of the relative field variation at 9.9 kmc/sec.

The power crossing any given cross section can be arbitrarily broken up into the power in the z direction, P_z; the power in the y direction in the air section, P_{yo}; and the power in the y direction in the dielectric section, $P_{y\epsilon}$; as indicated in Fig. 5. The proportioning for the low frequency approximation, indicated as zero frequency in Table II, could be arrived at using a TEM mode and simple geometry. The power in the z direction (perpendicular to the dielectric) is the largest proportion because the dielectric makes an angle of 32 degrees with the transverse direction. The total power in the y direction divides in proportion to the widths of the sections. The major change up to about 10.0 kmc/sec is the gain of power in the dielectric section, a familiar effect for microwave transmission lines. Further increase in frequency causes the propagation in the y direction to mount rapidly being entirely in the y direction at the critical frequency. At these higher frequencies, the efficiency could be expected to be seriously impaired because of the distorted mode and length of path of transmission.

Using the foregoing analysis, the attenuation values were calculated for $\frac{1}{2}$ inch Styroflex cable for all frequencies up to 11.31 kmc/sec, first critical frequency.

For the equivalent parallel plate line, the analysis gives exactly the ratio of the actual attenuation to the attenuation calculated using the low frequency approximation. Table III lists separately these ratios for the attenuation caused by conductor loss and that caused by dielectric loss. These factors are assumed to apply as correction factors to the attenuation of the coaxial structure calculated by the use of the low frequency approximation. These coaxial attenuation values are also listed in Table III for a dielectric loss

TABLE III

Attenuation Data for $\frac{1}{2}$ Inch O.D. Styroflex Cable

Freq. in kmc	Correction Factor Parallel Peak		Coax Line Low Freq. Approx.	
	$\frac{\alpha_c}{\alpha_{cLF}}$	$\frac{\alpha_\epsilon}{\alpha_{\epsilon LF}}$	α_{ccLF}	$\frac{\alpha_{\epsilon LF}}{\tan\delta=.0003}$
0	1	1	0	0
2	1.003	1.011	3.517	.7632
4	1.008	1.035	4.974	1.526
6.28	1.028	1.112	6.23	2.396
8.24	1.06	1.31	7.14	3.144
9.9	1.232	1.576	7.829	3.778
10.48	1.413	2.153	8.05	3.999
11.03	1.915	5.329	8.259	4.209
11.31	4.069	6.849	8.364	4.316

tangent of 0.0003. The curves for the corrected values of coaxial attenuation are shown plotted separately in Fig. 8 for the conductor and dielectric loss. The attenuation caused by conductor loss is noted to predominate virtually over the entire frequency band in spite of the fact that there is a more marked correction factor for the attenuation caused by dielectric loss.

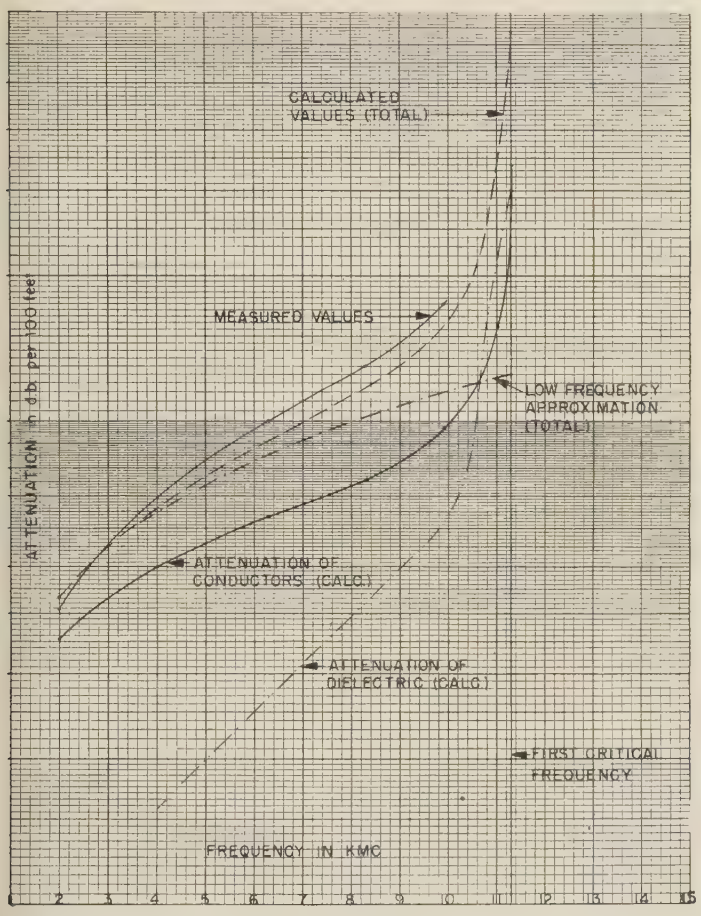

Fig. 8—Attenuation vs frequency, $\frac{1}{2}$ inch O.D. 50 ohm Styroflex cable. Loss Tangent = 0.0003.

The total calculated attenuation is plotted in Fig. 8 along with curves for measured values[4] and the total attenuation obtained from the use of the low frequency approximation. In particular, the attenuation values for the low frequency attenuation do not contain the rise toward peak values as the critrical frequency is approached, whereas the measured values and the values calculated from the foregoing analysis do show this rise; use of the logarithmic scale for attenuation should be noted. From the curve it is evident that the application of the correction factors of Table III appears to be warranted for frequencies above 4.0 kmc/sec. At 9.9 kmc/sec, the attenuation value for the low frequency approximation is 30 per cent below that of the more complete analysis. The agreement between measured values and those of the analysis are dependent on the value used for the loss tangent of the dielectric. A loss tangent value of 0.0003 which is representative of polystyrene at these frequencies was chosen for the calculated curve of attenuation for Fig. 8. At 9.9 kmc/sec, the measured value is 7.4 per cent above the calculated value. In view of the overlap of calculated and measured values at 2.5 kmc/sec, a lower value of loss tangent is perhaps appropriate for the lower frequencies. The measured values can be expected to exceed the calculated values because the measured surface resistance values of the metal are known to exceed theoretical values, particularly for frequencies approaching 10.0 kmc/sec. This effect would be emphasized by the existence of transverse components of surface currents which the analysis indicates. Further detailed investigation would be necessary to warrant closer detailed examination of the agreement between the theoretical and experimental results.

[4] Measured at Signal Corps Engineering Laboratories.

Comments

An equivalent parallel plate structure has been used to analyze the frequency limitations and performance characteristics of a coaxial line with a helical dielectric support. The key to equivalence of the parallel plate and coaxial structure is the imposed boundary condition that, at any given transverse cross section for the parallel plate, the fields at the sides are identical in magnitude and phase angle. An analysis in terms of component transmission lines, one parallel to the dielectric and the other perpendicular to the dielectric, may then be used to determine the detailed fields and their variation with frequency. The performance of the overall transmission line reflects the iterative line characteristics of the component transmission line perpendicular to the dielectric, and gives rise to pass bands and high attenuation bands for the over-all transmission line.

For $\frac{1}{2}$ inch Styroflex transmission line, analysis based on the low frequency approximation, which assumes cross sectional fields independent of angle and an equivalent dielectric constant corresponding to the air and dielectric sections in parallel, is accurate up to about 4.0 kmc/sec or about 35 per cent of the cutoff frequency. Above this frequency, the analysis indicates that the power component in the dielectric directed parallel to the dielectric grows at the expense of the power component directed perpendicular to the helix while the power component in the air directed parallel to the helix remains, for the most part, reasonably constant. The increase of the field in the dielectric corresponds with a reduction in the guide wavelength and would imply a reduction in the characteristic impedance of the line. Similar behavior would be expected for other coaxial lines with a helical dielectric support, but the details of operation would be dependent on the proportion of dielectric and the pitch angle.

In the analysis, the line has been assumed smooth in the direction parallel to the helix. Precise construction of the line would be necessary to maintain this condition since it is evident that eccentricity would give rise to a line with periodicities in this direction.

Improved Microwave Noise Measurements Using Ferrites*

C. H. MAYER†

Summary—The ferrite isolator and the ferrite circulator have been applied separately to improve the accuracy of measuring small microwave noise powers or small power differences. Either the isolator or the circulator effectively isolated the input circuit of a microwave receiver from the impedance of the source. As a result, the measurement errors introduced by mismatched source impedances were reduced by as much as 98 per cent. The added input circuit losses of the ferrite components reduced the receiver sensitivity by only about 10 per cent. Since the accuracy of measuring small noise power differences was limited principally by impedance errors, the addition of ferrite isolation to the receiver input circuit increased the sensitivity of measurement to near the theoretical limit.

The ferrite isolator was used as a passive transmission element in these experiments. The ferrite circulator, however, was used as an electrically-operated, microwave switch. This switch was used to replace the mechanical chopper in a Dicke-type radiometer. In addition to impedance isolation, the ferrite switch makes possible rapid comparison measurements of the microwave noise powers from any two sources, or of the noise powers from the same source in two different polarizations.

Introduction

THE MEASUREMENT of microwave noise powers is complicated by the similar characteristics of the signal power and the noise power generated in the measuring apparatus. When the signal power is small compared with the apparatus noise level, a measurement must be made of a small change in the total output noise power. The limiting sensitivity of a simple microwave receiver is generally determined by variations in the gain and noise factor of the receiver. The effects of receiver instabilities can be greatly reduced by adding the rapid comparison technique described by Dicke[1] to the simple receiver. The resulting apparatus is referred to as a microwave radiometer. In this system, the noise power output of the receiver is modulated by periodically substituting a second noise source for the source being measured. The modulation amplitude is a measure of the difference between the noise powers from the two sources. When the second noise source is a known standard, the noise power from the unknown source is measured relative to an absolute power level. With the microwave radiometer, the sensitivity of measurement approaches the theoretical limit set by the statistical nature of the receiver noise power. This limit can be controlled by adjusting the instrumental constants of the radiometer; in practice, noise power differences of the order of 0.1 per cent of the noise level of the apparatus should be detected with a one-second response time. For a typical microwave radiometer the minimum detectable power is about 10^{-16} watts.

With this high sensitivity, the measurement inaccuracies resulting from small changes in the radio-frequency impedance presented to the receiver input circuit become most important. The input impedance and consequently the noise power output of a microwave receiver are dependent on the radio-frequency source impedance. In the comparison radiometer, a changing impedance is presented to the receiver as the input is switched between the antenna, or other source of microwave noise power, and the comparison standard noise source. This change in impedance is synchronous with the desired modulation of the receiver noise level which corresponds to the difference between the power level of the source and the power level of the comparison standard. Since the desired and the undesired modulations pass through the receiver circuits together, the output reading of the radiometer is in error by an amount dependent on the radio-frequency impedance connected to the radiometer input, and on the coupling between the radio-frequency and intermediate-frequency circuits. When a superheterodyne receiver without image frequency rejection is used in the radiometer, the error in the radiometer output depends also on the length of the radio-frequency transmission line because of interference effects between the sum and difference frequency bands. Experimental observations indicate that when the receiver input circuit is a simple microwave converter, a source impedance mismatch corresponding to a voltage standing-wave ratio of 1.2 can cause errors in the output reading of a radiometer which are of the order of 100 times the minimum power which is detectable in the absence of reflection effects. These impedance errors place a serious limitation on the accuracy of measuring small microwave noise powers because of the difficulty of impedance matching antennas and other microwave components over the broad frequency bands used in microwave radiometry. Corrections for impedance error are uncertain and time consuming because of the complex dependence of the receiver response on frequency, input impedance, and line length. It is, therefore, desirable to isolate the receiver from the source impedance if this can be done with little sacrifice in receiver sensitivity. A balanced converter circuit can be made to minimize the interaction between the radio-frequency source impedance

* This paper was presented in part at the Joint Meeting of URSI and IRE, Ottawa, Canada, October 5, 1953; at the Washington Conference on Radio Astronomy, Washington, D. C., January 6, 1954; summary published in *J. Geophys. Res.*, vol. 59, pp. 188–191; March, 1954.

† U. S. Naval Res. Lab., Washington, D. C.

[1] R. H. Dicke, "The measurement of thermal radiation at microwave frequencies," *Rev. Sci. Instr.*, vol. 17, pp. 268–275; July, 1946.

and the intermediate-frequency circuit.[1,2] However, it has been found difficult to balance and maintain the critical factors in the converter circuit so that the impedance-induced output variations are consistently less than 10 or 20 times minimum detectable power.

Ferrite waveguide components with nonreciprocal transmission characteristics and small absorption losses provide a means of isolating the radiometer from the source impedance which does not depend on critical mixer characteristics. The applications of the ferrite isolater and the ferrite circulator[3] to the problem of receiver isolation were investigated experimentally. The results described in the following paragraphs indicate that either of these ferrite components can be used effectively to reduce the measurement errors caused by mismatched radio-frequency source impedances. In this application, the ferrite circulator was used as an electrically-controlled microwave switch and was substituted for the mechanical modulator in the radiometer referred to earlier. When used in this way the ferrite switch gives the added advantage of electrical switching and makes possible a wider variety of measurements with the radiometer.

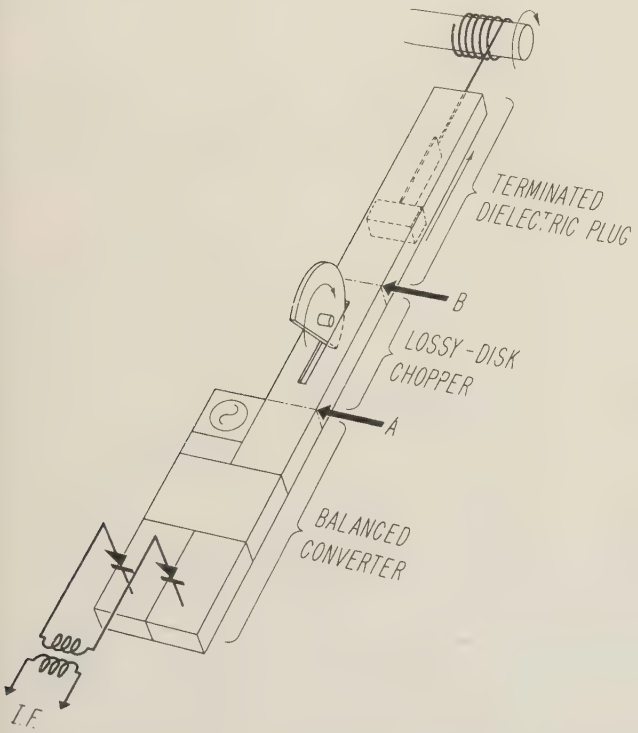

Fig. 1—The apparatus used to observe the effect of a mismatched source impedance on the noise power output of a microwave receiver at 3.15 cm wavelength. The dielectric plug was drawn through the input waveguide at a constant rate to simulate a source impedance with a variable line length.

Observation of Impedance Dependence

The apparatus shown in Fig. 1 was used to observe the effect of a mismatched source impedance on the noise power output of a microwave radiometer operating at a wavelength of 3.15 cm. The comparison radiometer system was preferred over a simple microwave receiver because of better stability in observations of receiver output variations corresponding to small power levels. The frequency response of the receiver was limited mainly by the bandpass of the intermediate-frequency amplifier; therefore, both the sum and difference bands of radio frequencies were converted to the intermediate frequency. The relative path lengths to the two crystals in the balanced mixer were adjusted for maximum coupling between the input impedance and the output noise power[1,2] so that the effect of a small impedance mismatch could be observed. A single crystal mixer was not used because of the added complexity of interpreting the data with greater leakage of local oscillator power into the antenna line. The receiver noise factor was about 13 db, the bandpass of the intermediate-frequency amplifier was 5.5 mc centered at 30 mc, and the output time constant was one-half second. A microwave noise source with constant power output and fixed radio-frequency reflection was approximated by fitting a resistively terminated dielectric plug into waveguide. The plug was drawn at a uniform rate through a long waveguide transmission line connected to the receiver input in order to change the impedance presented to the mixer in a systematic manner. The output of the radiometer was recorded with an Esterline-Angus graphic meter. The recorded output is not strictly proportional to power, however, the deviation from proportionality is small over the range of the measurements and has been neglected for simplicity of discussion.

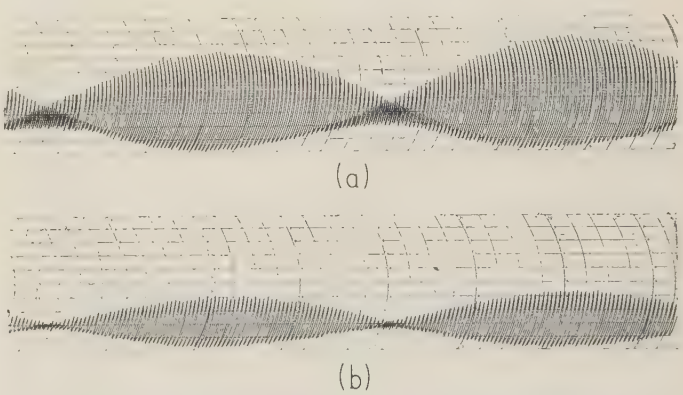

Fig. 2—Records of the variation in the noise power output of the receiver as a mismatched impedance was moved through a length of input waveguide of about 12 feet. The right-hand side of the records corresponds to the position of the impedance nearest to the receiver input circuit. (a) vswr of impedance 2.33; (b) vswr of impedance 1.50.

Fig. 2 shows recordings of the variation in the output of the radiometer when plugs with voltage-standing-wave-ratios of 2.33 [Fig. 2(a)] and 1.5 [Fig. 2(b)] were drawn through the waveguide. The short period of the variation corresponds to a change in the length of the input transmission line approximately equal to one-half of a local oscillator wavelength in waveguide. The long period envelope of the variation results from the re-

[2] R. V. Pound, "Microwave Mixers," McGraw-Hill Book Co., Inc., New York, N. Y., pp. 276–279; 1948.

[3] C. L. Hogan, "The ferromagnetic Faraday effect at microwave frequencies and its applications—the microwave gyrator," *Bell Sys. Tech. Jour.*, vol. 31 pp. 1–31: January, 1952.

sponse of the superheterodyne receiver to both the sum and the difference bands of radio frequencies which are separated by twice the intermediate frequency. This period corresponds to a length of input transmission line which is one-half wavelength longer for the signal than for the image, in this case about six feet. The recordings shown in Fig. 2 demonstrate qualitatively the dependence of the noise power output of the radiometer on the magnitude and phase of the source impedance, and on the length of transmission line separating the source impedance from the receiver input. A change in input noise power of 6×10^{-14} watts would be required to change the radiometer output by the amount of the peak variation shown in Fig. 2(a). The amplitude of the output variations shown in Fig. 2 would have been reduced by approximately 75 per cent by proper adjustment of the path lengths to the two crystals in the balanced mixer. The general reduction in the magnitude of the variation from right to left is due to waveguide attenuation.

Application of the Ferrite Isolator

The ferrite isolator[3] is a waveguide transmission-line component with greater attenuation for one direction of propagation than for the reverse direction. At centimeter wavelengths it is practical to make isolators with less than 0.5 db attenuation for one direction of propagation, and more than 30 db for the reverse direction. When the isolator is included in the input transmission line of a receiver, the reduction in the dependence of the receiver output noise power on a mismatched source impedance is comparable to one-half the difference between the reverse and the forward attenuations of the isolator, where all of factors are expressed in decibels.

A commercially built isolator (Uniline) of the ferrite rotator type was used for the experimental tests. At the wavelength of 3.15 cm the forward attenuation of the isolator was 0.5 db and the reverse attenuation was 20 db. Fig. 3(a) shows the recorded variation in the output of the radiometer as the plug with a voltage-standing-wave-ratio of 2.33 was drawn through the input waveguide. Fig. 3(b) shows the result of inserting the isolator in the transmission line at point A in Fig. 1 and repeating the test procedure. The variations in the noise power output of the radiometer caused by the mismatched impedance are reduced about 90 per cent. The reduction in the signal response by the forward attenuation of the isolator is indicated by the change in the measured level of the heated thermal-noise source when the isolator was inserted in the transmission line. The indication is not exact because of the impedance error when the isolator was out of the circuit. The isolator used was designed to operate over a band centered at 3.26 cm. Because of greater reverse attenuation at the band center, the reduction in the receiver output variations would have been about 96 per cent if the test had been made at this wavelength.

The isolation of the receiver from the source impedance can be increased by building an isolator with a higher ratio of reverse attenuation to forward attenuation, or by connecting several isolators in cascade. The deterioration of receiver sensitivity can be lessened by building an isolator with a forward attenuation which is smaller than 0.5 db loss of isolator used here. According to reported loss values for recently developed ferrite materials, it should be possible to construct isolators with transmission losses of less than 0.25 db.

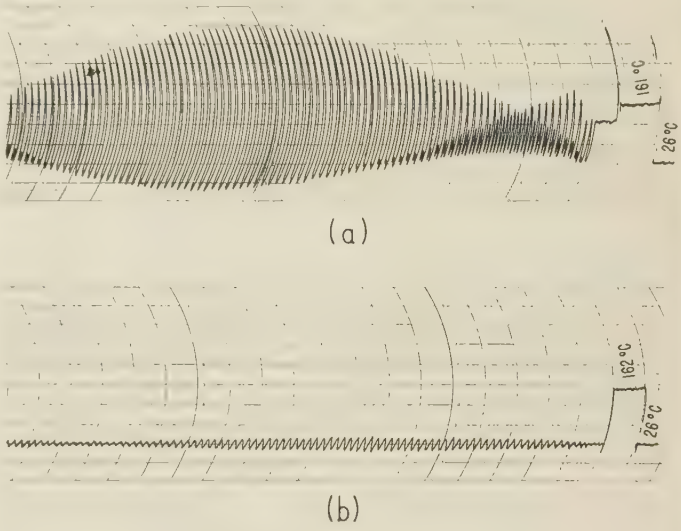

Fig. 3—The effect of inserting a ferrite isolator with attenuations of 0.5 db (forward) and 20 db (reverse) in the receiver input transmission line. The records show the variation in the noise power output of the receiver as the mismatched impedance with a vswr of 2.33 was moved through a length of input waveguide of about 6 feet. (a) Input circuit without ferrite isolator; (b) input circuit with ferrite isolator.

Application of the Ferrite Circulator

The ferrite circulator[3] is a four-terminal microwave network with nonreciprocal transmission characteristics. A circulator was assembled from laboratory components and a 90 degree ferrite rotator as shown in Fig. 4. The transmission properties are such that, for one direction of axial magnetization of the ferrite, power is transmitted from terminals 1 to 2, 2 to 3, 3 to 4, and 4 to 1 with small attenuation, while power transmitted in the opposite directions is highly attenuated. When the direction of the magnetic field applied to the ferrite rotator is reversed, the paths with low attenuation and the paths with high attenuation are interchanged. In this way, a microwave receiver connected to terminal 2 can be switched between a source of power connected to terminal 1 and a second source of power connected to terminal 3 by alternating the direction of the magnetic field applied to the ferrite rotator. To switch the circulator, an alternating magnetic field was applied to the ferrite by exciting a solenoid wound around the waveguide with an audio-frequency, square-wave current. This ferrite switch was used to replace the rotating lossy-disk chopper which dips into the input waveguide 30 times a second to act as both the comparison switch and the standard comparison noise source in the radiometer diagrammed in Fig. 1.

The nonreciprocal transmission properties of the ferrite switch provide good isolation of the receiver from the source impedance. In this application, the apparent isolation of the receiver is greater than would be indicated by the forward-to-reverse attenuation ratio of the switch. Because the circuit is symmetrical, the impedances presented to the receiver over the two halves of the switching cycle are nearly the same, even though the impedances of the two sources differ. The ferrite switch used for the experimental tests had attenuations of 0.4 db and 25 db for the two directions of propagation over the radio-frequency band of the receiver. In order to make a direct comparison between the characteristics of the radiometer when either the ferrite switch or the lossy-disk chopper were used, the solenoid around the ferrite was excited at 30 cycles per second to correspond to the modulation frequency of the mechanical chopper. The receiver was connected to terminal 2 of the ferrite switch, the input transmission line to terminal 1, and a resistive termination at room temperature, corresponding to the lossy chopper disk, was connected to terminal 3. A matched termination was connected to terminal 4, the unused terminal.

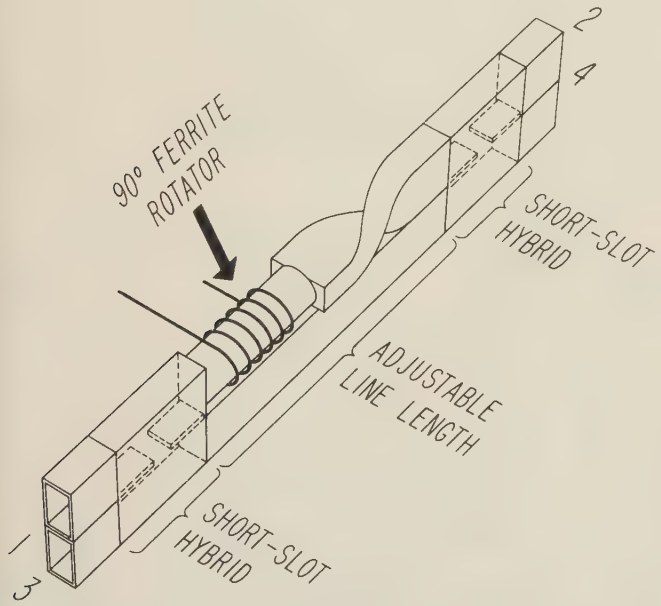

Fig. 4—The ferrite circulator used as a microwave switch in the radiometer. The polarization of the wave in the circular waveguide section was rotated from 90 degrees clockwise to 90 degrees counterclockwise 30 times a second by alternating the magnetic field applied to the ferrite. The periodic 180 degree phase shift introduced in one branch of the hybrid circuit made it possible to realize the advantages of rapid electrical switching along with the advantage of nonreciprocal transmission.

Fig. 5(a) shows the variation in the output of the radiometer with the lossy-disk chopper as the plug with a voltage-standing-wave-ratio of 2.33 was drawn through the input transmission line. Fig. 5(b) shows the variation in the output of the same radiometer when the ferrite switch was substituted for the lossy-disk chopper and the plug was again drawn through the input waveguide. When the ferrite switch was used, the magnitude of the variation in the output noise power of the receiver was about two per cent of the magnitude of the variations when the lossy-disk chopper was used. The reduction of signal response caused by the 0.4 db transmission loss of the ferrite switch is indicated by the response of the radiometer to the power from the heated thermal noise source. It is probable that a ferrite switch could be constructed to give performance which is superior to that of the experimental model used for these tests.

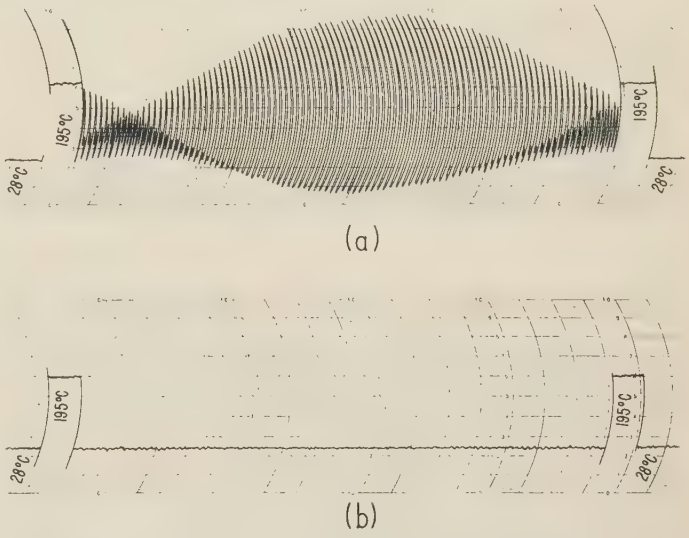

Fig. 5—The effect of substituting the ferrite switch for the mechanical chopper between the points marked *A* and *B* in Fig. 1. The records show the variation in the noise power output of the receiver as the mismatched impedance with a vswr of 2.33 was moved through a length of input waveguide of about 6 feet. (a) With the mechanical chopper in the input circuit; (b) with the ferrite switch substituted for the mechanical chopper.

The ferrite switch has several desirable characteristics in addition to impedance isolation when used as the comparison switch in a microwave radiometer. Since the switching is accomplished electrically rather than mechanically, the problems associated with mechanical vibrations of the crystal mixers, the local oscillator, and the amplifiers are reduced. The rate of switching can be increased to high audio frequencies to allow more rapid comparisons and a reduction of the lower limit on radiometer response time. Another desirable feature is that any two sources of microwave noise power can be connected to the ferrite switch and compared directly. For example, the receiver input can be switched between the outputs of two antennas at an audio-frequency rate to compare the radiations received from two directions in space or the radiations received in two different polarizations. If desired, a second receiver can be connected to the unused terminal of the switch for parallel operation with the first receiver.

Conclusions

The limitation to the accurate measurement of small microwave noise powers is imposed by the dependence of the receiver output noise power on the radio-fre-

quency source impedance. This limit was effectively reduced by the use of ferrite waveguide components in the radiometer input circuit. A reduction of 98 per cent in the effect of a mismatched radio-frequency source impedance was easily obtained and greater reductions are possible. The input circuit losses introduced by the ferrite components caused a degradation in receiver noise factor of about 10 per cent with a corresponding increase in the minimum detectable power of the system. The use of either a ferrite isolator or a ferrite circulator in the radiometer input circuit will allow accurate measurements of small powers even when some of the critical requirements on the design of the input circuit and antenna are relaxed. In addition, the use of the ferrite circulator as the radiometer comparison switch makes possible a wider variety of direct comparison measurements of microwave noise powers.

Acknowledgment

The author wishes to thank Mr. F. T. Haddock and Drs. W. R. Ferris and J. P. Hagen for many helpful suggestions.

The Characteristic Impedance of the Shielded Slab Line

R. H. T. BATES†

Summary—**The characteristic impedance of the shielded slab line is worked out exactly in terms of elliptic functions. A design graph is given to cover most practical applications.**

List of Symbols

THE NOTATION used for the elliptic functions follows E. T. Copson [1].

z, p, q, s, u, v	Independent complex variables.
a, b, d, t, w	Variable parameters.
$\wp(z)$	Weierstrasse's second order elliptic function.
sn z, cn, z, dn z	Jacobian elliptic functions.
k	Modulus of the elliptic functions.
K	Real quarter period of sn z.
jK'	Imaginary half period of sn z.
$\Theta(z)$	Jacobian theta function.
$Z(z)$	Jacobian zeta function.
ϵ_r	Relative permittivity of medium between shielding plates.

Introduction

The shielded slab transmission line has several advantages over the coaxial line, especially when it is used as a slotted-line standing wave indicator for wavelengths greater than one foot. The mechanical tolerances are less stringent for a given reading accuracy. A good account of the advantages and disadvantages of this type of standing wave indicator is given by Wholey and Eldred [2], who give design curves for a circular inner conductor.

In a recent paper Cohn [3] has given values of the characteristic impedance of the slab line, calculated from approximate formulas, for t/b less than 0.25, see Fig. 1. However, it is possible to solve the problem exactly, using elliptic functions. As these functions have been comprehensively tabulated, the labor involved in producing the design graphs is probably less than that necessary for evaluating the approximate expressions. Also, the exact formulas allow one to design lines having values of t/b up to unity.

This paper describes the conformal transformations whereby the characteristic impedance of the slab line is determined. The results are shown on a chart, with $\sqrt{\epsilon_r}Zo$ as parameter.

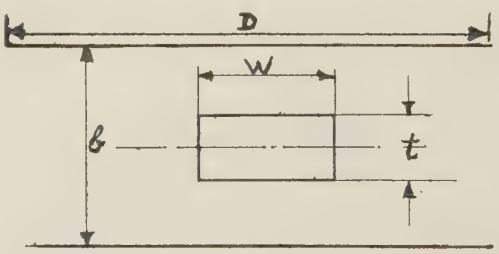

Fig. 1—Geometry of shielded slab line.

Effect of Finite Width of Shielding Plates

The characteristic impedance of the slab line from now on will be referred to as Zo.

In the calculation of Zo, the width, D, of the shielding plates is assumed infinite; see Fig. 1. In practice D does not have to be excessively large for this assumption to be valid. There is a convenient method of judging the effect of the finite value of D. The infinite plates are transformed into a cylinder. Then the angular width, θ radians, of the slot in the cylinder due to the finite width of the shielding plates is given by,

$$\theta = 4 \operatorname{cosech} \frac{\pi D}{b}$$

In Fig. 2, θ in degrees is plotted against D/b. It is that the effect of a finite D can easily be made negligible.

† Decca Radar Ltd., Tolworth, Surrey, Eng.

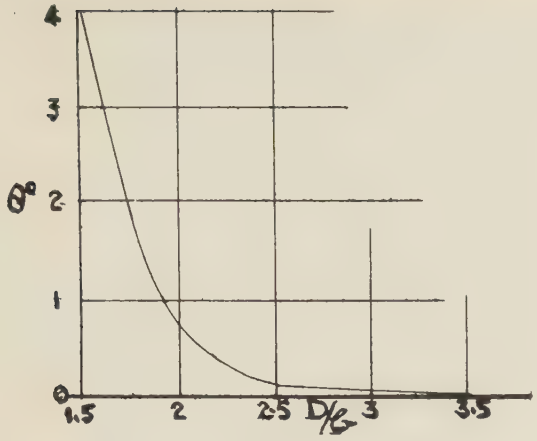

Fig. 2—Angular width of slot in equivalent circular cylinder.

Determination of Z_o

It is convenient to bisect the slab line along that axis of symmetry parallel to the shielding plates. Fig. 3 shows the transformations necessary to change the bisected system into two infinitesimally thin coplanar sheets, one finite and one infinite.

Fig. 4 shows how a system of two coaxial cylinders can be transformed into a parallel plate line [4], exactly equivalent to the one shown in the s plane in Fig. 3. The details of the transformation are shown in Fig. 4. The numerical evaluation is simple for,

$$\frac{\omega_1}{\omega_3} = \frac{K}{jK'}$$

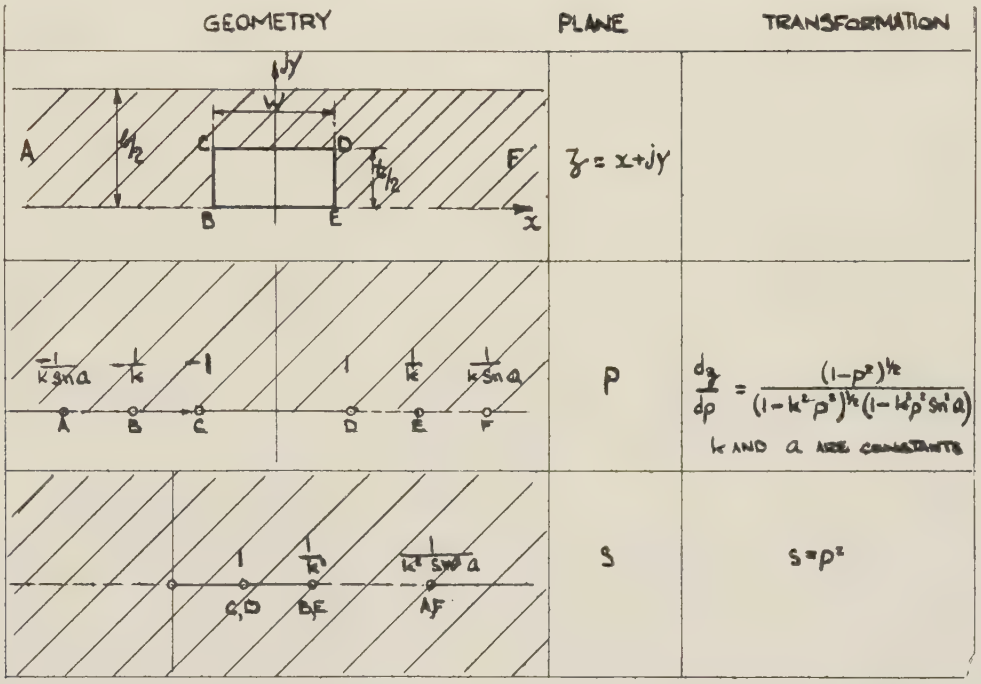

Fig. 3—Full lines represent constant potential boundaries; *i.e.*, conductors. Dotted lines represent streamlines of electric force. Hatching represents the region originally within the slab line after it has been transformed from plane to plane.

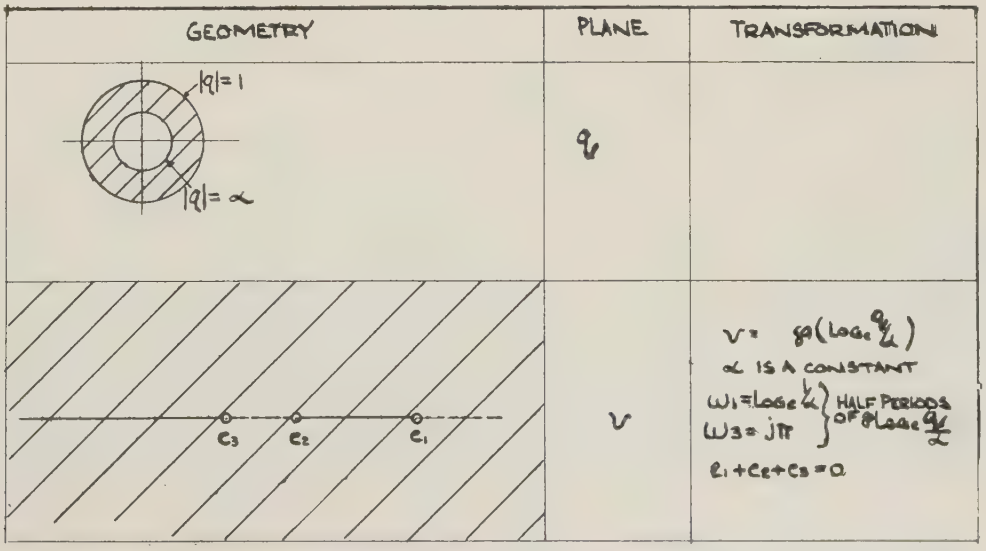

Fig. 4—Transformation of coaxial line into parallel plate line.

and $\omega_1 = \log_e (1/\alpha) = (1/60) \times$characteristic impedance of coaxial cylinders. K and jK' are complete elliptic integrals of the first kind as well as the real quarter period and imaginary half period of sn (z, k).

Only half the original system has been considered, so the characteristic impedance of the coaxial cylinders will be $2Zo$. Fig. 5 (opposite) is a plot of Zo vs $(e_2 - e_3)/(e_1 - e_3)$. With reference to Fig. 3 it is clear that

$$\frac{e_2 - e_3}{e_1 - e_3} = \mathrm{cn}^2\, a \tag{1}$$

The main part of the problem is the solving of the integral equation derived from the Schwarz-Christoffel transformation from z plane to the p plane, Fig. 3.

$$\int_0^z dz = \int_0^p \frac{(1 - p^2)^{1/2} dp}{(1 - k^2p^2)^{1/2}(1 - k^2p^2\mathrm{sn}^2\, a)} + M$$

where a and M are constants for one set of values of W, t, and b.

Make the substitution,

$$p = \mathrm{sn}\, u \tag{2}$$

Then,

$$z = \int_0^u \frac{(1 - \mathrm{sn}^2\, u) du}{1 - k^2\mathrm{sn}^2\, u\, \mathrm{sn}^2\, a} + M.$$

Refer to the chapter on Jacobian elliptic functions [1]. Transform the above integral into two Legendre elliptic integrals of the first and third kinds respectively. After a little manipulation the above equation reduces to,

$$z = u\left[1 - \frac{\mathrm{dn}\, a\, Z(a)}{k^2\, \mathrm{sn}\, a\, \mathrm{cn}\, a}\right] - \frac{\mathrm{dn}\, a}{2k^2\, \mathrm{sn}\, a\, \mathrm{cn}\, a} \cdot \log_e\left[\frac{\Theta(u - a)}{\Theta(u + a)}\right] + M. \tag{3}$$

Now sn a is always less than unity, so a is real. Since $\Theta(z)$ is an even function of z,

$$\frac{\Theta(-a)}{\Theta(a)} = 1.$$

So $z = M$ when $u = 0$. By inspection of Fig. 3 it can be seen that,

$$z = j\frac{t}{2} \quad \text{when} \quad p = 0.$$

From (2), $u = 0$ when $p = 0$. So,

$$M = j\frac{t}{2} \tag{4}$$

Also, $z = W/2$ when $p = 1/k$, $u = K + jK'$. Substituting into (3), using (4), and separating real and imaginary parts,

$$W = 2K\left[1 - \frac{\mathrm{dn}\, a(Z)a}{k^2\, \mathrm{sn}\, a\, \mathrm{cn}\, a}\right] \tag{5}$$

$$t = \frac{\pi\, \mathrm{dn}\, a}{k^2\, \mathrm{sn}\, a\, \mathrm{cn}\, a} \cdot \frac{a}{K} - 2K'\left[1 - \frac{\mathrm{dn}\, aZ(a)}{k^2\, \mathrm{sn}\, a\, \mathrm{cn}\, a}\right] \tag{6}$$

since,

$$\frac{\Theta(K + jK - a)}{\Theta(K + jK + a)} = e^{j\pi a/k}.$$

The constant b is found very simply by integrating along a small semi-circle in the upper half of the p plane about the point $1/k$ sn a, and equating the result to the equivalent change in the z plane. Since the residue at $p = 1/k$ sn a is

$$\frac{\mathrm{dn}\, a}{2k^2\, \mathrm{sn}\, a\, \mathrm{cn}\, a}$$

then,

$$b = \frac{\pi\, \mathrm{dn}\, a}{k^2\, \mathrm{sn}\, a\, \mathrm{cn}\, a}. \tag{7}$$

Numerical Evaluation of Zo

From (5), (6), and (7), the following normalized expressions can be formed,

$$\frac{W}{b} = \frac{2K}{\pi}\left[\frac{k^2\, \mathrm{sn}\, a\, \mathrm{cn}\, a}{\mathrm{dn}\, a} - Z(a)\right] \tag{8}$$

$$\frac{t}{b} = \frac{a}{K} - \frac{2K'}{\pi}\left[\frac{k^2\, \mathrm{sn}\, a\, \mathrm{cn}\, a}{\mathrm{dn}\, a} - Z(a)\right]. \tag{9}$$

The most convenient way of evaluating these formulas was found to be the following,

a) Take a given value of Zo.
b) From Fig. 5, see (1), find the corresponding value of cn a.
c) Substitute this value of cn a into (8) and (9) and calculate W/b and t/b for several values of k.

Sufficient tables for the calculations were found in Milne-Thomson [5, 6] and Jahnke and Emde. [7]

Fig. 6, on page 32, is a plot of the results of the calculations. $\sqrt{\epsilon_r}Zo$ is the parameter. The graph should cover the design of the majority of slab lines.

Conclusions

The tables of elliptic functions available to the author were not suitable for calculating values of $\sqrt{\epsilon_r}Zo$ less than about 30Ω and greater than about 200Ω. However, approximate formulas can give accurate answers for values of $\sqrt{\epsilon_r}Zo$ less than about 30Ω. The approximate formulas used by the author were similar to those used by Cohn and have therefore not been described.

The results given by Cohn [3] agree well with those of this paper, which shows that approximate expressions give good answers for small values of t/b. It appears, however, that the exact formulas, (8) and (9), are needed for calculating $\sqrt{\epsilon_r}Zo$ for values of t/b greater than about 0.25 and for values of w/b less than about 0 1.

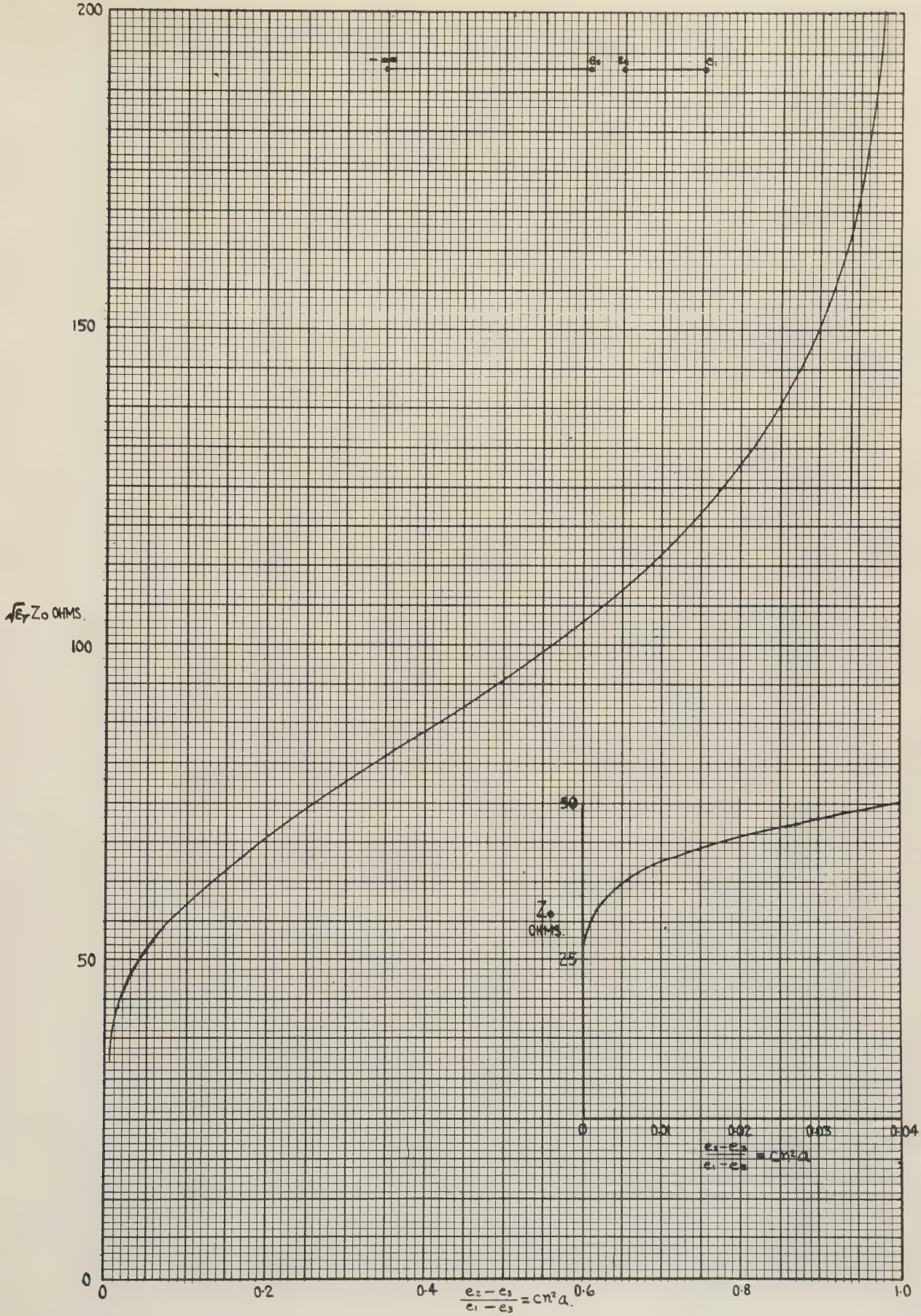

Fig. 5—*Zo* versus $cn^2\ a$.

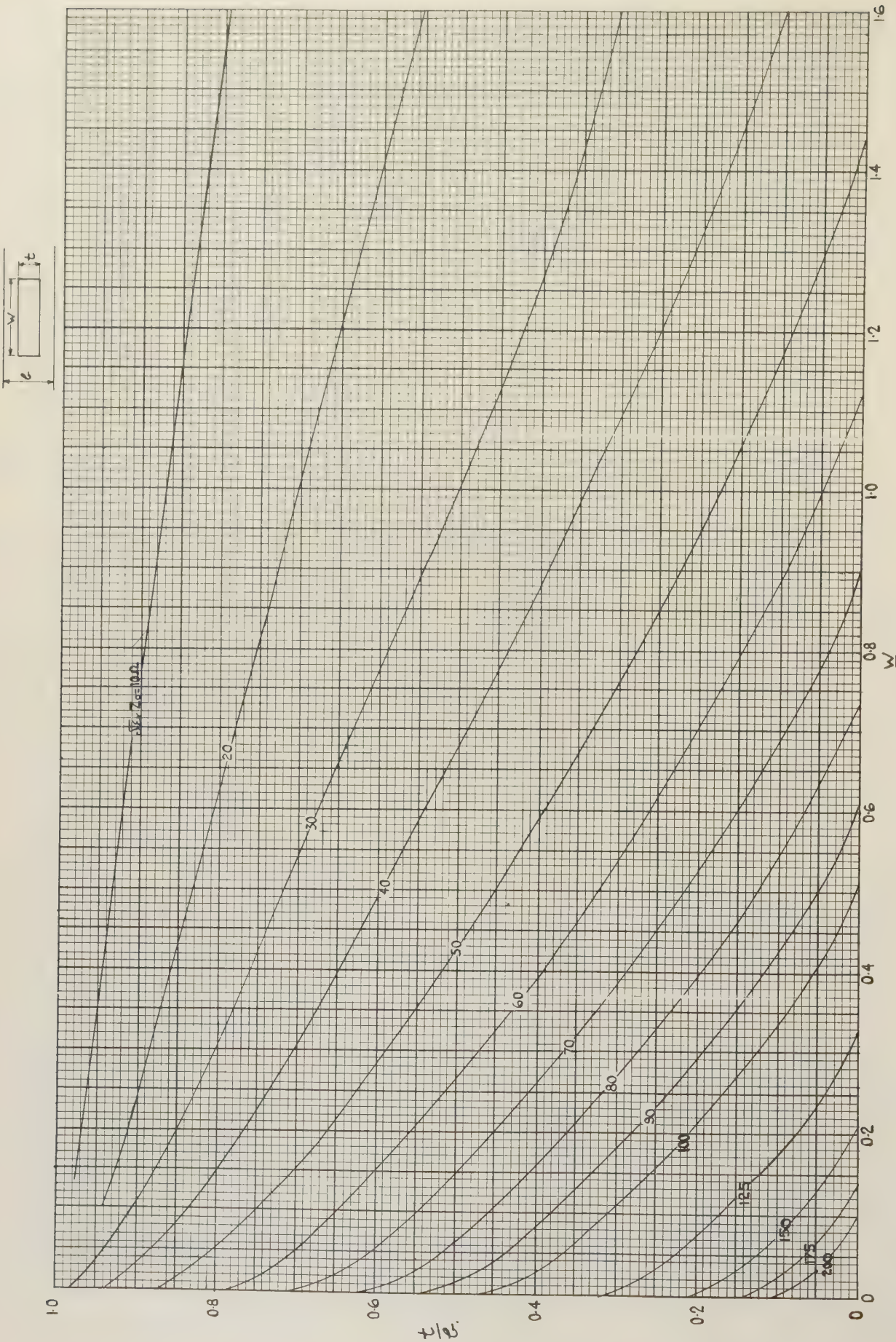

Fig. 6—t/b vs w/b with $\sqrt{\epsilon_r} Z_0 \Omega$ as parameter.

ACKNOWLEDGMENT

The permission of Vickers-Armstrongs Ltd. to publish this note is gratefully acknowledged.

BIBLIOGRAPHY

[1] Copson, E. T., *Functions of a Complex Variable*. Oxon. University Press. London, 1950.
[2] Wholey, W. B., and W. N. Eldred, "A New Type of Slotted Line Section." *Proceedings of the IRE*, Vol. 38, (March, 1950), pp. 244–248.
[3] Cohn, S. B., "Characteristic Impedance of the Shielded-Strip Transmission Line," *Transactions of the IRE* (PGMTT), Vol. MTT-2, (July, 1954), pp. 52–57.
[4] Kober, H., *Dictionary of Conformal Representation*, New York, Dover Press. New York, 1952.
[5] Milne-Thomson, L. M., *Die Elliptischen Funktionen von Jacobi*. Berlin, Springer, 0000.
[6] Milne-Thomson, L. M., "The Zeta Function of Jacobi." *Proceedings of the Royal Society of Edinburgh*, Vol. 52, Part II, No. 11 (1931, 1932).
[7] Jahnke, E., and F. Emde, *Funktionentafeln*. Leipzig & Berlin, Teubner.

Characteristics of a New Serrated Choke

KIYO TOMIYASU† AND J. J. BOLUS‡

Summary—**A new type of serrated choke will permit cuts or gaps anywhere on the walls of a rectangular waveguide. The low gap impedance is provided essentially by closely spaced, quarter-wavelength, open-ended, two-wire-line stubs. Low power and high power characteristics of many designs are presented.**

INTRODUCTION

A NEW choke has been designed and tested which will permit cuts, slots, or gaps on waveguide walls hitherto considered impossible. Previously, only slots on the center of the broad wall of a guide supporting the dominant TE_{10} mode as well as gaps in a transverse plane, such as a choke flange, were permitted. However, with the new serrated choke, slots or gaps are permitted anywhere on the guide walls; *e.g.*, on the narrow wall in the longitudinal direction, on the broad wall not at its center, cuts or gaps at any angle on any wall, etc. Applications of the new choke are possible in microwave components and scanning antennas.

Essentially the required low impedance across a gap is provided by closely spaced quarter-wavelength open-ended two-wire line stubs. A schematic diagram of a longitudinal serrated choke is shown in Fig. 1(a). The second conductors of the two-wire line stubs are provided by the images of the serrations as shown in Fig. 1(b) and Fig. 1(c).

It may appear feasible to design a longitudinal choke without the serrations. Such a choke was actually tried but without success. A section of a waveguide 12 inches long with unserrated choke was connected into a $1 \times \frac{1}{2}$ inch rectangular waveguide measuring setup. The input vswr varied from 1.05 to 3 and the insertion loss varied from 0.5 to 3 db as the effective length of the unserrated choke was varied using an adjustable short. The large variation in characteristics is due to the coexistence of two propagating waveguide modes in the choked waveguide region. These two modes could be considered as the $TE_{1/2,0}$ and $TE_{3/2,0}$ modes relative to the choked waveguide. The latter mode yields the dominant TE_{10} mode in unchoked rectangular waveguide. Inasmuch as these two modes have different cutoff wavelengths, whose ratio may be about 4, the respective propagation velocities will differ. This will result in a spatial beating and hence partial power transfer characteristics between the primary waveguide and the "choke" waveguide.[1] By serrating the choke, the $TE_{1/2,0}$ mode will not propagate and the desired low impedance will be provided across the gap.

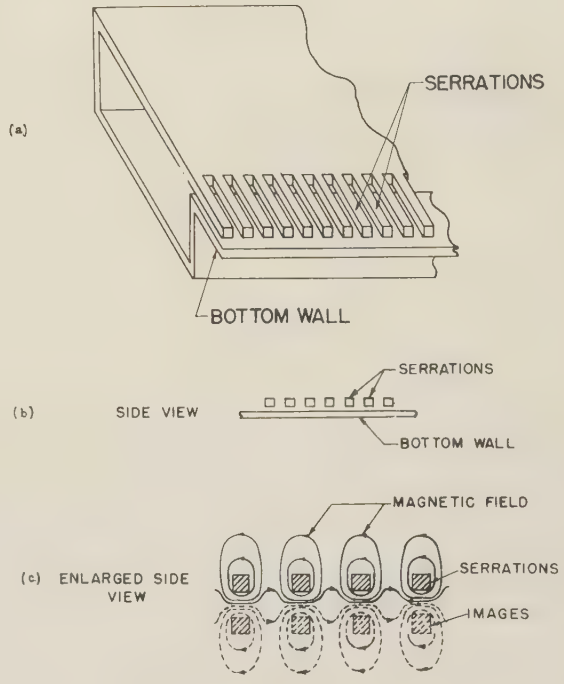

Fig. 1—The serrated choke.

† Formerly with Sperry Gyroscope Co., Great Neck, N. Y., now with Gen. Elec. Microwave Lab., Palo Alto, Calif.

‡ On leave from Sperry Gyroscope Co., now at Signal Corp Engrg. Labs., Ft. Monmouth, N. J.

[1] K. Tomiyasu and S. B. Cohn, "The transvar directional coupler," PROC. IRE, vol. 41, pp. 922–926; July, 1953.

An investigation was conducted to obtain information which would make possible the design of a choke having minimum vswr and insertion loss and also high power-handling ability. To make the data complete, the frequency and phase velocity characteristics of the choke were also obtained. Since fabrication is a factor in determining the design of a component, chokes having a circular cross section were studied along with those having a rectangular cross section.

Circular Cross Section Chokes

A cross section of the 12 inches long X band fixture used to test circular cross section chokes and a definition of symbols are given in Fig. 2. The choke pins, set in V shaped grooves, are held in place with a beryllium-copper strip and silver paint, thus allowing variation of pin length, diameter, and spacing. Image planes of various thicknesses, T, are used to vary the waveguide gap, G.

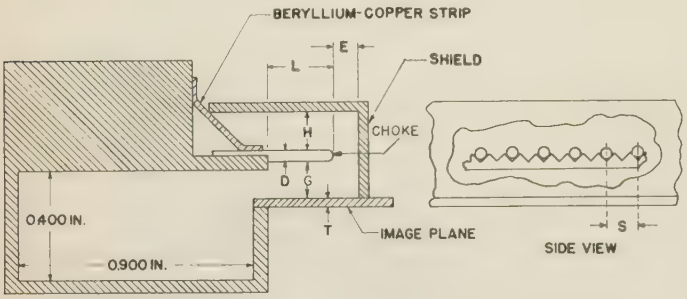

Fig. 2—Fixture used to test longitudinal serrated chokes, cross sectional view.

The first choke pins had a diameter of 0.040 inch, was spaced 0.060 inch center to center, and extended 0.312 inch. With the shield left off and a gap, G, of 0.060 inch, it was found that the radiation was quite excessive. The gap was reduced and it was noted that, even for a gap of approximately 0.015 inch, shielding was necessary. It was also determined that the position of the shield affected the operation of the chokes. When the enclosed volume of the shield is made too large, resonances within the shield structure occur; this resulted in high insertion losses at certain frequencies. With a fixed gap of 0.060 inch, the best characteristics were obtained when the shield was located at $H=0.150$ inch and $E=0.060$ inch.

Using the 0.040 inch diameter pin, the effect of pin length on the insertion loss is shown in Fig. 3 and on the vswr in Fig. 4. A residual insertion loss of 0.2 db of the fixture when the chokes were shorted out has been subtracted so that only the losses due to the chokes are plotted in Fig. 3. The data indicate that a length of approximately 0.312 inch ($0.99\ \lambda_0/4$ at 9,370 mc) gives the best results. λ_0 is the free-space wavelength. However, a length of 0.250 inch ($0.80\ \lambda_0/4$ at 9,370 mc) also gives good results, so that the length can be varied between these two values without greatly affecting the vswr and insertion loss.

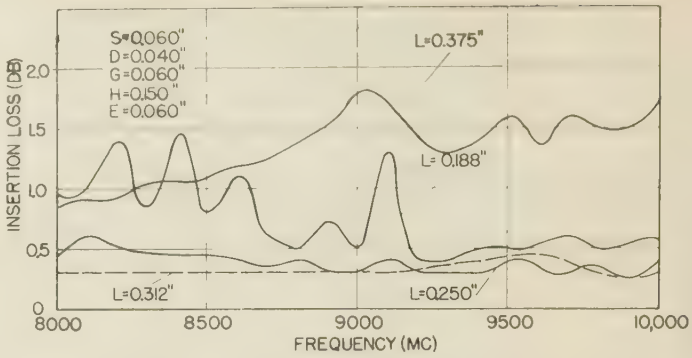

Fig. 3—Insertion loss as a function of frequency for circular cross section chokes with pin length as parameter.

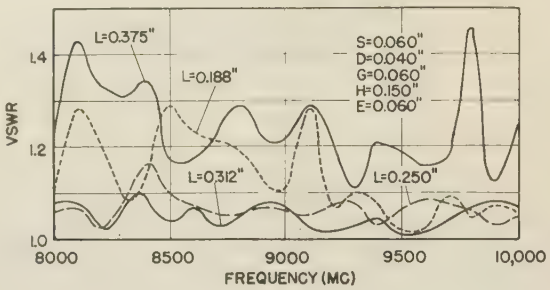

Fig. 4—Vswr as a function of frequency for circular cross section chokes.

Another characteristic of the chokes investigated is the phase velocity in the "choked" waveguide. This was measured by varying the position of a short circuit in the guide. With a fixed probe position in the slotted line, the short was moved through an integral number of half wavelengths to yield an average guide wavelength in the choked waveguide. By comparing this with the calculated value of guide wavelength for an unperturbed rectangular waveguide (obtained by measuring frequency), the change in guide wavelength or phase velocity in the choked waveguide was computed. The phase velocity characteristics for the several pin lengths

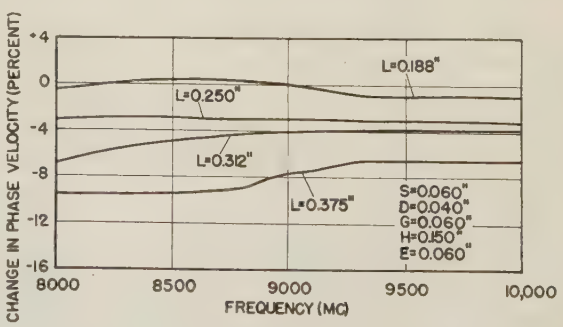

Fig. 5—Per cent change in phase velocity as a function of frequency for circular cross section chokes.

used are given in Fig. 5 and show that the phase velocity (or guide wavelength) in the choked portion is reduced.

Since the decrease in guide wavelength may be due not only to the loading effect of the chokes but to errors in the various parameters, an analysis of latter was made using general wavelength equation for TE_{10} mode:

$$\lambda_g = \frac{\lambda_0}{\sqrt{\epsilon_r - \left(\frac{\lambda_0}{2a}\right)^2}} = \frac{1}{\sqrt{\epsilon_r \left(\frac{f}{c}\right)^2 - \left(\frac{1}{2a}\right)^2}} \quad (1)$$

where

λ_g = guide wavelength
λ_0 = free-space wavelength
ϵ_r = relative dielectric constant of medium inside waveguide
f = frequency
c = velocity of light
a = inside broad dimension of waveguide.

Taking the natural logarithm of (1) and then the derivative results in the following:

$$\frac{\Delta\lambda_g}{\lambda_g} = -\frac{1}{2} h \frac{\Delta\epsilon_r}{\epsilon_r} - h\frac{\Delta f}{f} + h\frac{\Delta c}{c} - (h-1)\frac{\Delta a}{a} \quad (2)$$

where

$$h \equiv \epsilon_r \left(\frac{\lambda_g}{\lambda_0}\right)^2.$$

By using typical values of errors in these parameters it was found that the factor $\Delta a/a$ ($\approx 1/900$) gave the greatest contribution to a 0.35 per cent change in phase velocity at the low frequency end of the waveguide band ($h = 3.1$). Since the measured change in phase velocity exceeds 0.35 per cent it can be deduced that the loading effect of the chokes is the greater factor.

To determine the effect of pin spacing, this dimension was increased from 0.060 to 0.120 inch. Since the vswr and phase velocity were not appreciably changed by this increase, the pin spacing was determined as not being critical, but should be about two times the pin diameter, D.

With respect to pin diameter, it was found that 0.040 to 0.050 inch gave the best over-all results at X band frequencies. The insertion loss of the 0.062 inch pins was higher than that for 0.040 inch pins and the 0.062 inch pins reduced slightly the change in phase velocity.

When all factors are considered, a pin length of 0.90 $\lambda_0/4$ seems to yield a good compromise in the characteristics of vswr, insertion loss and phase velocity change.

Rectangular Cross Section Chokes

For particular applications where choking action is desired over a considerable length, fabrication of circular cross section chokes may become a problem. For this reason, a choke having a rectangular cross section of the type shown in Fig. 6 was investigated in the fixture in Fig. 2. Several test sections were fabricated, each having a different choke width, W (dimension in the direction of propagation). The separation between choke pins was 0.125 inch in all cases. The thickness of all chokes was 0.125 inch and the length, L, was varied by removing material from the ends of the chokes. These choke sections were tested in the fixture shown in Fig. 2 by removing beryllium-copper strip and adding a mounting block to which choke sections could be bolted.

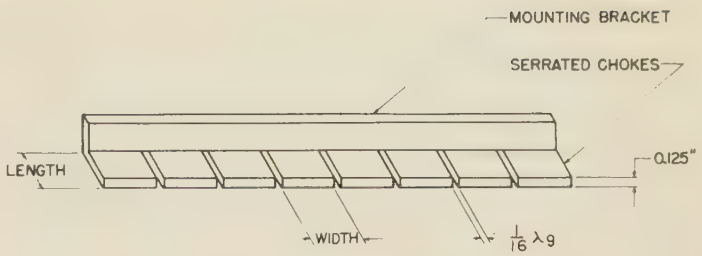

Fig. 6—Rectangular cross section choke which was mounted on fixture in Fig. 2.

It was found that this type of choke was particularly useful in places where no shielding could be used and the gaps encountered were less than 0.025 inch. For this particular application, it was found that chokes having a width, W, of 0.450 inch gave the best results when no shield was used. It is believed that this is due to the smaller amount of radiation obtained from this choke configuration. The effect of length was also investigated, and it was found that a length of 0.320 inch gave optimum performance. The vswr characteristics for this choke as a function of gap size are shown in Fig. 7. Furthermore, the insertion loss and phase velocity measurements show that for $G = 0.010$ inch they are about 0.3 db and -2 per cent change respectively over the same frequency band.

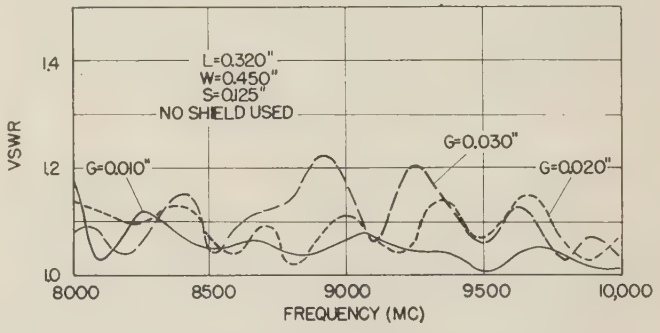

Fig. 7—Vswr as a function of frequency for rectangular cross section chokes with gap size as parameter.

High Power Measurements

The circular and rectangular cross section chokes were tested at high power using a fixed tuned 4J50 magnetron operating at 9,375 mc. The pulse width used was 1.2 μsec, with a repetition rate of 800 cps and a peak power of approximately 240 kw. The air gap, G, used when testing the circular cross section chokes was approximately 0.010 inch. The choke pin diameter was 0.040 inch, and the center-to-center distance, S, was 0.060 inch. These chokes were able to carry the maximum available peak power of 240 kw without any evidence of breakdown for choke lengths ranging from 0.280 to 0.320 inch.

Rectangular cross section chokes having widths, W, of 0.225 and 0.450 inch, spacing between chokes of 0.125

inch, and a thickness of 0.125 inch were tested. The gap was varied from 0.030 to 0.070 inch and the length was varied from 0.320 to 0.280 inch without any sign of the breakdown at the peak power of 240 kw. The corners and edges of these chokes were not rounded in any way. These high-power measurements indicate that both types of chokes are able to carry full rated waveguide power.

Remarks

While it is possible to use the serrated choke on waveguides other than rectangular in cross section, it should be noted that since effective gap impedance is actually nonzero, higher order modes are generated at gap.

In considering the use of the new choke for specific applications and configurations, the array of choke pins and its image plane can be interchanged. Also greater utility may be achieved by rotating the plane of the chokes to any other angle about an axis parallel to the longitudinal axis of the waveguide.

Acknowledgment

The initial limited development on this choke, carried out in 1950, was a part of a program sponsored by the Bureau of Ships under Contract No. Nobsr-42419. The greater portion of the data presented here was obtained under a subsequent contract AF30(120)-440 with the Rome Air Development Center.

Microwave Filters Utilizing the Cutoff Effect

P. A. RIZZI†

Summary—**Two band-rejection microwave filters employing the waveguide cutoff effect are discussed. One type utilizes the cutoff property in the series arm of an *E* plane tee to improve the filter's characteristics, while the other utilizes this property in the *E* and *H* arms of a magic tee. Experimental data for both single and multistage filters are presented. Methods of obtaining low standing wave ratios over a broad pass-band are also presented.**

Introduction

IN GENERAL, the design of microwave filters has been treated from an equivalent circuit point of view. That is, low frequency filter theory is used to determine the configuration and from this the microwave analog is constructed. For example, by using resonant cavities and irises, the microwave equivalent of the series, shunt, and ladder type filters have been made.[1–4] In addition, *m* derived filter theory has been applied to microwaves for the design of band-rejection filters.[5] On the other hand, the design of a microwave filter sometimes entails the use of a property peculiar to waveguides. An example of this is the cutoff filter. In normal waveguide theory, the application of the boundary conditions at $x=0$ and $x=a$ (Fig. 1) to Maxwell's field equations reveals the fact that the electromagnetic wave (rectangular TE_{10} mode) will only propagate unattenuated above the frequency f_c, where

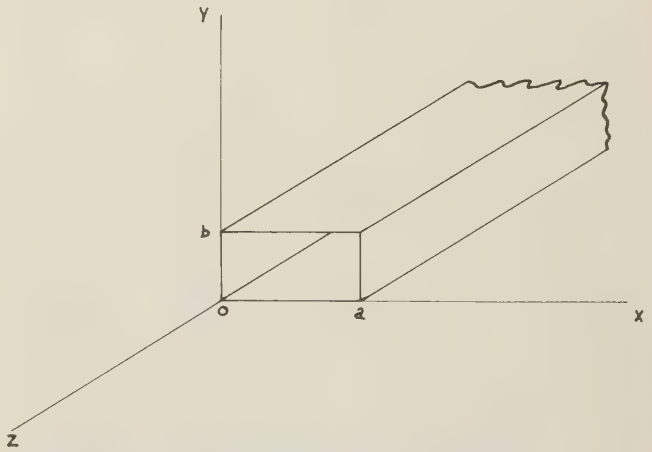

Fig. 1—Rectangular waveguide structure.

$$f_c = \frac{1}{2a\sqrt{\mu\epsilon}}.^{6} \tag{1}$$

For frequencies below f_c, the wave will attenuate at the rate of α nepers per meter, where

$$\alpha = \frac{\pi}{a}\sqrt{1-\left(\frac{f}{f_c}\right)^2}. \tag{2}$$

† Raytheon Mfg. Co., Missile and Radar Div., Bedford, Mass.

[1] R. M. Fano and A. W. Lawson, Jr., "Microwave filters using quarter-wave couplings." Proc. IRE, vol. 35, pp. 1318–1323; November, 1947.

[2] W. W. Mumford, "Maximally-flat filters in waveguide," *Bell Syst. Tel. Jour.*, vol. 27, pp. 684–713; October, 1948.

[3] W. L. Pritchard, "Quarter-wave coupled waveguide filters," *Jour. Appl. Phys.*, vol. 18, pp. 862–872; October, 1947.

[4] J. Reed, "Low-Q microwave filters," Proc. IRE, vol. 38, pp. 793–796; July, 1950.

[5] M. E. Breese and S. B. Cohn, "Diplexing Filters," 1954 IRE Convention Record, Part 8, "Communications and Microwaves," pp. 125–133.

[6] The Rationalized MKS system of units will be used in this discussion.

Thus it is seen that the rectangular waveguide (or, in fact, any closed waveguide) is, by virtue of the cutoff effect, a high-pass filter. Consequently if a high-pass microwave filter is desired which passes frequencies above f_1, one merely sets the width of the waveguide (a) so that f_1 is the cutoff frequency of the waveguide section. That is, let

$$a = \frac{1}{2f_1\sqrt{\mu\epsilon}}. \tag{3}$$

By adjusting the length of the cutoff section, any required attenuation at frequencies below f_1, can be obtained.

Having reviewed the manner in which the cutoff property can be used to design a high-pass microwave filter, we will now show how this effect in conjunction with waveguide tees can be used to construct band rejection and possibly low-pass filters.

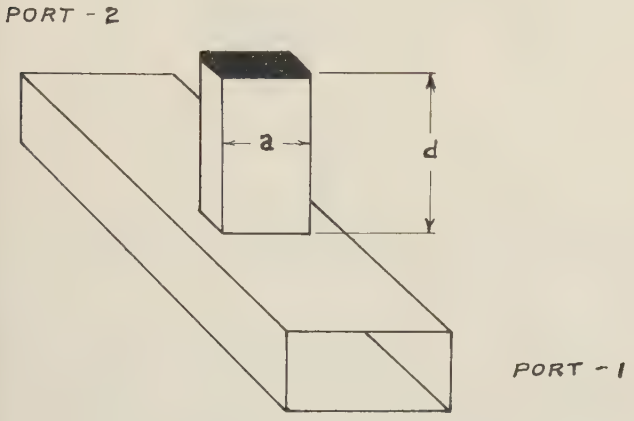

Fig. 2—A single-stage E plane cutoff filter.

The E Plane Tee Cutoff Filter

One method of constructing a band-rejection filter is to make use of the cutoff effect in the series arm of an E plane tee.[7] Fig. 2 shows a single stage E plane cutoff filter. At frequencies below the cutoff frequency of the series arm (1) and above the cutoff frequency of the main guide, the microwave energy will be transmitted from port 1 to 2 with practically no loss. That is, since the series arm is beyond cutoff, the wave will "see" it not as a transmission line but as a small reactive element in series with the main guide. Above the cutoff frequency of the series arm, the section behaves like a normal series tee; namely, a six terminal network. Therefore, by shorting the series arm a distance d from its input terminals, the filter section will reject frequencies at which d is approximately a quarter wavelength long. By choosing the cutoff frequency of the series arm close to the resonant frequency of the shorted series arm, one obtains an attenuation curve which rises very rapidly with frequency. A typical attenuation curve for a single stage filter is shown in Fig. 3.

[7] This can also be done with an H plane tee, but each filter section is physically longer.

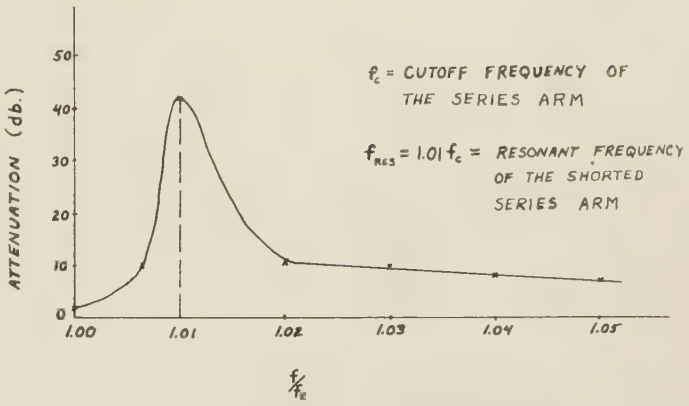

Fig. 3—Attenuation curve for single-stage E plane cutoff filter.

At frequencies below the cutoff frequency of the series arm, the vswr of the filter section is practically constant (Fig. 4). Since the series arm is below cutoff ($f/fc<1$) in the filter's pass band, the vswr is independent of the shorting distance d. This is very important from a practical viewpoint since it allows the problem of good vswr in the pass band and good rejection in the stop band to be treated separately. That is, the filter sections may be spaced so as to give a good impedance match across the pass band. Then the shorts may be adjusted to give good rejection in the stop band without in any way affecting the match in the pass band. Since the tuning of the series-tee cutoff filter, unlike the quarter-wave coupled filter, is independent of the pass band match, the individual stages may be stagger-tuned. Consequently a given rejection over a frequency band can be obtained with a smaller number of filter elements.

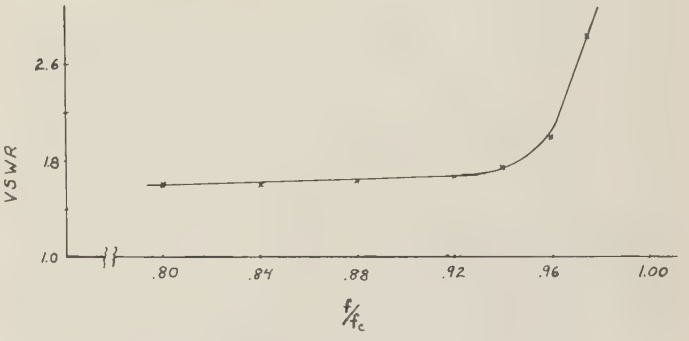

Fig. 4—Vswr for single-stage E plane cutoff filter.

Three types of E plane tee cutoff filters which have been made for application at X band are shown in Fig. 5. The vswr in the pass band and the attenutaion in the stop band for the filter shown in Fig. 5(a) is given in Fig. 6. By spacing the first two filter sections $\lambda/4$ apart, the reflections from the individual sections tend to cancel. Likewise $\lambda/4$ spacing for the next two sections also causes the reflections to cancel. Finally by spacing the two *pairs* $3/4\lambda$ apart, second order cancellation is obtained. That is, at frequencies where the mismatch of each pair becomes bad, the $3/4\lambda$ spacing tends to cancel

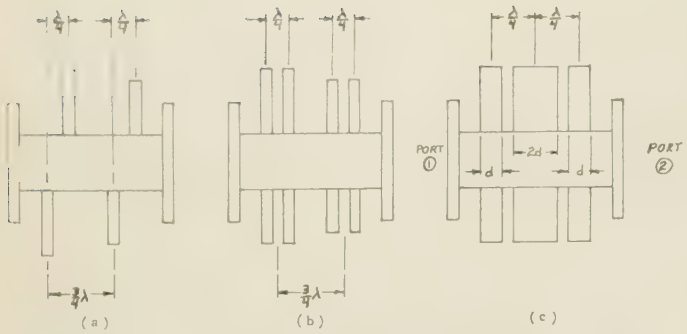

Fig. 5—*E* plane tee cutoff filters.

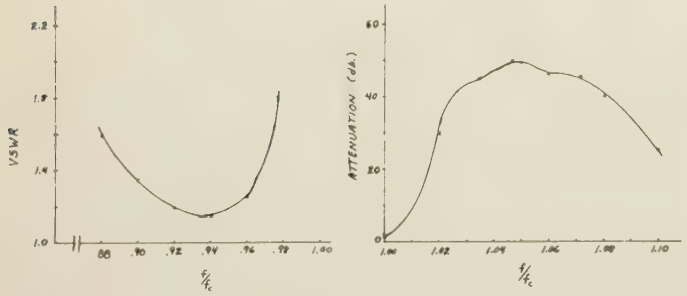

Fig. 6—Vswr and attenuation for filter shown in Fig. 5(a).

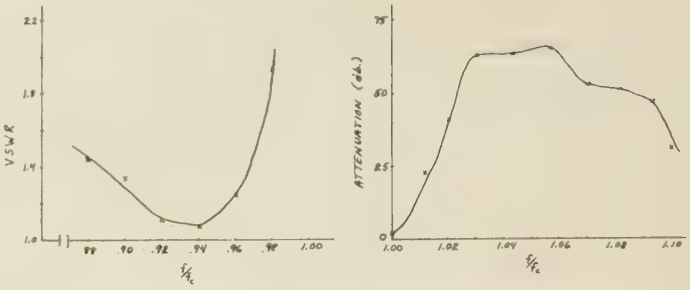

Fig. 7—Vswr and attenuation for filter shown in Fig. 5(b).

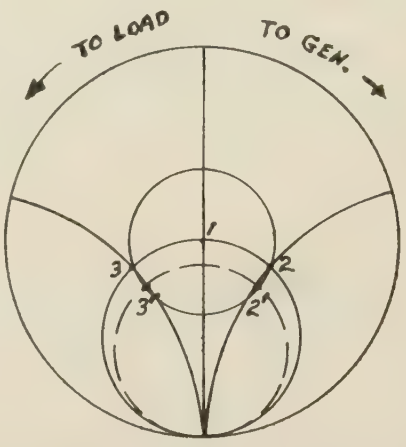

Fig. 8—Matching technique for filter shown in Fig. 5(c).

these reflections and thereby keep the vswr of the complete filter fairly low. The filter shown in Fig. 5(b) also uses the matching technique described above. In this case the number of filter elements is doubled in order to obtain greater attenuation in the stop band. The vswr and attenuation data is given in Fig. 7.

The matching technique used in the filter shown in Fig. 5(c) can be described more conveniently by the use of a Smith Chart. Assuming a generator of internal impedance Z_0 at port 1 and a matched load ($Z = Z_0$) at port 2, the Smith Chart analysis (Fig. 8) proceeds as follows:

1) Starting from the matched load at port 2, the first series stub is encountered. Since this is a small reactive element, impedance is transformed from point 1 along a constant resistance circle to some point 2.

2) Moving approximately $\lambda/4$ toward the generator transforms the impedance to the point 3. Introduction of the next stub which has twice the reactance of the first stub moves the impedance along the constant resistance circle to point 2.

3) Again moving approximately $\lambda/4$ toward the generator on a constant vswr circle moves the impedance to point 3.

4) Insertion of the final stub which has a reactance equal to that of the first stub transforms the impedance to the point 1; that is, a matched condition.

If the operating frequency is now changed, the electrical length between the stubs also is changed. To show that this change in electrical length does not disturb the matched condition to any appreciable degree, let us repeat the above analysis for a decrease in the operating frequency.

1) Starting at point 1, the first stub again transforms the impedance to the point 2.

2) Since the frequency has been decreased, the electrical length between the stubs is now less than $\lambda/4$. Therefore, moving along the first section of line brings the impedance to the point 3′ instead of the point 3. Insertion of the larger stub now transforms the impedance to the point 2′.

3) Since the impedance is at point 2′ instead of point 2, the second length of line (which is also less than $\lambda/4$) moves the impedance to the *point 3*.

4) Insertion of the final stub again transforms the impedance to the center of the Smith Chart.

Hence by virtue of the matching technique used, the change in electrical length between the first and second series stubs is compensated for by the change in length between the second and third stubs; thereby, yielding a good vswr over a considerable frequency band. Fig. 9 shows the vswr and attenuation of this filter [shown in Fig. 5(c)] vs frequency.

As mentioned, individual filter elements were staggertuned in all the above filters. This enabled required attenuation to be obtained in shortest possible length. The three filters in Fig. 5 have been designed for *X* band and are all less than two inches in length.

The Magic-Tee Cutoff Filter

Another method of constructing a band-rejection filter is to make use of the cutoff effect in the *E* and *H* arms of a magic tee. Fig. 10 shows a magic tee in which the width of the *E* and *H* arms have been reduced to the value "*a*". At frequencies below the cutoff frequency of

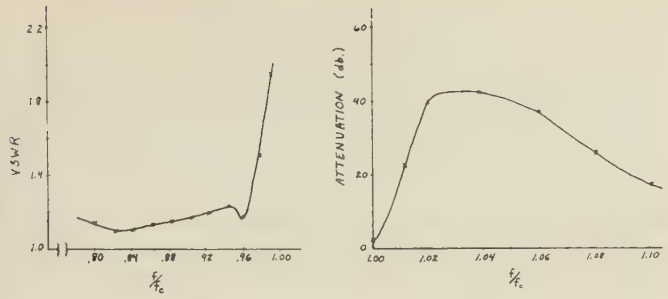

Fig. 9—Vswr and attenuation for filter shown in Fig. 5(c).

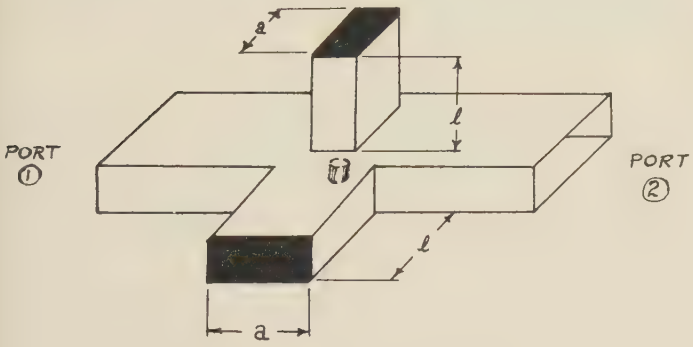

Fig. 10—A magic-tee cutoff filter.

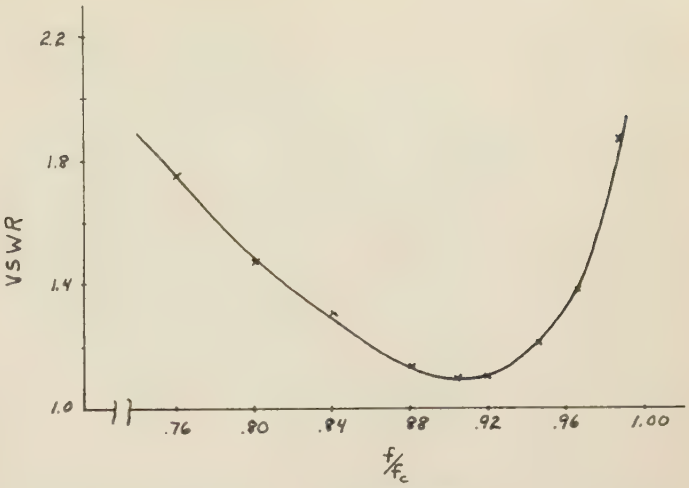

Fig. 11—Vswr for the magic-tee cutoff filter shown in Fig. 10.

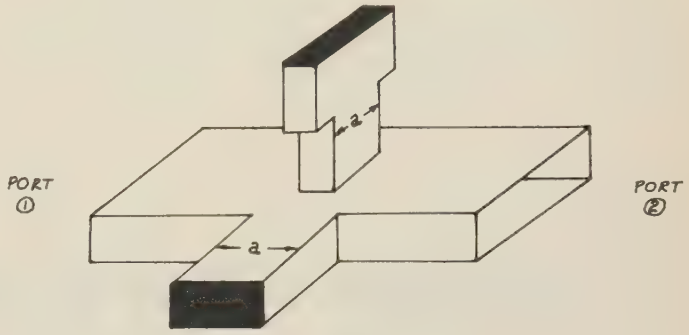

Fig. 12—A broadband magic-tee cutoff filter.

the E and H arms, the microwave energy propagates from port 1 to 2 with practically no loss. In other words, the wave propagating through the main guide will "see" the E and H arms not as transmission lines but as a small reactive effect. The vswr due to this effect can be reduced by placing a small capacitive button in the main guide at the center of the magic tee as shown in Fig. 10. Since the mismatch is corrected at the source of the discontinuity, no long line lengths are involved and consequently a low vswr is maintained over a considerable frequency band as shown in Fig. 11.

Above the cutoff frequency of the E and H arms, the device behaves like an ordinary magic tee. Therefore if shorts are placed in the E and H arms equidistant from their input terminals, the energy entering port 1 will split between the E and H arms and by virtue of the phase relations in a magic tee will all be reflected back to port 1. The only additional requirement on the distances l to the shorts is that they be long enough to attenuate frequencies below the cutoff frequency of the E and H arms before the energy reaches the shorts. Usually 10 db attenuation is adequate to make the shorts "invisible" in the pass band. The required length for any attenuation can be determined from (2).

Since the operation of this filter in the stop band only requires that the electrical length to the shorts in the E and H arms be equal, good rejection should be obtained for all frequencies above the cutoff frequency of the E and H arms. That is, the magic-tee cutoff filter is basically a low pass filter. However, in practice, this wideband rejection is difficult to obtain. The reason is that although the electrical length from the input terminals to the shorts are equal, the actual length of E and H plane stubs are not necessarily equal. For example, the electrical length of the E plane stub is determined by the actual length of the shorted E arm *plus* the distance from the top wall of the main guide to the apparent input terminal of the series arm. This apparent input terminal is located approximately one-quarter of the guide height down from the top wall of the main guide. Similarly, the electrical length of the H arm is a combination of the actual length of the shorted H arm plus the distance from the side wall to the apparent input terminal of the shunt arm. This terminal is located at approximately the center of the main guide. Since the shift in apparent input terminal is different for the E and H arms, different lengths of E and H plane stubs are required to give the same electrical length from the input terminals to the short circuits. Consequently, the frequency sensitivity of the two line lengths are different and adjustment of the line lengths for good rejection at one frequency will not necessarily yield good rejection at all frequencies. To compensate for this, one can add a section of guide of appropriate width and length behind either the E or H arm cutoff section which will tend to cancel the difference in frequency sensitivity between the E and H plane stubs. This idea is similar, in principle, to that presented by H. Sohon.[8] For example, Fig. 12 shows a magic-tee cutoff filter which employs an additional section of guide in the E arm to reduce the difference in frequency sensitivity between the shorted stubs.

[8] H. Sohon, "Wide band phase delay circuits," Proc. IRE, vol. 41, pp. 1050–1052; August, 1953.

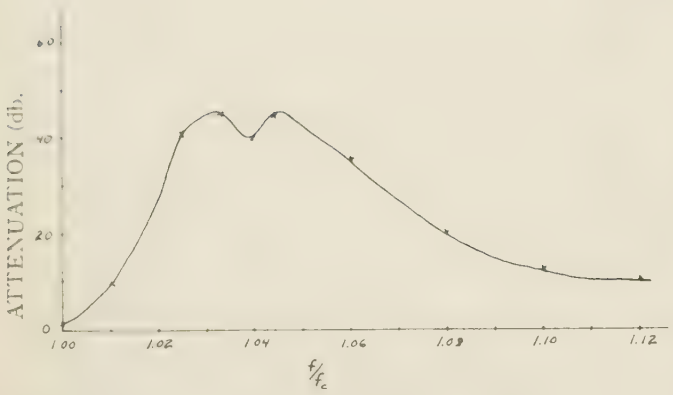

Fig. 13—Attenuation of a magic-tee cutoff filter.

The attenuation vs frequency characteristic of this filter is given in Fig. 13. To obtain greater rejection in the stop band, two or more filters can be cascaded. Another method is to employ a double magic tee; *i.e.*, one with two E arms and two H arms.

Conclusions

Two band-rejection filters employing the waveguide cutoff effect have been discussed. They are the E plane tee cutoff filter and the magic-tee cutoff filter. By appropriate matching techniques, E plane tee cutoff filters have been designed with a vswr of less than 1.5 over 8, 10, and 16 per cent pass bands while maintaining greater than 25 db rejection over 8, 10, and 6 per cent bands, respectively. A magic-tee cutoff filter has also been constructed which has a vswr of less than 1.7 over a 20 per cent frequency band. By proper design of the shorted E and H arms, greater than 10 db rejection has been obtained over a 12 per cent band.

Acknowledgment

The author wishes to acknowledge the assistance of Mr. G. C. Shaw in formulating some of the ideas presented here. He also wishes to express his gratitude to Dr. Ernest Wantuch and Mr. T. S. Saad for their suggestions.

Technique of Pulsing Low Power Reflex Klystrons

J. I. DAVIS†

Summary—**Very little published information is available on pulsing low power reflex klystrons. Since low power reflex klystrons have been generally designed for cw operation as local oscillators, a minimum of effort has been directed toward the development of specific low power pulse reflex klystrons.**

This paper summarizes an effort that has been directed toward pulsing typical low power reflex klystron with a description of the techniques evolved and a summary of the limitations and merits of each technique. Included also is a description of a pulse klystron "priming" technique that minimizes the effects of pulse shortening and leading edge jitter associated with typical pulse operation.

Introduction

IT HAS BEEN apparent for some time to designers of microwave equipment that there has been little or no attempt by the klystron tube manufacturers to design low power klystrons for pulse application. In general, the low power klystrons have been designed for local oscillator use in radar and beacon receivers, and in equipment such as spectrum analyzers. A great deal of effort of late has been devoted toward pulsing high power klystrons for use in generating high speed particles and for use in large anti-jamming radar systems. This has forced the designers of low power beacons and rf signal generators to rely almost wholly on their wit and ingenuity to find suitable techniques for pulsing low power klystrons for optimum pulse fidelity and minimum pulse jitter. In addition to the lack of information from manufacturers on pulsing klystrons there has been very little written in the literature on suitable techniques for pulsing klystrons to yield minimum leading edge jitter and pulse shortening.

Because many of the new guided missile systems have stringent requirements for rf pulsed coded modulation to meet their tactical requirements, a great deal of effort has been expended in advancing the state of the art of pulse circuit design. The circuitry itself has preceded the pulsed rf techniques primarily because of the availability of new components to the circuit designer. These components consist essentially of improved pulse transformers, more reliable thyratrons, and improved hard tube modulator tubes. The basic difficulty of reliable pulsed rf systems has been associated primarily with the pulsing of the klystron itself.

Starting of Pulse Reflex Klystron

It is well known that all electronic oscillators are started by noise or circuit transients associated with the oscillator. This concept applies equally well to the starting of reflex klystron oscillators. However, when one is concerned with pulse operation of reflex klystrons there exists the distinct possibility that the oscillation could have been started by shock excitation of the resonant cavity by the pulsed beam current.

† Litton Industries, Beverly Hills, Calif.

It will be shown that the initial excitation produced by shot noise in the beam exceeds that induced by the current transient by a very large factor. Had it been found that the microwave voltage produced by the high-frequency components of the pulse was larger than the voltage produced by shot noise, the voltage produced by the pulse would always have been the same and there would have been no evidence of leading edge jitter associated with the rf pulse. This, of course, is not the case and accounts for typical rf pulse leading edge jitter.

The relative effects of Johnson noise and shot noise in building up oscillation can be expressed by the following ratio:[1]

$$\frac{Is^2}{It^2} = \frac{eI_o}{kTG} = \frac{11{,}600I_0}{TG};$$

where

I_s = shot noise current,
I_t = Johnson noise current,
I_0 = gap current,
k = Boltzmann's constant
1.374×10–23 Joule per °K,
e = charge of an electron
1.59×10–19 coulombs,
G = conductance defined as M/Q,
M = admittance of mode,
Q = loaded Q of klystron cavity.

For a typical klystron such as a V-153 operating at 9,500 mc with a beam voltage of 300 volts, and operating in the $4\frac{3}{4}$ mode the following values can be approximated:[2]

$$T = 293°K \ (20°C)$$
$$I_0 = 8.8 \times 10^{-3} \text{ amperes}$$
$$M = 2.22 \times 10^{-4} \text{ mhos}$$
$$Q = 150$$

then

$$\frac{I_s^2}{I_t^2} = 1.57 \times 10^3.$$

From this ratio it becomes evident that the shot noise is of greater magnitude and importance than Johnson noise in the tube.

To proceed further, it is now desirable to compute the relative effects of shot noise compared with high-frequency transients induced by the applied video pulse, in starting klystron oscillations. This can be expressed by the following ratio:[1]

$$\frac{Vs^2}{V^2} = \frac{eQ\Delta t^2\omega_0^3}{2I_0};$$

where

V_s = shot noise voltage,
V = transient voltage,
$\omega_0 = 2\pi \times$ (klystron frequency),
Δ_t = rf pulse build-up time.

Assuming the following approximate values for the V-153 Klystron:

$$I_0 = 8.8 \times 10^{-3} \text{ amperes},$$
$$Q = 150,$$
$$\Delta t = 2 \times 10^{-8} \text{ seconds},$$
$$\omega_0 = 5.96 \times 10^{10} \text{ radians per second},$$

then

$$\frac{V_s^2}{V^2} = 115.$$

This ratio points out clearly that the oscillations are built up from shot noise rather than from high-frequency transients induced by the pulse.

Practical Applications and Considerations

Experience has indicated that the application of a video modulation pulse to one klystron will not, of necessity, yield the same detected rf video pulse when applied to another type of klystron. As an example, the V-260 and V-280 klystrons were pulsed with the same circuit techniques. The detected video pulses were significantly different, the leading edge jitter also differed, and the spectrums as noted on a spectrum analyzer were noticeably different. In discussion of this problem with the klystron manufacturer it was indicated that both klystrons operated satisfactorily as local oscillators, the function for which they were designed and tested, and that the results of pulsing these klystrons would be of great interest to them. They suggested that further laboratory tests would probably yield optimum repeller modes for best pulse operation of each klystron. It was also pointed out that there may exist an optimum direction for pulsing into a klystron mode; that is to say, the pulse spectrum may be noticeably different when the klystron is pulsed from a high static repeller voltage into a particular mode rather than from lower static repeller voltage into the same mode. Tests indicated in this regard that there was no noticeable difference when this was tried on the $4\frac{3}{4}$ and $5\frac{3}{4}$ modes of the klystron under test.

It might be pointed out that:[3]

1) That a klystron would have the best starting time characteristics if it were operated in a mode associated with the longest drift time in the drift space;
2) That the operating characteristics would be a function of external circuit loading;
3) That the rise time of the applied pulse and klystron Q were important considerations;

[1] Bell Tel. Labs. Staff, "Radar Systems and Components," D. Van Nostrand Co., Inc., New York, N. Y., pp. 702–705; 1949.
[2] Approximate values as furnished by Mr. Arnold Acker of Varian Associates.
[3] Bell Labs. Staff, *op. cit.*, p. 498.

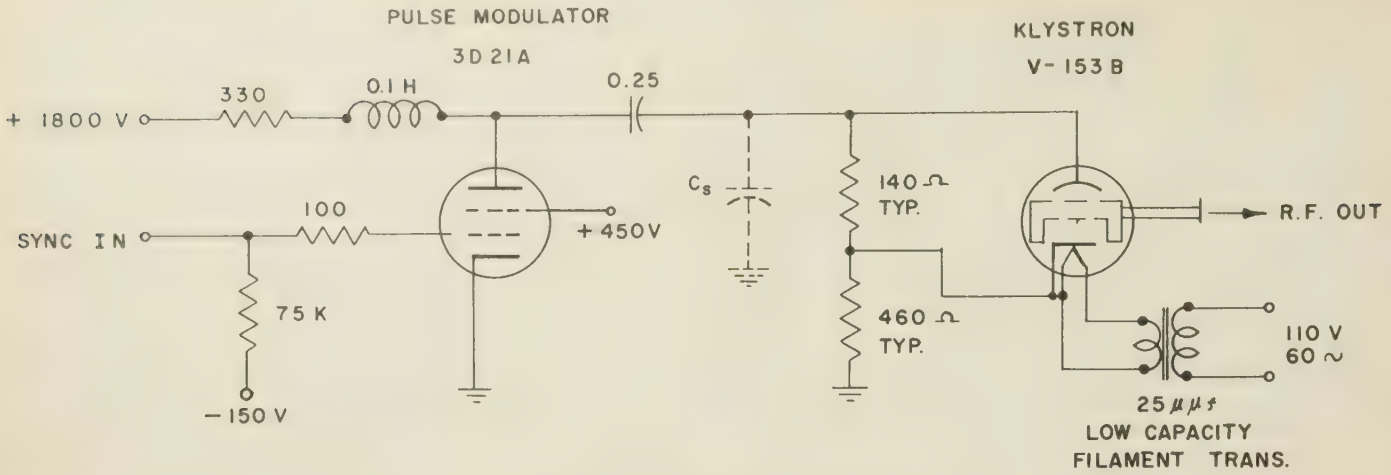

Fig. 1—Klystron beam and repeller pulsing.

4) The general klystron operation is a direct function of the basic electron optics design.

With the above considerations noted, concerted effort was directed towards determining the best technique for pulsing klystrons so as to yield best pulse modulation operation. Basically, three pulse techniques were explored:

1) Pulsing the the beam voltage only.
2) Pulsing the repeller voltage only.
3) Pulsing repeller and beam voltage simultaneously.

The results follow.

Simultaneous Beam and Repeller Pulsing

Pulsing both elements simultaneously appeared to give the poorest results. The results were interpreted by observing the detected rf video rectangular pulse as well as comparing the observed spectrum on a spectrum analyzer for theoretical $(\sin X/X)^2$ distribution of energy. It was interesting to note that the detected video pulse was quite misleading, for it looked to the uncritical eye very much like the applied video pulse. Closer observation, however, indicated pulse shortening, leading edge jitter, and poor rise time.

The spectrum consisted essentially of almost random spectrum lines with no definite nulls, symmetry or pattern. It is quite possible that the circuitry employed (Fig. 1) to pulse simultaneously both the repeller and beam elements of the klystron, in this case the V-280, could have been optimized and perhaps yielded better results. It was taken as a good engineering guess, however, that since the same circuitry was used in pulsing elements of the klystron with better results, improving the basic pulse circuitry would not, in itself, significantly improve the spectrum.

It was concluded from empirical observations with consideration of the electrical characteristics of klystrons, that it would be most difficult to pulse simultaneously the repeller element, which is a high impedance element, and the beam element (or cathode), which is a relatively low impedance element, and expect both elements to have the same volts per unit time, change in potential with identically applied pulses. To enlarge upon this point, we might add that it would be a coincidence, indeed, if the rise time of the beam voltage and the repeller voltage were identical even if the pulse modulating circuitry were matched to the pulsing elements of the klystron. This is primarily due to the fact that the high impedance of the repeller would remain constant during pulse modulation, while the beam element impedance would vary with time and therefore yield a complex impedance match even for an optimum designed pulse modulating circuit. It becomes clear that the rise time of the beam element of the klystron would be different from the rise time of the repeller element to the applied modulating pulse. The great amount of detectable frequency modulation as noted by spectrum analysis is therefore understandable, because of the changing voltage ratio of the beam element to the repeller element of the klystron.

It might be interesting to note at this point that pulsing both the repeller and beam elements of the 2K25 klystron has resulted in a relatively good spectrum. With this klystron, however, the rise time of the pulse applied to the repeller and to the beam elements was made adjustable to give an optimum spectrum. This adjustment had to be varied to suit the particular tube being pulsed and was called a "spectrum control" adjustment. This type of solution, though practical, is not desirable in military equipment where tube replacement is preferred without the necessity of adjusting circuitry.

In continuing the investigation of pulsing reflex klystrons, both the repeller and beam elements of the klystron were pulsed individually, keeping all other circuit parameters constant. That is to say, only the repeller was pulsed and the beam voltage was held constant. No effort was made to pulse tubes with control grids although, in that case, the control grid would also have been held as a constant in the test procedure.

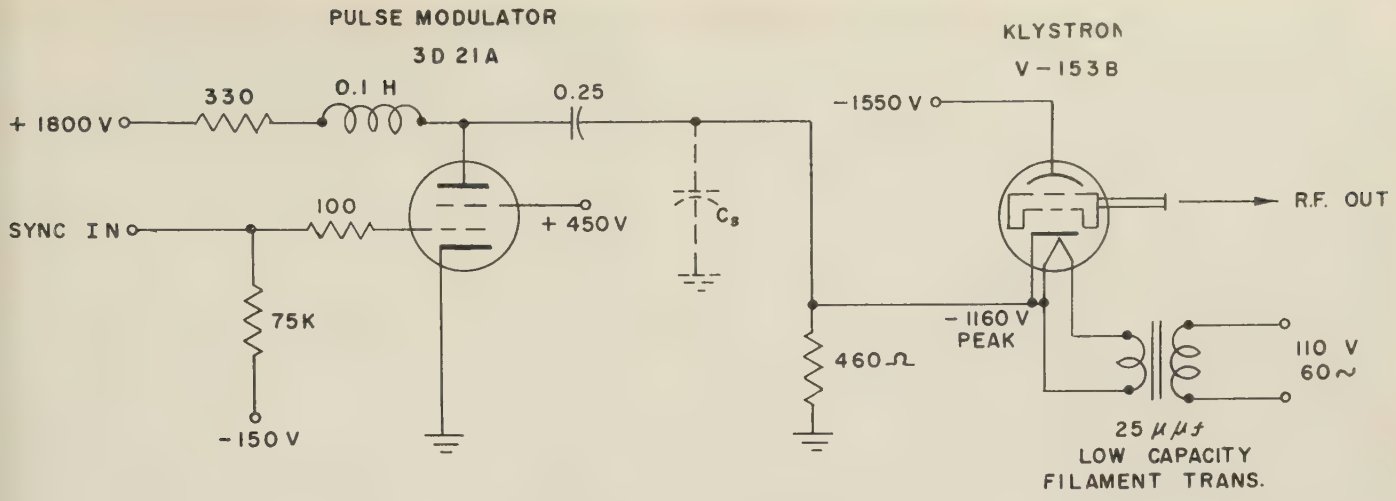

Fig. 2—Klystron beam pulsing.

Beam Voltage Pulsing

In pulsing the beam (or cathode) one has to design suitable matching circuitry to match the pulse circuitry to the characteristics of the tube being pulsed. There are, for example, a number of klystrons that operate with 300 volts beam voltage as recommended by the manufacturer, and often have the same operating repeller voltages; however, the amount of beam current drawn by the tubes could be significantly different. One can deduce, therefore, that even though several klystrons may have the same static operating voltages, the pulse impedance of the cathode or beam element of the klystrons may vary widely. The design of the pulse circuitry (Fig. 2) for optimum pulsing of the beam element of the klystron would be very similar to that of a magnetron pulser because of the requirement of operating into a circuit with a complex impedance. This has led to a compromise in impedance matching of the output pulse circuit driving the klystron beam element.

Another element of concern in pulsing the beam element of a klystron is the need for a low capacity filament transformer associated with the klystron since, in most cases, the filament is tied to the cathode of the klystron and would bypass to ground any video pulse applied to the cathode filament circuit. In general, the following conclusions were reached in pulsing the beam element of a klystron.

The detected rf video pulse seemed to have good fidelity as compared with the applied modulating video pulse, but the spectrum had no noticeable nulls generally associated with the spectrum analysis of a theoretical rectangular video pulse. It seemed to have the same kind of spectrum as associated with a theoretical applied Gaussian video pulse. This is undoubtedly due to an apparent time constant phenomenon of the beam circuit wherein the cathode circuit could not follow the rise time associated with the applied video pulse. It can be surmised that the cathode emission characteristics, electronic optics geometry, and klystron mode operation would influence this pulse characteristic of the beam element of the klystron. Some of the advantages of pulsing the beam of the klystron are: 1) The elimination of a typical high current beam power supply since the average power under pulse condition would be low; 2) The cooling blower needed with most klystrons is unnecessary because of the low average applied power.

It was also observed that as a result of the tube running relatively cool, changes of frequency due to ambient temperature variations were negligible as compared with its normally higher temperature operation during cw oscillation.

Of particular importance in beam voltage pulsing of the reflex klystrons is the fact that this technique lends itself to a very high rf peak power generation. Since the average power generated by a klystron under normal pulse operation is low, the operation of the pulse klystron at higher than rated voltages and currents is possible without exceeding the average power requirements of the tube.

The limits of the applied pulse voltage are primarily determined by the value at which voltage arc-over occurs and the point at which the maximum peak cathode current has been reached. Normally, the arc-over limit occurs first, but it is possible to provide high voltage insulation by immersing the klystron in an oil bath. This facilitates the application of higher pulse voltage necessary for peak cathode current operation. The maximum duty cycle is generally determined from the value of the maximum allowable average dc power input called out by the klystron operating characteristics. The average dc power input can be expressed by the following formula:

$$\text{Average dc power input} = (E_b)(I_b)\ \text{(Duty Cycle)}$$

It is noted that the higher the desired value of peak power required, the lower is the duty cycle and conversely, the lower the desired peak power, the higher is

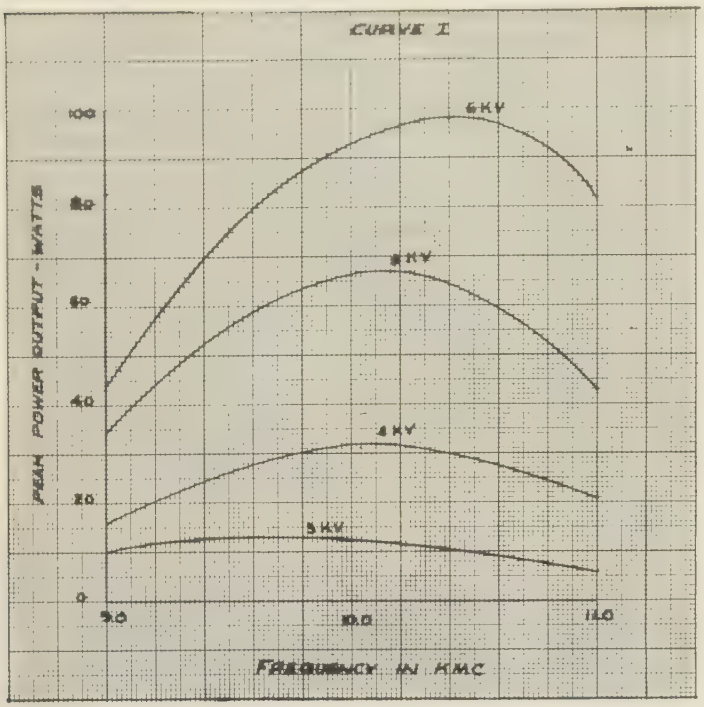

Fig. 3—2K39 pulsed power output: Curve 1—Frequency vs peak power output for various values of beam voltage. (Best mode used at each frequency. Results of three tubes averaged.)

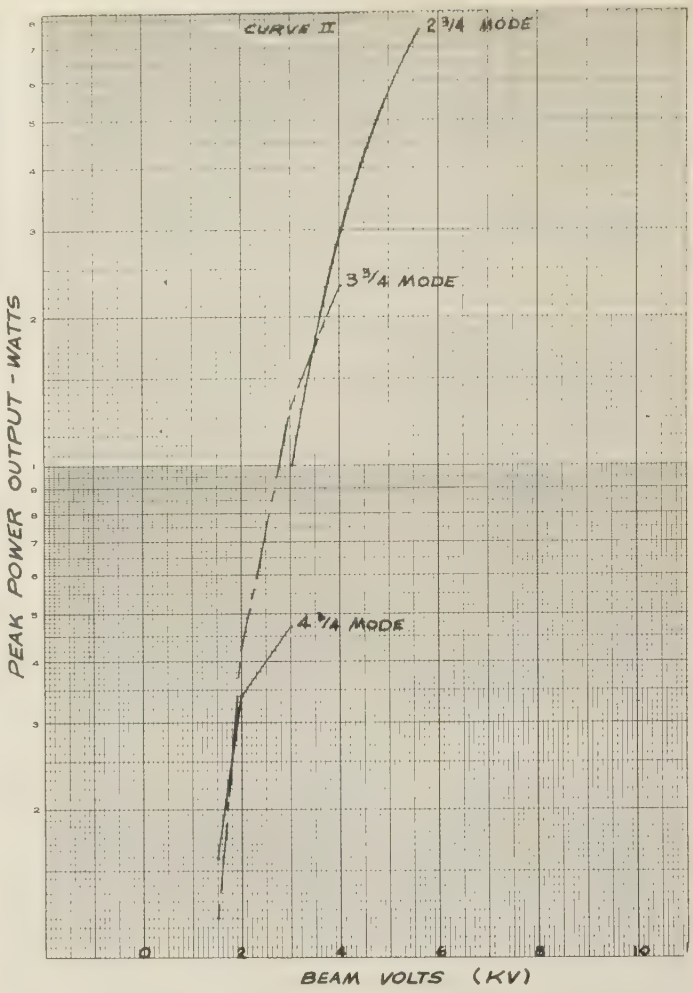

Fig. 4—2K39 klystron, frequency 9,600 mc: Curve 2—Beam voltage vs peak power output for various modes of operation.

the duty cycle. During high power pulse operation, no need for additional cooling other than that called for by cw operation is required, as long as the average input power remains the same as that recommended for cw operation. Under these operating conditions, it is felt that pulse operation will not appreciably affect the life of the klystron.

Data has been taken on the 2K39 and 2K43 reflex klystron in pulse operation,[4] and a summary of test results, will be shown graphically. In general, the pulse operation of the 2K39 reflex klystron indicated that peak power in the order of 50 to 100 watts can be achieved in the frequency range of 9 to 11 kc with applied beam voltage between 5 and 6 kilovolts. The klystron testing was carried out using a pulse repetition rate of 500 cycles per second. The rise time of the rf pulse enevelope was 0.3 microseconds and the beam voltage was about 5,000 volts. It was found that the pulse rise time did not appear to vary appreciably with load, mode, or frequency as long as the klystron was not coupled too tightly to the load. The attached curves (Figs. 3, 4, and 5) show in detail the data that was collected on 2K39 reflex klystron in pulse operation. The other klystron testing for pulse operation was the 2K43 klystron. The 2K43 Klystron is a "C" Band klystron having a minimum tuning range of 4,200 to 5,700 mc, and the typical cw operating characteristics are described as follows: Beam voltage 1,000 volts, Beam current 45 milliamperes, Power output 0.25 watts over the tuning range. The particular klystron selected for pulse operation was first tested in normal cw operation at 5,070 mc with 1,000 volts on the beam and 1,350 volts on the repeller. The average power output under these conditions was 0.50 watt. When the beam and repeller elements were pulsed to the same cw operating voltages a peak power of 0.50 watt was measured. A PRR of 500 cps and pulse length of 2 microseconds was used for the pulse operation. By increasing the peak beam voltage, to 4,000 volts and remaining in the same repeller mode with a repeller voltage of 4,380 volts, the peak power output was increased to 18 watts. This follows closely the equation $Po = KE^{5/2}$ which governs the increase of power with beam voltage.

With the same applied beam voltage, the frequency was changed to 5,380, 5,600, and 6,000 mc. Under these conditions the power output was the same or greater. At 5,380 mc, a peak power output of 38 watts was obtained with a repeller voltage of 4,800 volts. It was noted that higher voltage repeller modes were more sensitive to external circuit loading and a variable susceptance tuner was used to optimize the load. Fig. 6 (Curve 4) shows a plot of beam voltage versus repeller voltage for four repeller modes.

Further testing at a PRR of 1, 2, and 4 kc did not result in any change in peak power output. At 4,000 volt beam operation the cathode current density was calculated to be 0.91 amps/cm-2 and the area of the cathode determined to be approximately 0.4 square centi-

[4] Notes on "Pulse Operation of 2K Series Klystrons," Sperry Gyroscope Corp., January 8, 1951.

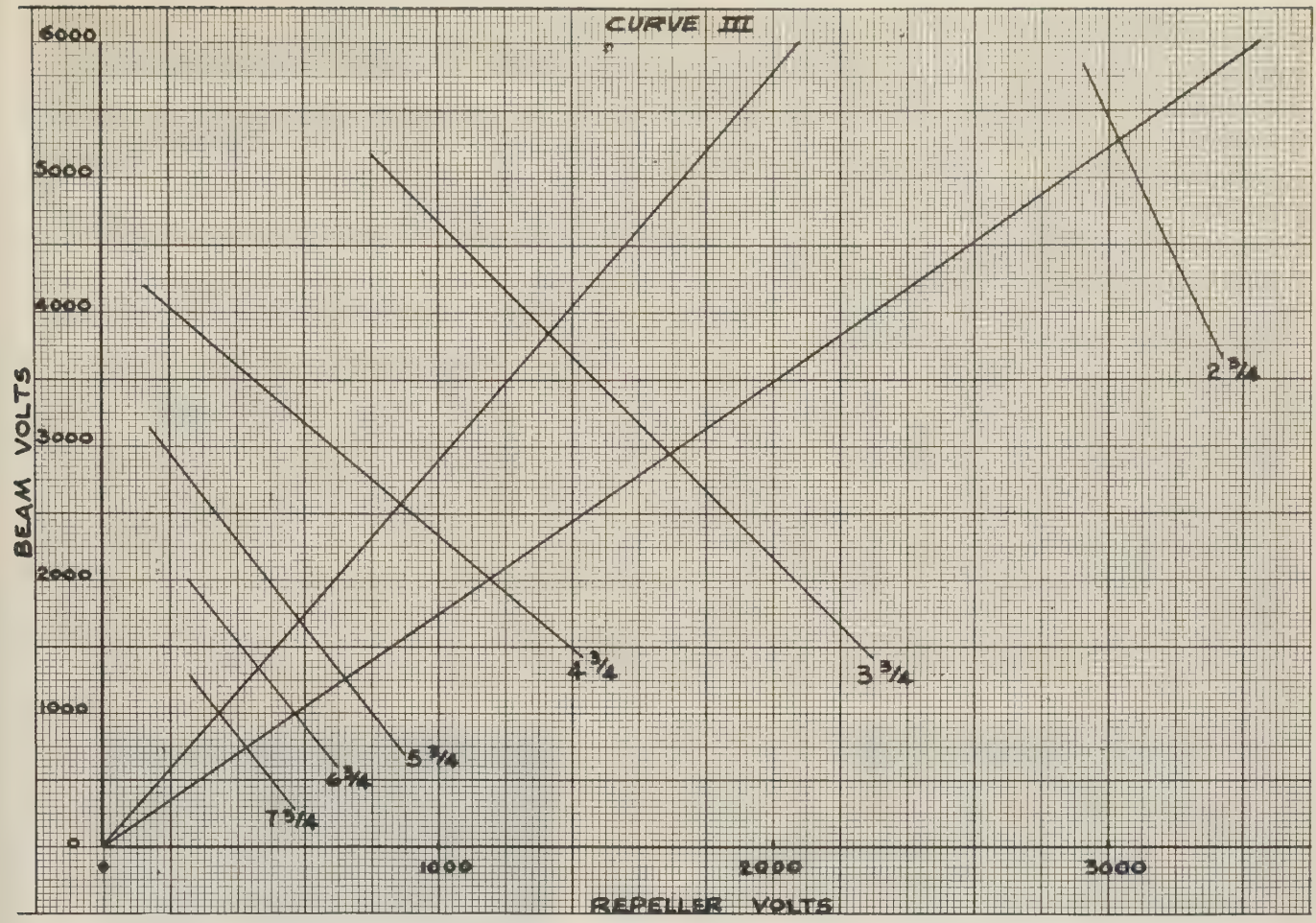

Fig. 5—2K39 klystron, pulsed frequency 9,600 mc: Curve 3—Repeller voltage vs beam voltage for various modes of oscillation.

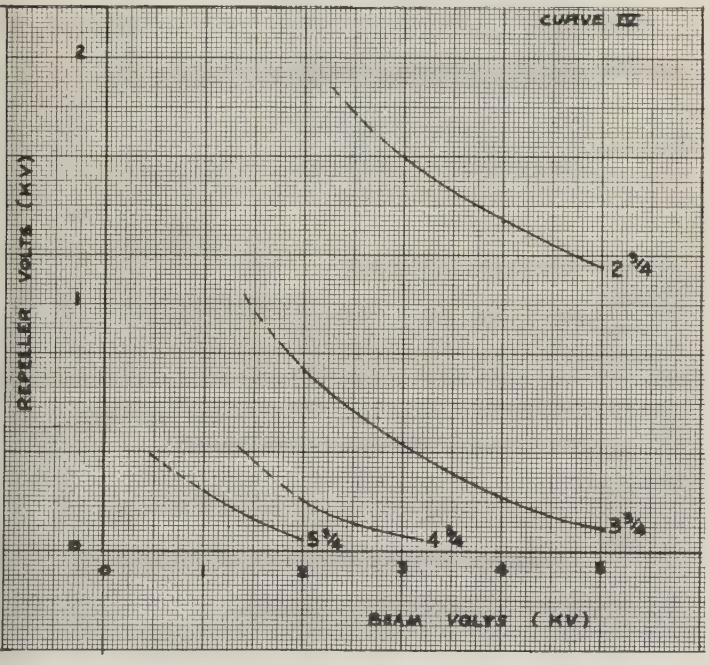

Fig. 6—2K43 klystron repeller modes, frequency 6,000 mc: Curve 4—Beam voltage vs repeller voltage for four repeller modes.

meters. To limit the repeller current to a safe operating value a parallel RC network was placed in the repeller circuit. The time constant of the RC circuit was chosen so that it was large compared to the maximum applied pulse width.

It was interesting to note that at these voltages the klystron showed no evidence of arc-over. It was also noted that as the beam voltage was increased to 5,000 volts the power output was not appreciably greater than that for 4,000 volt operation. It is suspected that klystron efficiency was dropping off at a higher beam voltage due to cathode emission limitations. Some of the disadvantages of pulsing the beam are listed below:

1) Most production klystrons currently being manufactured appear to have slightly different mode characteristics, average current characteristics, and rf matching characteristics. When optimizing the pulse circuitry for a particular klystron, there can be no assurance that any two klystrons of the same stock number will behave similarly in the same pulse circuit. This is true because the beam currents, and therefore the beam impedances, in general differ. This presents a handicap to the circuit designer who endeavors to design equipment needing a minimum of adjustments during maintenance and replacements of faulty components.
2) When pulsing beam element of a klystron, a special low capacity filament transformer is required.
3) The rf pulse is noticeably shorter than the applied video modulating pulse.
4) Modulation sensitivity of beam element is generally one-fifth that of klystron repeller modulation.

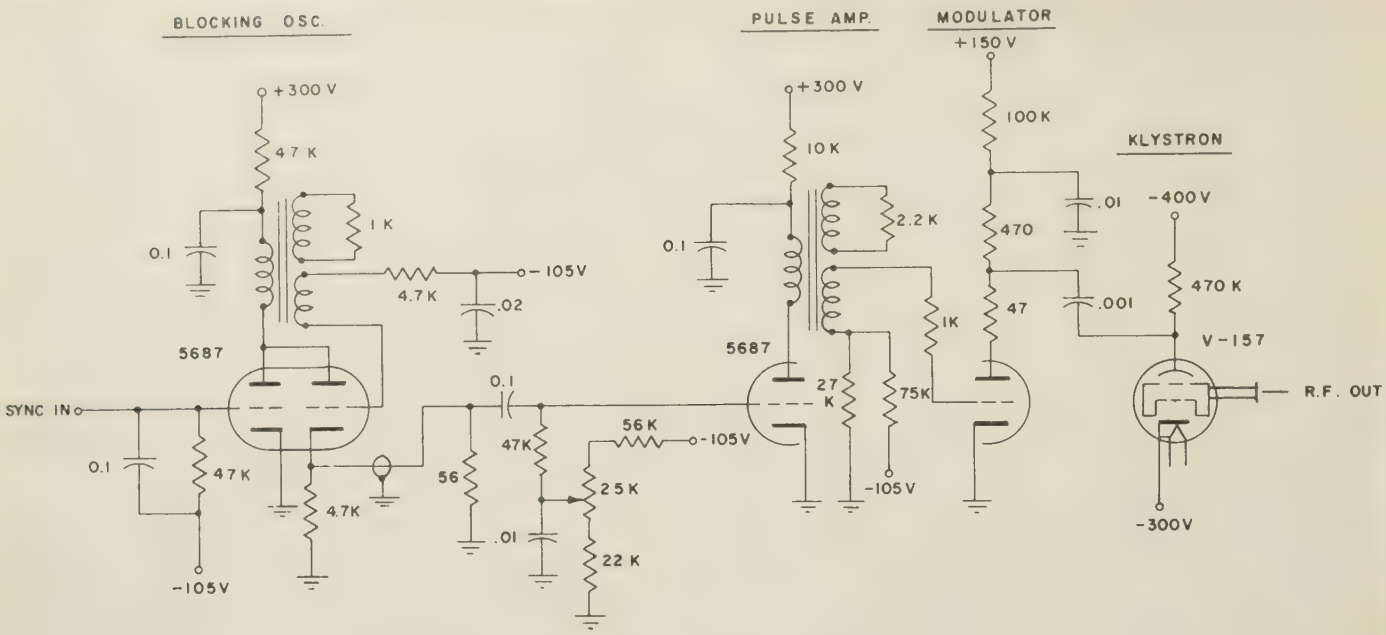

Fig. 7—Klystron repeller pulsing.

Repeller Voltage Pulsing

Pulsing the repeller of a klystron has presented the best results to pulse modulation operation. The repeller, being a high impedance circuit, does not require the special adjustment of the associated modulating pulse circuitry (Fig. 7) as for pulsing the beam element of a klystron. For this reason, interchangeability of klystrons in modulating circuitry could be rapidly accomplished without the requirements for circuit readjustment. Some of the advantages of pulsing the repeller element of the klystron are listed below:

1) It gives the best spectrum with the least amount of pulse shortening to the applied video modulating pulse.
2) It has the highest modulation sensitivity. This is particularly important when the tube is used in afc circuitry where the frequency of the klystron is controlled by changes in modulation voltage to the repeller.
3) Pulsing the repeller element does not require any special filament transformer.

Some of the disadvantages of pulsing the repeller are:

1) It requires a high current beam voltage supply.
2) High peak powers equivalent to beam pulsing cannot be realized.
3) A cooling blower is generally required.

RF Priming Technique

As a result of this background, attempts were made in the laboratory to determine optimum pulse techniques to yield minimum pulse shortening and leading edge jitter as evidenced by monitoring the detected video pulse, and qualitatively by noting the observed spectrum. Several approaches to this problem were tried,

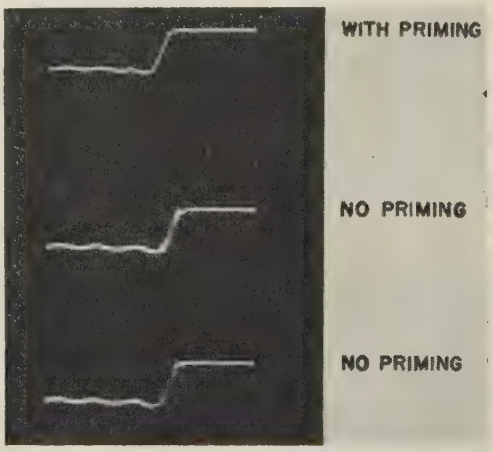

Fig. 8—Effects of priming on rf leading edge jitter.

with one yielding the best results. The technique of supplying a small amount of rf power into the cavity of the klystron to be pulsed appeared to clear up all discernible pulse jitter and pulse shortening as evidenced by observation of the detected video pulse as shown by Fig. 8. The amount of energy required to prime the pulse klystron was surprisingly small. Table I shows

TABLE I

Priming Frequency vs Priming Level Below Peak Pulse Power

Frequency (mc)	Primary level
9100	−10 db
9200	−25 db
9300	−34 db
9340	−40 db
9400	Jitter did not clear up
9500	Jitter did not clear up

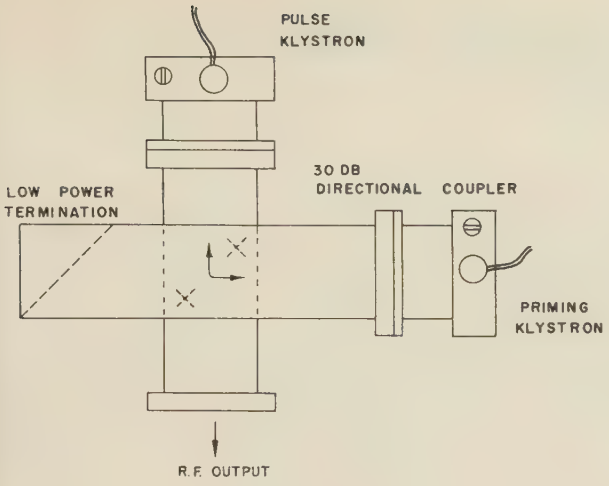

Fig. 9—Klystron priming circuit.

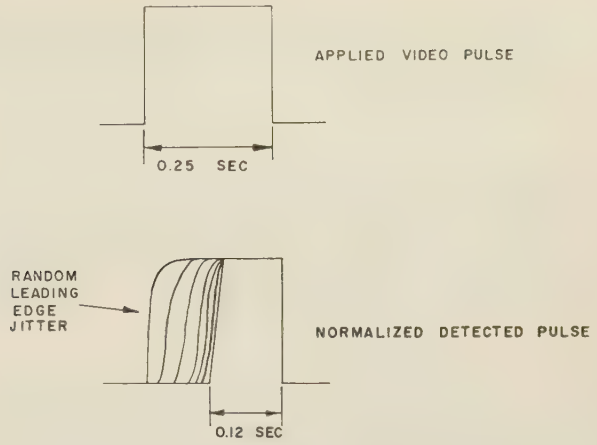

Fig. 10—X-26E klystron pulse shortening.

relative power and frequency required to prime pulse klystron. Pulsed klystron was operated at 9,360 mc and generated about +20 dbm of peak pulse power.

In general, it was observed that the frequency of the priming cw energy should be lower than the frequency of the pulse klystron and that it need be only of a very low power level. Applying priming rf above the operating frequency did not seem to clear up pulse jitter and pulse shortening. The cw priming signal was injected into the pulse klystron by means of a directional coupler (as shown in Fig. 9) but could have been injected just as well by applying some rf energy to the repeller lead of the klystron.

Fig. 8 shows the effects of cw priming of the pulse klystron. With priming there seems to be no evidence of rf leading edge jitter. Without priming the statistical leading edge jitter can be easily discerned. The synchroscope sensitivity was calibrated to be 25 millimicroseconds per centimeter and the pulse rise time was measured to be about .020 microsecond.

One other method of priming the klystron was tried, but was only a laboratory interest. In general, the technique of pulsing the repeller is accomplished by setting the static repeller voltage between operating modes of the klystron and applying a pulse to the repeller element, thus gating the tube into operation. By setting the static repeller voltage just at the edge of the lower mode of oscillation so that a very minute amount of energy was generated, and then pulsing into the middle of the next higher order mode, the jitter and pulse shortening problem was cleared up. This technique makes full use of rf energy from the lower klystron mode to prime the klystron for a higher order mode pulse operation. This technique is not recommended for equipment use because of the stringent requirements for stabilized voltages and possible spurious oscillations of the klystron operating in this marginal manner.

In one case where a 0.25-microsecond pulse was applied to the repeller of an X-26E klystron, the detected rf video pulse was only 0.12 microsecond long as shown in Fig. 10 with about 0.10 microsecond leading edge jitter. By the injection of a small amount of rf energy through a directional coupler into the cavity of the pulse klystron, the detected rf pulse assumed the 0.25-microsecond video pulse width applied to the klystron with no noticeable leading edge jitter. The minimum discernible leading edge jitter that could be accurately measured with the techniques used in this experiment was in the order of 5 millimicroseconds.

Conclusions

Rf circuit designer in selecting klystrons for pulse operation should thoroughly investigate pulse characteristics of several klystrons before making a firm choice.

External circuitry influencing the rf loading of the klystron, quality of the applied video modulating pulse, and the proper selection of klystron mode of operation are of prime importance in pulsing low power klystrons.

For generating high rf peak pulse power, beam element pulsing is recommended. Where rf pulse fidelity is required, repeller pulsing is recommended. Only in special cases where klystron tuning is accomplished during high pulse power operation, is simultaneous repeller and beam element pulsing recommended.

Acknowledgment

I wish to thank Hycon Manufacturing Company for its cooperation in making data and photographs available, Sperry Gyroscope Company and Varian Associates for their technical assistance, and the members of the Technical Staff at Litton Industries for their encouragement and cooperation necessary to prepare the paper.

Bibliography

[1] Harrison, A. E., *Klystron Tubes*. New York, McGraw-Hill Book Co., Inc., 1947.
[2] *Radar Systems and Components* (Bell Telephone Laboratories). New York, D. Van Nostrand Company, Inc., 1949.
[3] Sarbacher, R. I., and Edson, W. A., *Hyper and Ultra High Frequency Engineering*. New York, John Wiley & Sons, Inc., 1943.
[4] Ramo, S., and Whinnery, J. R., *Fields and Waves in Modern Radio*. New York, John Wiley & Sons, Inc., 1943.
[5] Hamilton, D. R., Knapp, J. K., and Kuper, J. B., *Klystrons and Microwave Triodes*. New York, McGraw-Hill Book Co., Inc., 1947.

Some Properties of Image Circles

H. F. MATHIS†

Summary—Some properties of image circles for four-terminal networks are discussed. A procedure for correcting an image circle, obtained with a lossy short, is presented. Indirect methods for determining the open and short circuit impedances of a symmetrical four-terminal network are discussed.

The Image Circle

THE IMAGE circle for a linear and bilateral four-terminal network, or two-port waveguide structure, is obtained in the following manner:

a) A variable reactance, or a movable short, is connected to the output terminals, or port. It is assumed that the reactance, or short, is lossless.

b) The input impedances, or voltage reflection coefficients, for several values of reactance, or positions of the short, are measured.

c) The input impedances, or reflection coefficients, are plotted on a circular transmission line chart; *i.e.*, Smith ($R-X$) or Carter ($Z-\theta$) chart, or polar graph paper.[1] Any convenient normalizing impedance can be used with the transmission line chart.

d) The image circle is drawn through these points. If all of the points do not lie on a circle, this is due to experimental errors. Hereafter, it is assumed that the image circle is drawn on a Smith chart.

The image circle has several interesting properties which were discussed in many papers and research reports. Here two experimental procedures are presented making use of the image circle. Theoretical basis for these is discussed in Appendix. Before presenting these procedures, it is desirable to consider the input impedance when network is terminated in a resistance.

Input Impedance for Resistive Load

The input impedance $\boldsymbol{Z}_A$, when the network is terminated in a resistance R_2, can often be determined by direct measurement. If R_2 is the characteristic impedance of the transmission line or waveguide containing the movable short, the input impedance can be determined by indirect methods which make use of the image circle.[2–5] These methods do not require that the image circle be obtained with a lossless short.

These indirect methods pair points on the image circle corresponding to positions of the movable short which are separated by one-quarter wavelength. The *cross-over point*, which is used later, is defined as the intersection of the straight lines connecting these pairs of points. If the network is terminated in a variable reactance, these indirect methods can be used if the points on the image circle corresponding to the reactances X and $-R_2^2/X$ are paired.

A Procedure for Correcting an Image Circle Obtained with a Lossy Short

The magnitude Γ of the voltage reflection coefficient of the short is determined. The points for the image circle are plotted. The center $\boldsymbol{Z}_B$ of the image circle is located and the image circle is drawn, as shown in Fig. 1. The value of the input impedance $\boldsymbol{Z}_A$ for R_2 equal to the characteristic impedance of the line containing the movable short is determined and plotted.

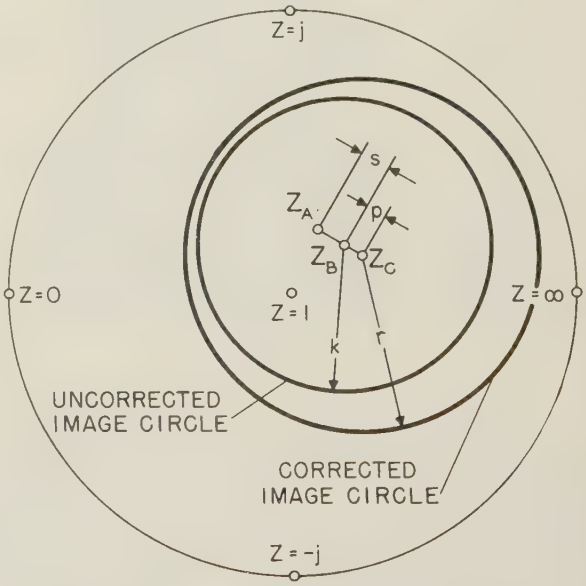

Fig. 1—A circular impedance diagram that illustrates the procedure for correcting an image circle.

The radius k of the image circle and the distance s between the points $\boldsymbol{Z}_A$ and $\boldsymbol{Z}_B$ are measured. The value of

$$p = \frac{(1 - \Gamma^2)k^2 s}{\Gamma^2 k^2 - s^2} \tag{1}$$

is calculated. The center $\boldsymbol{Z}_C$ of the corrected image circle is located on the straight line through $\boldsymbol{Z}_A$ and $\boldsymbol{Z}_B$, as shown in Fig. 1. The point $\boldsymbol{Z}_B$ always lies between $\boldsymbol{Z}_A$ and $\boldsymbol{Z}_C$. The radius r of the corrected image circle is given by

† Aerophysics Dept., Goodyear Aircraft Corp., Akron, Ohio.

[1] The reader should recall that plotting impedances on a circular transmission line chart is equivalent to plotting voltage reflection coefficients.

[2] G. A. Deschamps, "A new chart for the solution of transmission line and polarization problems," Trans. IRE, vol. MTT-1, pp. 5–13; March, 1953; also, *Electrical Communications*, vol. 30, pp. 247–54; September, 1953.

[3] G. A. Deschamps, "Determination of reflection coefficients and insertion loss of a waveguide junction," *Jour. Appl. Phys.*, vol. 24, pp. 1046–50; August, 1953; also, *Electrical Communications*, vol. 31, pp. 57–62; March, 1954.

[4] G. A. Deschamps, "A Hyperbolic Protractor for Microwave Impedance Measurements and Other Purposes," Federal Telecommunication Laboratories, Nutley, N. J.; 1953.

[5] J. E. Storer, L. S. Sheingolb, and S. Stein, "A simple graphical analysis of a two-port waveguide junction," Proc. IRE, vol. 41, pp. 1004–13; August, 1953.

$$r = \frac{(k^2 - s^2)\Gamma k}{\Gamma^2 k^2 - s^2}. \tag{2}$$

Finally, the corrected image circle is drawn using the center Z_C and the radius r.

Indirect Procedures for Determining Z_{sc} and Z_{oc} of a Symmetrical Four-Terminal Network

For some convenient value of R_2, the value of Z_A is determined. The points for the image circle and the point Z_A are plotted, using R_2 as the normalizing impedance. The center Z_C of the image circle is located and the image circle is drawn, as shown in Fig. 2.

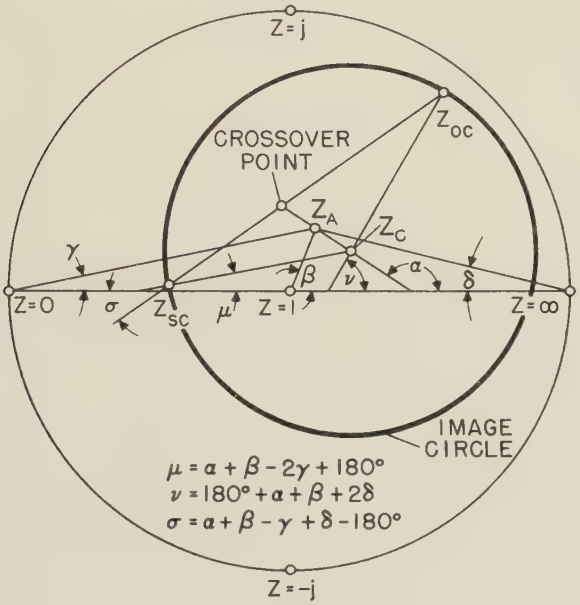

Fig. 2—A circular impedance diagram that illustrates the graphical procedure for determining Z_{sc} and Z_{oc}.

Straight lines are drawn through the points Z_A and the points Z_C, $Z=0$, 1, and ∞. The angles α, β, γ, and δ are measured. Lines are drawn through the points Z_C which makes the angles

$$\mu = \alpha + \beta - 2\gamma - 180° \tag{3}$$

and

$$\nu = \alpha + \beta + 2\delta + 180° \tag{4}$$

with the $X=0$ line. The intersections of these lines with the image circle are Z_{sc} and Z_{oc}, respectively.

If the crossover point is known, the line through this point which makes the angle

$$\sigma = \alpha + \beta - \gamma + \delta - 180° \tag{5}$$

with the $X=0$ line intersects the image circle at Z_{sc} and Z_{oc}. When the crossover point is above the $X=0$ line, the point Z_{sc} is nearer the $X=0$ line if $0<\sigma<180°$ and Z_{oc} is nearer if $180°<\sigma<360°$. When the crossover point is below the $X=0$ line, Z_{oc} is nearer the $X=0$ line if $\sigma<\sigma<180°$ and Z_{sc} is nearer if $180°<\sigma<360°$. If $0=0$, Z_{sc} is left of Z_{oc}; and if $\sigma=180°$, Z_{sc} is right of Z_{oc}.

The triangles whose vertices are $Z=0$, Z_{oc}, $1/Z_{sc}$, and $Z=0$, Z_A, $1/Z_A$ should be similar. These triangles can be drawn and used to check the results.

The values of Z_{sc} and Z_{oc} can also be determined from the values of Z_A and Z_C by using

$$Z_{sc} = \frac{(Z_A + \bar{Z}_A)Z_C - Z_A\bar{Z}_A(1 + Z_C)}{Z_A - \bar{Z}_A Z_C} \tag{6}$$

and

$$Z_{oc} = \frac{Z_A - \bar{Z}_A Z_C}{1 - Z_A - \bar{Z}_A + Z_C}, \tag{7}$$

where $\bar{Z}_A$ is the conjugate of Z_A. Let K_A, $\bar{K}_A$, and K_C denote the voltage reflection coefficients corresponding to Z_A, $\bar{Z}_A$, and Z_C, respectively. Eqs. (6) and (7) are equivalent to

$$Z_{sc} = -\frac{K_A + \bar{K}_A - K_C + K_A\bar{K}_A(K_C + 2)}{K_A - \bar{K}_A - (1 - K_A\bar{K}_A)K_C}, \tag{8}$$

$$Z_{oc} = -\frac{K_A - \bar{K}_A - (1 - K_A\bar{K}_A)\bar{K}_C}{K_A + \bar{K}_A - K_C + K_A\bar{K}_A(K_C - 2)}, \tag{9}$$

$$K_{sc} = \frac{K_A - K_C + K_A\bar{K}_A(K_C + 1)}{\bar{K}_A + K_A\bar{K}_A}, \tag{10}$$

and

$$K_{oc} = -\frac{K_A - K_C + K_A\bar{K}_A(K_C - 1)}{\bar{K}_A - K_A\bar{K}_A}. \tag{11}$$

The writer has found that the graphical procedure which was described first gives the most accurate results of any of the procedures presented in this paper for determining Z_{sc} and Z_{oc}.

Appendix

General Theory

According to well-known circuit theory, the input impedance Z_1 and the load impedance Z_2 of a linear and bilateral four-terminal network are related by

$$Z_1 = \frac{AZ_2 + B}{CZ_2 + D}. \tag{12}$$

Let K_1 denote the voltage reflection coefficient at the input terminals relative to the resistance R_1; *i.e.*

$$K_1 = \frac{Z_1 - R_1}{Z_1 + R_1}; \tag{13}$$

and let K_2 denote the voltage reflection coefficient at the output terminals relative to the resistance R_2; *i.e.*

$$K_2 = \frac{Z_2 - R_2}{Z_2 + R_2}. \tag{14}$$

Eqs. (12)–(14) can be combined to obtain

$$K_1 = \frac{aK_2 + b}{cK_2 + d}. \tag{15}$$

Eqs. (12) and (15) are called bilinear transformations. Bilinear transformations map circles into circles.

Eq. (15) can be written

$$K_1 = \frac{a\bar{c}K_2\bar{K}_2 - b\bar{d}}{c\bar{c}K_2\bar{K}_2 - d\bar{d}} - \frac{(\bar{cK_2 + d})(ad - bc)K_2}{(cK_2 + d)(c\bar{c}K_2\bar{K}_2 - d\bar{d})}, \quad (16)$$

where the bars above the symbols denote conjugates. If K_2 lies on a circle whose center is at the origin and whose radius is Γ, it follows from (16) that K_1 lies on a circle whose center K_B and radius k are given by

$$K_B = \frac{a\bar{c}\Gamma^2 - b\bar{d}}{c\bar{c}\Gamma^2 - d\bar{d}} \quad (17)$$

and

$$k = \left| \frac{ad - bc}{c\bar{c}\Gamma^2 - d\bar{d}} \right| \Gamma. \quad (18)$$

If $Z_2 = jX$, where X is a variable reactance; K_2 lies on the circle defined by $\Gamma = 1$ and K_1 lies on the circle which is called the image circle. The center and radius of the image circle are denoted by K_C and r, respectively. When $Z_2 = R_2$, $K_2 = 0$, and (15) reduces to

$$K_A = b/d. \quad (19)$$

If the image circle is obtained with a lossy short, $\Gamma < 1$. In this case, (17)–(19) can be solved for $a\bar{c}$, $b\bar{d}$, $c\bar{c}$, and $d\bar{d}$ to obtain

$$a\bar{c} = \frac{\Delta[k^2K_A - (k^2 - s^2)K_B]}{\Gamma k(k^2 - s^2)}, \quad (20)$$

$$b\bar{d} = \frac{\Delta\Gamma k\, K_A}{k^2 - s^2}, \quad (21)$$

$$c\bar{c} = \frac{\Delta s^2}{\Gamma k(k^2 - s^2)}, \quad (22)$$

and

$$d\bar{d} = \frac{\Delta\Gamma k}{k^2 - s^2}; \quad (23)$$

where

$$|\Delta| = |ad - bc| \quad (24)$$

and

$$s = |K_A - K_B|. \quad (25)$$

The center of the corrected image circle is given by

$$K_C = \frac{a\bar{c} - b\bar{d}}{c\bar{c} - d\bar{d}} = K_B + (p/s)(K_B - K_A), \quad (26)$$

where p is given by (1). The radius r is given by

$$r = \left| \frac{\Delta}{c\bar{c} - d\bar{d}} \right| = \frac{(k^2 - s^2)\Gamma k}{\Gamma^2k^2 - s^2}. \quad (2')$$

Thus (1) and (2) can be used to correct an image circle which was obtained with a lossy short.

In the following discussion, it is assumed that the four-terminal network is symmetrical. Now, $A = D$ and $b = -c$. The center K_C of the image is given by

$$K_C = -\frac{a\bar{b} + b\bar{d}}{b\bar{b} - d\bar{d}}. \quad (27)$$

Eqs. (19) and (27) can be solved for a/d to obtain

$$\frac{a}{d} = -\frac{K_A - (1 - K_A\bar{K}_A)K_C}{\bar{K}_A}. \quad (28)$$

If $Z_2 = 0$, $K_2 = -1$ and (15) can be written

$$K_{sc} = -\frac{\frac{a}{d} - \frac{b}{d}}{\frac{b}{d} + 1}. \quad (29)$$

If the values of a/d and b/d given by (28) and (19) are substituted in (29), the result is (10). When $Z_2 = \infty$, $K_2 = 1$ and (15) can be written

$$K_{oc} = -\frac{\frac{a}{d} + \frac{b}{d}}{\frac{b}{d} - 1}. \quad (30)$$

If the values of a/d and b/d given by (28) and (19) are substituted in (30), the result is (11). Eqs. (6)–(9) can be obtained from (10) and (11).

It follows from (10) and (11) that

$$K_{sc} - K_C = \frac{(K_A - K_C)(1 + \bar{K}_A)}{\bar{K}_A(1 + K_A)}, \quad (31)$$

$$K_{oc} - K_C = -\frac{(K_A - K_C)(1 - \bar{K}_A)}{\bar{K}_A(1 - K_A)}, \quad (32)$$

and

$$K_{sc} - K_{oc} = 2\frac{(K_A - K_C)(1 - K_A\bar{K}_A)}{\bar{K}_A(1 + K_A)(1 - K_A)}. \quad (33)$$

The angles of the vectors in (31)–(33) must satisfy

$$\angle(K_{sc} - K_C) = \angle(K_A - K_C) + \angle K_A - 2\angle(1 + K_A), \quad (34)$$

$$\angle(K_{oc} - K_C) = 180° + \angle(K_A - K_C) + \angle K_A - 2\angle(1 - K_A), \quad (35)$$

and

$$\angle(K_{sc} - K_{oc}) = \angle(K_A - K_C) + \angle K_A - \angle(1 + K_A) - \angle(1 - K_A). \quad (36)$$

Eqs. (34)–(36) are equivalent to (3)–(5).

It follows from (10) and (11) that

$$\frac{1 + K_{oc}}{1 - K_{sc}} = \frac{1 + K_A}{1 - K_A}. \quad (37)$$

This equation requires that the triangles $(-1, K_{oc}, -K_{sc})$ and $(-1, K_A, -K_A)$ be similar. This is equivalent to requiring that the triangles whose vertices are $Z = 0$, Z_{oc}, $1/Z_{sc}$ and $Z = 0$, Z_A, $1/Z_A$ be similar.

Determination of the Parameters of Cavities Terminating Transmission Lines

R. A. LEBOWITZ†

Introduction

PAST methods available for measuring parameters of cavities terminating transmission lines are often considered too involved for production line testing.[1,2] One common method requires many individual standing wave ratio measurements at frequencies slightly lower and higher than the resonant frequency of the cavity. These measurements take not only an excessive length of time but also require an accurately controlled variable frequency oscillator for precision measurements. A second method in which an oscillographic display of reflected power is used, while much faster, requires more complicated equipment and calls for use of unconventional measurement procedures.

The method presented herein was devised to meet time and accuracy requirements on the production line. Its speedy results can be obtained from equipment and calculations with which production line personnel are familiar. Use is made of the same common sweep frequency method utilized in testing transmission and absorption cavities. This paper presents a derivation of the theory of the method, a description of the apparatus used, and a comparison of the results obtained with this and the point by point method.

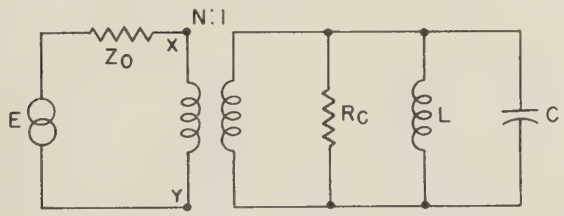

Fig. 1—Simplified equivalent circuit of cavity.

Theory

Cavity Coupling Factor

An equivalent circuit of a cavity that terminates a radio frequency transmission line of characteristic impedance Z_0 is illustrated in Fig. 1. Here, it is assumed that there is no line loss, no resistive loss in the coupling mechanism between the cavity and the line, and that the generator is matched to the line. The points labeled X and Y are considered to be the points on the transmission line at which the cavity presents the impedance Z. The impedance looking into the cavity is

$$Z = \frac{N^2}{\frac{1}{R_c} + j\left[\omega c - \frac{1}{\omega L}\right]} \tag{1}$$

where

R_c = equivalent cavity shunt resistance
L = equivalent cavity shunt inductance
C = equivalent cavity shunt capacitance
N = equivalent transformation between line and cavity.

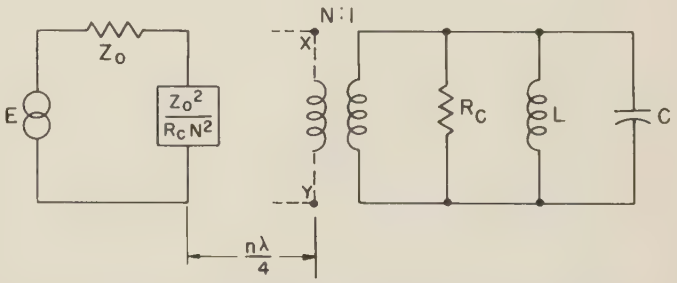

Fig. 2—Equivalent impedance of cavity at resonance at point on line one-quarter wavelength from cavity.

At resonance, $\omega c = 1/\omega L$ and $Z = R_c N^2$. If the voltage across the line is measured at a point on the line an odd multiple of one-quarter wavelengths from the cavity (see Fig. 2), the voltage is

$$E_1 = \frac{\frac{Z_0^2}{R_c N^2} E}{Z_0 + \frac{Z_0^2}{R_c N^2}}. \tag{2}$$

Far from resonance, $Z = 0$ and the impedance across the line an odd multiple of one-quarter wavelengths from the cavity is infinite. In this case, the voltage measured across this point on the line is equal to E.

The ratio of the voltage far from resonance to that at resonance is

$$R = \frac{E}{E_1} = \frac{R_c N^2}{Z_0} + 1. \tag{3}$$

The cavity coupling factor—commonly symbolized as β—is used in specifying the performance of line terminating cavities. It is defined as the normalized cavity impedance at resonance or

† Microwave Product Engrg., Polytechnic Res. and Dev. Co., Inc., Brooklyn 1, N. Y.

[1] C. G. Montgomery, "Technique of Microwave Measurements," McGraw-Hill Book Co., Inc., New York, N. Y., pp. 334–336; 1947.

[2] E. D. Reed, "A sweep frequency method of Q measurement for single-ended resonators," *Proc. NEC*, vol. 7, pp. 162–172; 1951.

$$\beta = \frac{R_c N^2}{Z_0} \tag{4}$$

By substituting β for $R_c N^2/Z_0$ in (3) and rearranging, there results

$$\beta = R - 1. \tag{5}$$

Cavity Q Factor

If it were possible to measure the voltage at the cavity itself, its loaded Q may be found from

$$Q_L = \frac{f_0}{2\Delta f} \tag{6}$$

where f_0 = the resonant frequency of the cavity, Δf = the difference between the resonant frequency and the frequency at which the voltage is .707 of that at resonance. Since it is usually impossible to measure the voltage at the cavity, it may be measured at multiples of a half-wavelength from the cavity.

If the cavity Q is high and the distance between the point of measurement and the cavity is small, negligible error will result. As the distance from the cavity increases and as the Q becomes lower, an error is introduced. This error is caused by the fact that the measurement point is only a multiple of a half-wavelength at one discrete frequency. Thus if the point is exactly a multiple of one-half wavelength for the resonant frequency, it will be slightly more or less for the .707 voltage points. Under these conditions, a correction term must be added to the impedance of the cavity when it is off resonance.

To simplify the expressions, normalized admittance will be used and N will be assumed to be unity. The admittance of the cavity near resonance may be written as

$$Y = G_c + jG_cQ_0\frac{\Delta f}{f_0} \tag{7}$$

and the equivalent circuit of the cavity may be shown as in Fig. 3(a) and 3(b).

At resonance the cavity admittance reduces to $Y = G_c$ and Fig. 3(a) applies at points a multiple of half-wavelength from the cavity.

Near resonance at points a multiple a half-wavelengths from the cavity Fig. 3(d) applies. The correction term[3] added due to the small shift in wavelength is

$$dY = jn\pi\left(\frac{\lambda_g}{\lambda_0}\right)^2(1 - [jy]^2) \tag{8}$$

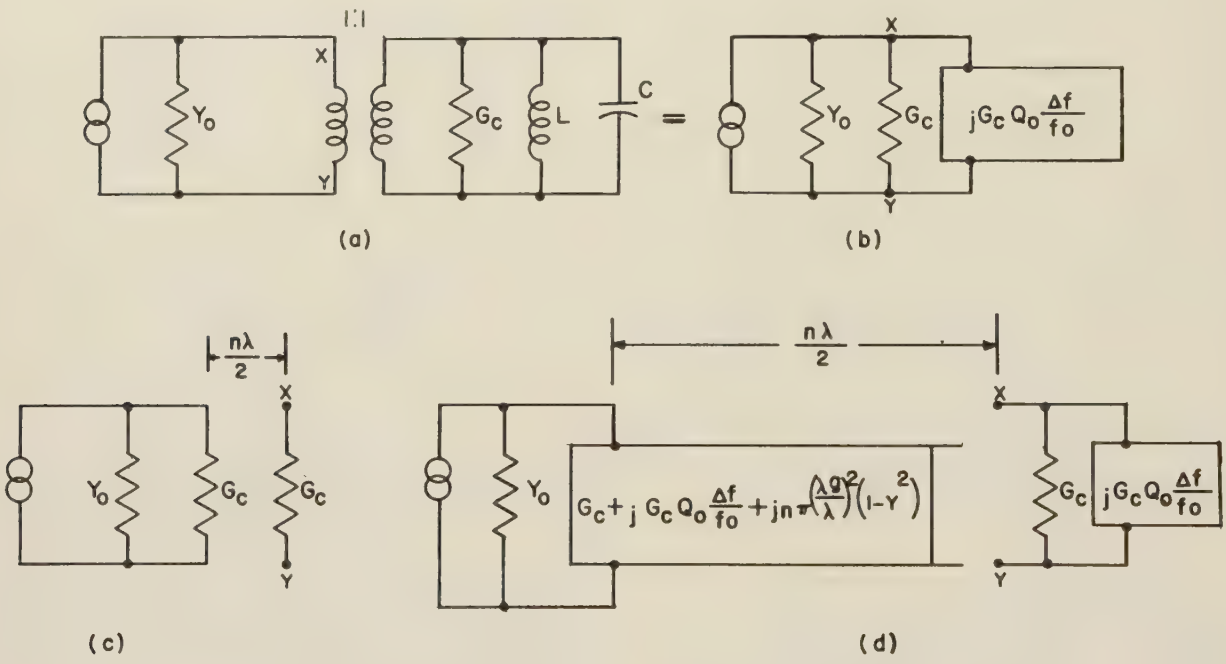

Fig. 3—Equivalent circuit of cavity in terms of admittance.

where

G_c = the conductance of the cavity
n = the number of half wavelengths between the point of measurement and the cavity
λ_g = guide wavelength
λ_0 = free space wavelength.

If the magnitude of the voltage at a frequency Δf from resonance is set equal to $\sqrt{2}/2$ times its magnitude at resonance, there results

$$\frac{.707}{Y_0 + G_c} = \frac{1}{Y_0 + G_c + jG_cQ_0\frac{\Delta f}{f_0} + jn\pi\left(\frac{\lambda_g}{\lambda_0}\right)^2(1 - Y^2)} \tag{9}$$

[3] N. Marcuvitz, "Waveguide Handbook," McGraw-Hill Book Co., Inc., New York, N. Y., p. 13; 1951.

solving for Q^L there finally results

$$Q_L = \frac{f_0}{2\Delta f}\sqrt{1 - 2n\pi\left(\frac{\lambda^g}{\lambda_0}\right)^2\left(\frac{1+\beta}{\beta}\right)\frac{1}{Q_L} - n^2\pi^2\left(\frac{\lambda^g}{\lambda_0}\right)^4\left(\frac{1+\beta^2}{\beta^2}\right)\frac{1}{Q_L{}^2}}\,. \tag{10}$$

Discussion

The equipment used for measurement is very similar to that described by Montgomery,[4] except that a slotted section and probe are placed before the cavity. The output of this probe is used for the vertical deflection of the oscilloscope. The law of the crystal detector must be taken into account when determining the various measured voltages.

The coupling parameter is found by presenting a complete klystron mode on the oscillograph screen, and adjusting the probe in the slotted section to a position a multiple of quarter-wavelengths from the point in the line at which the cavity is effectively a short circuit. This probe position produces a maximum mode height (Fig. 4(a)). The cavity is then tuned so that its dip lies on the center of the mode. The value of R is obtained as shown in Fig. 4(b).

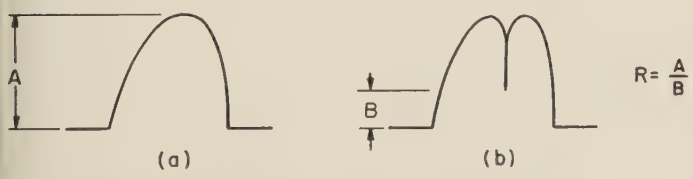

Fig. 4—Oscilloscope patterns obtained when measuring the cavity coupling parameter.

The cavity loaded Q is found by adjusting the probe position to a multiple of half-wavelengths from the cavity. This position is obtained when the mode height on the oscilloscope is made a minimum with the cavity off resonance. The cavity is then tuned to produce a cavity band pass characteristic at the center of the mode. Alternately, if the β measurement had been made first and the cavity and oscillator were set to the correct frequency the probe position may be varied to produce a symmetrical band pass characteristics on the oscilloscope (Fig. 5). The loaded Q of the cavity is then obtained by measuring 2 Δf by any of the well known methods.

The following assumptions were made in deriving the theory of these measurements:

1) Zero line loss between cavity and point of measurement
2) Zero coupling loss
3) High cavity Q factor
4) Negligible probe or voltmeter error and loading
5) Matched generator.

[4] Montgomery, *op. cit.*, p. 396.

At microwave frequencies assumptions 1, 2, 3, and 4 are usually true and 5 can be accomplished by tuning or by using matched attenuators. Hence, the errors in the measurements due to these factors are negligible for production line testing.

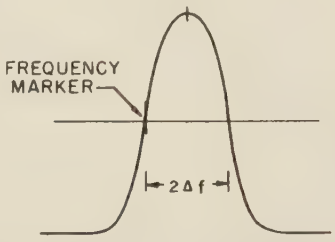

Fig. 5—Oscilloscope pattern obtained when measuring the cavity Q factor.

Tests were made on various cavities at X and C bands with this method and the point by point VSWR method. The apparatus available for the tests by the VSWR method allowed measurement of 2Δf to no better than $\pm$0.8 mc/sec. The results obtained by both methods compare quite well. Table I gives a comparison of the results obtained on C band cavities when the probe was set at a position three half-wavelengths from the cavity.

TABLE I
Comparison of Results by Two Methods

Cavity	Simplified method		Point by point vswr method	
	β	Q_L	β	Q_L
No. 1	0.48	11300	0.50	14000
No. 2	1.00	11300	1.01	11300
No. 3	1.11	6900	1.13	6900
No. 4	0.74	5400	0.74	5650
No. 5	2.16	2350	2.20	2350

A cavity with a loaded Q of 2700 and a coupling parameter of 1.4 was tested for Q at a probe position 9/2 wavelengths from the cavity and at a second point 3/2 wavelengths from the cavity. The difference in measured Q between these two points was $1\frac{1}{4}\% \pm \frac{1}{4}\%$ per wavelength. The theoretical correction using equation 10 is $1\frac{1}{8}\%$. There is good correlation between the measured and theoretical corrections both of which are low. Thus, for most production line measurements the application of the correction is unnecessary, and the loaded Q is obtained from (6).

Acknowledgment

The author wishes to thank Mr. W. E. Waller for his aid in preparing this paper.

Correspondence

"Double-Ridge Waveguide"

Dr. Seymour Cohn has pointed out that the equation for attenuation as shown on page four of the article "Double-Ridge Waveguide for Commercial Airlines Weather Radar Installation"[1] by the undersigned should be corrected to read as follows:

$$\alpha = 6.01 \times 10^{-7} k \sqrt{f} \left(\frac{\frac{1}{b_1} + \frac{2}{a_1}\left(\frac{f_c}{f}\right)^2}{\sqrt{1 - \left(\frac{f_c}{f}\right)^2}} \right) \frac{60\pi^2 \left(\frac{b_1}{a_1}\right)}{Z_{0c}}.$$

Using a value for K of 1.2 which seems reasonable for this geometry, Dr. Cohn has computed the attenuation for the double ridge guide and obtained numbers of 0.0407 decibel per foot at 5,400 mc and 0.028 decibel per foot at 9,375 mc, which agrees rather well with measured data.

I would like to call your attention to the fact that the b_1 in the attenuation formula represents the total height of the ridge waveguide rather than as shown in Fig. 2 of the above article.

T. N. Anderson
Airtron, Inc.
Linden, N. J.

[1] Trans. IRE, vol. MTT-3, pp. 2–9; July, 1955.

On a Variable Impedance Termination for Testing High Power Components

In testing microwave components for electrical breakdown under high power it is generally desirable to simulate conditions encountered in a system. For proper evaluation it is necessary, therefore, to employ a termination, the reflection coefficient of which is variable and which will handle high powers. Our attempt to manufacture a variable mismatch device similar to those described in the literature[1] were unsuccessful, since we could not obtain sufficiently high insertion vswr without electrical breakdown of the tuner.

[1] Ragan, M.I.T., vol. 9, p. 489.

One can introduce a variable reflection coefficient by using a short slot hybrid junction with two of the arms short circuited by movable plungers which are displaced from each other by an angle θ as shown in Fig. 1.

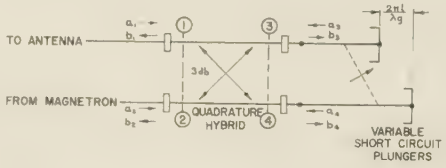

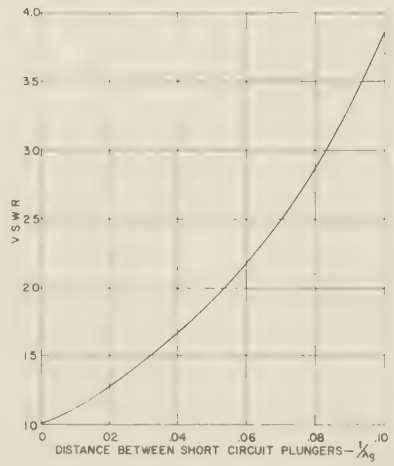

Fig. 1—Insertion vswr of high power phase shifter.

The vswr introduced into the line as a function of $l/\lambda g = \theta/2\pi$ is also shown. A device of this type has been built and used successfully at 250-kw peak power with an insertion vswr of 2:1 without any signs of breakdown.

An analysis of this device can be made employing the scattering matrix $|S|$. If a_1, a_2, a_3, and a_4, are the incident waves on terminals 1, 2, 3 and 4, and b_1, b_2, b_3, and b_4 are the waves scattered from these terminals, then the relationship

$$|S| \; |a| = |b| \tag{1}$$

describes the junction performance.

The scattering matrix is easily written as

$$|S| = \begin{vmatrix} 0 & 0 & -j & e^{-j\theta} \\ 0 & 0 & 1 & -je^{-j\theta} \\ -j & 1 & 0 & 0 \\ e^{-j\theta} & -je^{-j\theta} & 0 & 0 \end{vmatrix}, \tag{2}$$

which includes the displacement of terminal 4 by the angle θ.

From (1) is obtained 4 simultaneous equations:

$$-ja_3 + a_4 e^{-j\theta} = b_1\sqrt{2} \tag{3}$$

$$a_3 - ja_4 e^{-j\theta} = b_2\sqrt{2} \tag{4}$$

$$-ja_1 + a_2 = b_3\sqrt{2} \tag{5}$$

$$a_1 e^{-j\theta} - ja_2 e^{-j\theta} = b_4\sqrt{2}. \tag{6}$$

These equations are subjected to the following boundary conditions:

$$a_1 = 1 \text{ (Normalization)} \tag{7}$$

$$a_2 = 0 \text{ (Matched termination)} \tag{8}$$

$$a_3 + b_3 = 0 \text{ (Short circuit on terminal 3)} \tag{9}$$

$$a_4 + b_4 = 0 \text{ (Short circuit on terminal 4).} \tag{10}$$

The reflection coefficient on the input arm is

$$\frac{b_1}{a_1} = \Gamma_1. \tag{11}$$

From the above equations one obtains

$$\Gamma_1 = \frac{1 - e^{-2j\theta}}{2} = je^{-j\theta} \sin\theta. \tag{12}$$

The voltage standing wave ratio in terms of the magnitude of the reflection coefficient is

$$\text{VSWR} = \frac{1 + |\Gamma_1|}{1 - |\Gamma_1|} = \frac{1 + \sin\theta}{1 - \sin\theta}.$$

Similar results may be obtained by using a "folded magic tee" or other hybrid junction.

R. J. Stegen and
Alvin Clavin
Canoga Corp
Van Nuys, Calif

Roster of PGMTT Members

Region 1

Binghamton

Cour, G. J.
Miller, H. T., Jr.

Boston

Achramowicz, M. J.
Alexander, H. C.
Alter, R. S.
Altman, J. L.
Altshuler, E. E.
Angulo, C. M.
Armstrong, D. G.
Ayer, D. R.
Barker, H. R., Jr.
Barrett, R. M.
Bayliss, R. E.
Beauregard, W. G.
Bixby, W. L.
Blaisdell, A. A.
Blanchard, R. L.
Bliss, Z. R.
Braden, R. S.
Bronwell, A. B.
Brown, D. F.
Brunschweiger, Alfred
Brunton, D. A.
Brunton, R. H., III
Butler, J. L.
Carlson, E. S.
Carr, K. L.
Cho, Yohan
Clark, N. F.
Cohen, Albert
Cole, B. R.
Connor, T. J.
Crandell, P. A.
Cuming, W. R.
Devane, M. E.
Duffy, John M.
Duncan, K. W.
Dye, N. E.
Edelberg, Seymour
Ewen, H. I.
Faflick, C. E.
Faigen, I. M.
Fallows, E. M.
Fano, R. M.
Favaloro, C. J.
Feigenson, Arbey
Feldman, E. J.
Fine, E. C.
Foster, A. E.
Freeman, L. D.
Frost, A. D.
Fulton, D. A.
Galagan, Steven
Goldberg, H. B.
Goldman, E. M.
Goldstein, Irving
Gottschalk, W. M.
Goulder, M. E.
Graham, J. W.
Graham, J. S.
Gregory, J. G.
Gunn, K. C. C.
Haddad, S. G.
Hadge, Eugene
Hagan, R. A.
Hall, R. T.
Hall, W. M.
Harris, J. M.
Hellenbrand, C. M.
Helm, G. D.
Hiatt, R. E.
Hogan, W. D.
Holmes, K. O.
Horrigan, J. B.
Howe, S. E.
Huang, Chaang
Keller, E. W.
Kenyon, R. W.
King, R. P.
Klane, C. H.
Klemm, G. H.
Kline, Jack
Kohler, H. M.
Kostriza, J. A.
Lanciani, D. A.
La Rue, A. D.
Lehr, C. G.
Lester, D. R.
Le Van, J. D.
Lippincott, Southard
Loewenthal, Morton
Lowe, W. R., Jr.
Mack, R. B.
Maillet, A. J.
Maple, T. G.
Mayer, Alex
McLeod, W. W., Jr.
Mercer, W. R.
Michelson, Max
Mingins, C. R.
Moats, R. R.
Murphy, E. J.
Nans, E. A., Jr.
Nash, H. F., Jr.
Nelson, A. A.
Nichols, A. J.
O'Hara, F. J.
O'Neil, J. F., Jr.
Osepchuk, J. M.
Paananen, R. A.
Paine, B. B.
Parke, N. G., III
Pascalar, H. G.
Pathe, J. F.
Peters, J. D., Jr.
Petteruti, A. J.
Pippin, J. E.
Prickett, R. J.
Pritchard, W. L.
Purdy, W. E.
Reed, John
Ricardi, L. J.
Richter, Edwin
Riska, G. G.
Rivers, R. A.
Rizzi, P. A.
Rotman, Walter
Rubin, Samuel
Rutledge, P. D.
Ruze, John
Saad, T. S.
Salzberg, Edward
Santos, R. F.
Scharfman, Howard
Segal, Sumner
Senseman, R. W.
Sheingold, L. S.
Shekel, Jacob
Sherburne, A. E.
Sibley, R. C.
Simmons, W. J., Jr.
Skolnik, M. I.
Smith, C. L.
Smith, M. K.
Smith, R. V.
Smullin, L. D.
Soorsoorian, S. A.
Spencer, R. C.
Stein, Seymour
Stewart, R. F.
Stockman, Harry
Stone, M. L.
Strum, P. D.
Swing, R. E.
Tenenholtz, Robert
Thomas, H. J., Jr.
Trunfio, A. P.
Tucker, Nathaniel
Tyler, E. M.
Ulm, E. H.
Vant, L. M.
Walker, R. M.
Wantuch, Ernest
Watson, W. H.
Wheeler, G. J.
Willenbrock, F. K.
Zucker, F. J.

Buffalo-Niagara

Barnes, J. A.
Borkowski, C. J.
Buranich, G. F.
Champness, N. A.
Earl, H. D.
Flood, W. A., Jr.
Horvath, J. O.
Kasper, H. W.
Kell, R. E.
Kinsell, W. L.
Nuckolls, R. G.
Page, R. S.
Pelton, F. M.
Rhodes, D. R.
Sarkees, Y. T.
Schlichter, E. S.
Snyder, W. W.
Stengel, C. J., Jr.
Tanner, W. E.
Welch, D. P.

Connecticut Valley

Allen, T. F.
Carey, G. D.
Carlotto, A. J.
Cutler, M. A.
Dickon, A. J.
Getsinger, W. J.
Hoehn, A. F.
Liucci, C. A.
Loeb, J. M.
Lovell, B. W.
Marchand, Nathan
Molday, B. V.
Owen, S. F., Jr.
Reich, H. J.
Simko, R. S.
Winchell, A. M.
Warner, E. J.

Elmira-Corning

Clarke, R. L.
Guyer, E. M.
Hayter, W. R., Jr.
Larson, R. G.
Lempert, Joseph
Margolin, A. R.
Upshaw, Vert
Scullin, C. H.

Ithaca

Charton, P. W.
Evans, K. R.
Harmuth, H. F.
Hazebrook, Harry
Holden, W. D.
Ingalls, C. E.
Kantor, Gideon
Maresca, T. J.
Matt, Sol
Pike, Neal
Schmidt, R. A.
Shalloway, A. M.
Shnurer, Florian
Smith, F. G., Jr.
Stanton, J. W.
Travis, J. B., Jr.
Warriner, Ben

Rochester

Evans, J. E.
Heit, J. C.

Rome-Utica

Bates, E. L.
Chasek, N. E.
Cruickshank, J. E.
De Mesme, T. A.
Ellis, T. E., Jr.
Grimm, R. S.
Handelsman, Morris
Haycock, Alfred, Jr.
Ladwig, H. A.
Orear, E. R.
Pritchard, H. T.
Romanelli, P. A.
Scott, E. C.
Smith, S. L.
Worthington, J. W., Jr

Schenectady

Allen, C. C.
Babits, V. A.
Boyd, M. R.
Branch, G. M., Jr.
Bristol, T. R.
Cohoon, R. L.
Curtis, T. P.
Dehn, R. A.
Griffin, G. J., Jr.
Jarek, J. J.
Matthews, E. W., Jr.
Maurer, J. W.
Owens, O. G.
Quine, J. P.
Raschke, R. R.
Reynolds, M. T.
Smith, G. F.
Watson, R. P.

Syracuse

Baker, L. T.
Baxter, L. M.
Biele, R. J.
Cheng, D. K.
Conger, W. H.
Demaree, G. A.
Eber, L. O., Jr.
Evans, H. J.
Fitzmorris, S. R.
Grimm, H. H.
Gutt, A. J.

Hu, Ming-Kuei
Johnson, M. A.
Kluender, E. C.
Knox, R. L.
Kuecken, J. A.
Lepage, W. R.
Marvin, H. B.
Mather, D. L.
Michalek, A. R.
Mullen, E. B.
Plavcan, C. T.
Poppe, J. R.
Reich, R. J.
Smoll, A. E.
Strawn, R. K.
Whistler, W. T.
Williamson, J. C.

Region 2

Long Island

Agree, Irvin
Angevine, R. A.
Bachman, H. L.
Badoyannis, G. M.
Barash, L. F.
Barber, Edward
Basil, Alexander
Beamer, F. E.
Bellare, David
Berlly, Edward
Biss, R. P.
Blass, Judd
Bogner, R. D.
Bourke, W. A.
Breese, M. E.
Brenner, Milton
Busharis, J. G.
Carter, P. S.
Casper, Stuart
Churchill, D. B.
Cohen, Harold
Cornes, R. W.
Cortizas, A. P.
Dagavarian, H. O.
Damast, M. A.
Day, W. B.
Delore, G. E.
Denman, E. D.
De Size, L. K.
Dettinger, David
Dewaal, J. J.
Di Toro, M. J.
Dobson, D. A.
Dong, H. L. H.
Dong, J. G.
Duggan, J. R.
Duncan, B. J.
Dunefsky, Marcus
Eriksen, E. M., Jr.
Ettenberg, Morris
Farber, Herman
Fisch, Jerome
Frerking, H. W.
Friedman, E. D.
Fromm, W. E.
Fubini, E. G.
Garretson, G. M.
Garrett, B. R.
Gebhardt, J. W.
Greene, J. C.
Griemsmann, J. W. E.
Gorelick, George
Gould, R. V.
Hall, J. D.
Hana, T. C.
Hannan, P. W.
Hanover, A. M.
Hansell, C. W.
Harges, M. T.
Harris, W. T.
Harrison, R. I.
Haussig, Lester
Heacock, W. J., Jr.
Hellmann, R. K.
Hendler, A. J.
Henning, R. E.
Hershler, Abe
Hoffman, George
Hronek, R. L.
James, A. V.
Jasik, Henry
Kaye, Murray
Kearney, J. W.
Keim, D. Y.
Kiel, J. H.
Kiesling, J. D.
Kleinberger, Robert
Kraemer, E. H.
Kurzrok, R. M.
Lally, P. M.
La Rosa, Richard
Learned, Vincent
Lebenbaum, M. T.
Lee, T. K.
Levin, R. M.
Lizzio, Joseph
Loomis, S. A.
Loth, P. A.
Lowman, R. V.
Luber, Lawrence
Magenheim, Bertram
Malech, R. G.
Marston, R. S.
Matylewich, T. D.
McBee, W. D.
McFarland, J. E.
Michel, C. A.
Mieher, W. W.
Milukas, V. V.
Neiland, A. C.
Nielsen, Peter
Okwit, Seymour
Olthuis, R. W.
Orazio, A. F.
Ottenberg, E. C.
Packard, K. S., Jr.
Pensiero, L. R.
Perenic, L. J.
Peterson, H. O.
Pleasure, Myron
Price, R. C.
Regis, Robert
Reynolds, M. R.
Rickert, H. H.
Robinson, H. L.
Rubin, S. W.
Ruderfer, Martin
Russell, D. H.
Sartorio, D. R.
Savarese, R. T.
Schaefer, A. E.
Schiffres, Paul
Schindler, J. P.
Selbmann, R. W.
Sferrazza, P. J.
Shepherd, J. E.
Sherry, R. S.
Shnitkin, Lothar
Simkovich, J. R.
Simmonds, Jules
Sion, Elio
Smith, A. G.
Smith, P. G.
Sonnenschein, A. H.
Spector, Norman
Spencer, N. A.
Spillane, L. R.
Spira, J. S.
Stephenson, J. G.
Stevens, Stanley
Striednig, L. J.
Stuart, A. F.
Swern, Leonard
Tanenbaum, M. S.
Tennenbaum, Frank
Tiger, H. S.
Timms, R. J.
Tricamo, V. A.
Vafiades, B. C.
Vaupel, G. E.
Waller, W. E.
Wathen, R. L.
Watson, W. C.
Webber, H. E.
Weibel, G. E.
Weichardt, H. H.
Wengenroth, R. D.
Wershoven, G. A.
Wheeler, H. A.
Whitten, C. L.
Wilson, L. B.
Wind, Moe
Winzemer, A. M.
Woods, W. C., Jr.
Wu, W. I. L.
Young, C. B., Jr.
Young, V. J.
Zanichkowsky, Martin

New York

Abeyta, Isaac
Altschuler, H. M.
Ammirati, Salvatore
Arnold, J. W.
Bady, Isidore
Beck, A. C.
Becker, J. E.
Berger, R. M.
Berl, Siegmund
Bernstein, George
Bernstein, M. H.
Bertan, L. L.
Betts, R. W.
Bifano, V. J.
Bolton, Arthur
Brathwaite, Augustus
Bresler, A. D.
Buttner, H. H.
Caldwell, W. C.
Carlin, H. J.
Chanzit, Lawrence
Chavkin, Leon
Chays, Seymour
Chen, Tsung-Shan
Clark, A. R.
Cohen, Morton
Collins, Kenneth
Crivello, A. A., Sr.
Dawson, R. W.
Deschamps, G. A.
Di Fusco, F. J.
Douglas, R. H.
Doundoulaiks, G. J.
Dowling, T. J.
Espersen, George
Evans, G. E.
Falconer, Stanley
Feibish, H. L.
Felsen, L. B.
Ferri, R. I.
Fink, F. G.
Flower, R. A.
Fox, A. G.
Fraser, J. T.
Freed, Arthur
Freudenberg, Boris
Friedman, Felix
Friis, H. T.
Galligan, T. J.
Gamertsfelder, G. R.
Gauvenet, A. J.
George, D. E.
Giannattasio, A. R.
Goldfarb, A. T.
Goldmuntz, L. A.
Goldsmith, A. N.
Goodall, W. M.
Govinsky, Walter
Hammer, Harry
Hearn, R. B.
Hefter, Murray
Heidgen, Bernard, Jr.
Isaacson, H. B.
Kahn, W. K.
Kaplowitz, Morris
Kavanaugh, J. C.
Kilgore, C. R.
King, A. P.
Klug, S. H.
Koppl, W. J.
Korewick, John
Krevsky, Seymour
Kullback, Irving
Laas, I. E.
Lamb, R. U.
Lavi, Yeshayahu
Lawton, L. M., Jr.
Lerner, David
Lesman, Edward
Levey, Lawrence
Levine, Seymour
Likel, H. C.
Lipetz, Nathan
Mack, Alfred
Maedel, G. F.
Marcy, S. P.
Mazziotti, I. J.
McClean, J. F.
McGinnis, Frank
Menhennett, G. H.
Meserole, W. E.
Meslener, G. J.
Miller, S. E.
Mongan, A. J.
Monteleone, T. A.
Morris, W. P.
Novick, Gabriel
Nowogrodzki, Markus
Ohm, E. A.
Oliner, A. A.
Orefice, Gaetano
Parisier, Maurice
Pelner, Nathan
Pickholtz, R. L.
Piumsombun, Chuan
Pokorny, G. E.
Racker, Joseph
Rapaport, Harold
Reder, F. H.
Rivera, J. J.
Robertson, S. D.
Rojak, F. A.
Rolnik, J. A.
Rosenthal, S. W.
Rothman, H. S.
Rowley, B. G. H.
Rudner, B. S.

Rusinow, Kalman
Sahud, L. R.
Saltzman, Henry
Sawelson, A. I.
Schafer, J. P.
Scheier, Lester
Schelleng, J. C.
Schlaack, N. F.
Schneider, Seymour
Sharpless, W. M.
Shubel, E. J.
Simon, Harold
Singer, L. M.
Slobodin, Leo
Smithline, Herbert
Stavis, Gus
Stein, V. J.
Stern, Ernest
Stock, D. J. R.
Suttenberg, Stewart
Sweet, L. O.
Taub, J. J.
Thomas, R. O.
Torgow, E. N.
Tudor, J. E.
Vaughan, J. A.
Victor, H. W.
Walton, J. S. V.
Weber, Ernst
Weiss, M. T.
West, C. B.
Westheimer, Manfred
Wheeler, G. W.
Winkler, Arthur
Zenchoff, Philip

Northern New Jersey

Albrecht, H. W.
Arams, F. R.
Arditi, Maurice
Ashbrook, J. M.
Assadourian, Fred
Augenblick, H. A.
Beltz, W. F.
Benenson, C. A.
Benner, T. A.
Bradburd, E. M.
Brown, B. B.
Bryant, J. H.
Bucher, F. X.
Campanaro, P. L.
Chisholm, D. A.
Clavier, A. G.
Cox, A. L.
Currier, P. J.
Dardano, L. B.
Davis, M. G.
Dayem, A. H.
Del Vento, J. M.
De Rosa, L. A.
Dishal, Milton
Dorney, P. E.
Drexler, Jerome
Engelbrecht, R. S.
Engelmann, H. F.
Evans, N. L., Jr.
Farese, V. C.
Fay, C. E.
Feher, George
Ferrar, R. C.
French, H. A.
Friis, R. W.
Glomb, W. L.
Gray, G. E.
Green, M. W.
Haenichen, J. C.
Harkless, E. T.
Havstad, Harald
Henry, T. J.
Hensel, M. L.
Houghton, E. W.
Hughes, R. W.
Ingalls, David
Irby, R. F.
Jacobs, G. W.
James, W. M.
Jenny, H. K.
Klein, M. S.
Kompfner, Rudolph
Kovach, Leslie
Kreer, J. G., Jr.
Kulesha, K. J.
Kups, E. F.
Kuras, H. F.
Lamb, J. M.
Laport, E. A.
Levine, Sam
Lundburg, F. J.
MacVeety, R. C., Jr.
Maggio, J. B.
Mansfield, E. C.
Marchese, T. J.
Marsten, R. B.
Martin, J. F. P.
Mattingly, R. L.
McDowell, H. L.
McEwan, A. W.
Morgan, S. P.
Mottram, E. T.
Mulligan, J. H., Jr.
Mumford, W. W.
Nicodemus, K. L.
Ostlund, E. M.
Pattan, B. A.
Petrich, L. G.
Pomeroy, A. F.
Reading, Anne
Robertson, G. H.
Roetken, A. A.
Ronald, T. T.
Salzer, R. M.
Sandsmark, P. I.
Schafersman, R. L.
Scheibner, J. F.
Seidel, Harold
Shangraw, C. C.
Sichak, William
Siekanowicz, W. W.
Snyder, H. H.
Southworth, G. C.
Spanos, W. M.
Sproul, P. T.
Stebbins, M. D.
Stinehelfer, H. E., Sr.
Sullinger, W. B.
Tahan, E. N.
Talpey, R. G.
Tatsuguchi, Isamu
Terry, C. B.
Tulchin, Henry
Vaccaro, F. E.
Weber, R. M.
Wehrle, A. W.
Welber, Irwin
Westbrook, E. P.
White, R. E.
Wickliffe, P. R., Jr.
Williams, N. T.
Zayac, F. R.

Princeton

Beam, W. R.
Blattner, D. J.
Braden, R. A.
Brown, H. R.
Davis, Hector
Ginsberg, L. H.
Hautzik, R. M.
Hensperger, E. S.
Hoffmann, K. G.
Houser, B. E.
Kaplan, Martin
Kihn, Harry
Knechtli, R. C.
Miller, Robert
Norman, F. H.
Peter, R. W.
Rankin, J. B.
Snyder, C. L.
Thomas, G. W.
Woodward, O. M.

Region 3

Atlanta

Berry, G. C.
Birchfield, W. P.
Bowers, T. N.
Burgener, R. C.
Duggan, R. S., Jr.
Fellers, R. G.
Kennedy, C. L., Jr.
Long, M. W.
Masters, W. C.
McClung, W. C.
Pettyjohn, J. G., Jr.
Roth, F. P.
Schultz, F. V.
Smith, D. L.
Smith, R. T.
Thomason, J. G.
Waterman, H. B.

Baltimore

Barrack, C. M.
Barthel, D. R.
Behrends, P. O.
Boenning, C. B.
Bolt, C. A., Jr.
Brodwin, M. E.
Bucciero, Joseph
Claborn, K. D.
Clark, F. K.
Clark, T. H.
Cohn, Marvin
Combellick, T. A.
Crane, R. B.
Dempsey, M. E.
De Socio, George
Eby, J. T.
Ecker, J. L.
Foley, W. V.
Goodman, S. N.
Grauling, C. H., Jr.
Gray, A. R.
Griffith, B. H., Jr.
Hanks, H. C., Jr.
Hardy, F. S.
Helderman, T. E.
Herwald, S. W.
Hom, W. R.
Hsu, Chih-Chi
Jackson, H. L.
Jurich, Samuel
King, D. D.
Kudo, F. M.
MacKenzie, J. E.
Mannas, R. G.
May, H. A.
McBride, J. F.
McDonough, J. T.
Mueller, E. J.
Mueller, M. T.
Munson, L. A.
Neau, O. T
Olin, I. D.
Packard, R. F.
Platt, J. F., Jr.
Pratt, Amasa
Quenstedt, R. E.
Rabinowitz, S. J.
Roediger, F. E.
Ruth, H. O.
Sanner, G. E.
Scanga, W. A.
Schmid, Otto, Jr.
Schmidt, E. R.
Schrank, H. E.
Schreyer, S. D.
Schutz, Harald
Seman, A. E., Jr.
Shaw, G. D.
Shelor, E. G., Jr.
Sichelstiel, B. A.
Siegel, William
Slager, D. M.
Smith, E. L., Jr.
Spencer, P. H.
Stebbins, W. J.
Stout, G. P.
Sudia, A. T.
Tharp, N. B.
Thomas, C. E., Jr.
Trinter, V. E.
Undesser, Karl
Wallace, B. E., Jr.
Watson, T. E.
Watts, H. M.
Wentworth, F. L.
Wheeler, M. S.
Wiltse, J. C., Jr.
Wing, Jack
Woodyard, R. H.
Young, Leo

Central Florida

Aitken, K. M.
Apriletti, C. A.
Davidson, J. K.
Dietz, D. P.
Miller, L. S.
Moline, J. C.
Painter, Parker, Jr.
Rolfs, J. C.
Scharla-Nielsen, Hans
Shaw, L. R.
Walter, E. R.
West, K. A.

Huntington

Dicker, P. E.
Edens, S. V.
Everhard, F. U., Jr.
Lowery, H. R.
Rodriquez, P. T.
Schumann, Fred
Walker, B. J.

Miami

Boundy, G. G.
Driest, C. W.
Harrington, J. F.
Kimball, E. W.
Markley, P. F.
Neely, E. H.

North Carolina-Virginia

Brooker, E. G., Jr.

Brownfield, L. B.
Bush, T. K.
Fisher, R. W.
Grymes, J. R., Jr.
Harris, O. R.
Harvey, C. C.
Hastings, C. E.
Joly, C. D.
Keast, P. M.
Langston, J. W.
McGahey, E. W., Jr.
Peebles, N. A.
Pitsenberger, J. W.
Rhett, T. G., Jr.
Severance, F. D.
Taylor, M. L.
Tilley, J. H.
Ward, D. L.
Whisenhunt, J. A.

Northwest Florida

Howard, F. E., Jr.

Philadelphia

Allerton, G. L.
Anderson, W. G.
Angel, K. W.
Arnold, P. H.
Bargellini, I. P. L.
Bazan, S. J.
Beardwood, J. T., III
Beaver, J. A., Jr.
Benner, R. H., II
Bennett, R. G.
Benson, S. E.
Bollman, J. H.
Bradford, C. E.
Bradley, W. E.
Cantafio, L. J.
Capek, S. J.
Ciletti, V. J.
Colby, N. C.
Cooley, C. C., Jr.
Cottingham, J. H.
Crosby, D. R.
Dahlberg, R. S., Jr.
Davis, C. E.
Doughty, S. D.
Fast, Herbert
Follensbee, W. R.
Forbes, E. J.
Friend, A. W.
Fulmer, R. J.
Funk, R. E.
Godshall, J. L.
Greenfield, Alexander
Gumacos, Constantine
Hamm, N. G.
Hawthorne, E. I.
Hobgood, M. P.
Hochman, Daniel
Hockeimer, H. E.
Homer, E. G.
Honda, Hajime
Hricko, R. M.
Jackson, Robert, Jr.
Jacobs, Ernest
Kall, A. R.
Kassler, Raymond
Kelly, P. J.
Kennedy, Peter
Kolts, R. C.
Latham, N. D.
Laurent, G. J.
Lewis, E. S.
Li, Kam
Linden, D. A.
Lisicky, A. J.
Lombardini, P. P.
Mathwich, H. R.
McEnroe, J. M., Jr.
McKnight, C. F.
Messenger, G. C.
Million, J. W., Jr.
Moritz, K. C.
Mueller, P. L.
Munson, I. K.
Pastell, D. L.
Peterson, C. E.
Polk, Charles
Reiss, H. R.
Richter, Filmore
Ringland, R. S.
Rose, F. L.
Rothmel, B. J.
Sayer, T. C.
Schoenberg, J. P.
Schwartz, A. J.
Schwartz, R. F.
Schwartzberg, H. L.
Shellock, J. V.
Sheppard, W. H.
Sher, Nisson
Silverman, Elliot
Smith, A. E.
Smyton, S. A.
Sumerlin, W. T.
Thompson, L. E.
Twist, G. A.
Ussler, William, Jr.
Warren, W. L.
Wenzel, J. H.
Whitby, L. S.
Williams, A. J., Jr.
Wolin, Samuel
Wood, J. R.

Washington, D. C.

Adams, J. T.
Algor, M. M.
Anderson, H. W.
Ballard, J. L.
Bawer, Robert
Beck, E. A.
Bernstein, Benjamin
Bickart, T. A.
Blanks, R. T., III
Bowman, D. F.
Cacheris, J. C.
Calhoon, T. G.
Carpenter, Max
Chase, D. G.
Chen, Y. M.
Cook, F. W.
Cooper, H. W., III
Davis, L. B.
Diehl, L. G.
Dropkin, H. A.
Ford, R. R.
Francis, C. J.
Friedberg, I. S.
Gabriel, W. F.
Gerig, J. S.
Gessner, R. J.
Gould, W. I., Jr.
Grantham, R. E.
Gruber, J. R.
Herring, R. A., Jr.
Hockensmith, R. P.
Hwang, Y. C.
Isaacson, Sheldon
Jones, A. E.
Katzin, Martin
Klamm, G. E.
Kohler, H. W.
Kriz, Joseph
Kropf, R. G.
Lowy, W. M.
Masterson, J. P.
Miller, J. W.
Moore, C. G., Jr.
Ornstein, Edward
Ould, R. S.
Packert, D. E.
Polak, Henri
Portmann, P. A.
Potter, R. S.
Puro, W. O.
Randall, Henry
Ray, H. A., Jr.
Read, A. H.
Redden, M. S., Jr.
Reed, M. D.
Renner, J. J.
Reynard, A. I.
Ringenbach, M. E.
Rohrer, R. E.
Rueger, L. J.
Sakiotis, N. G.
Salisbury, L. L., Jr.
Schetzen, Martin
Shapiro, Gustave
Sidorov, A. G.
Silins, Andrejs
Simmons, A. J.
Stewart, R. B.
Stickley, C. M.
Summers, C. R.
Tai, J. H. Y.
Tozzi, L. M.
Turnage, H. C.
Turner, W. P.
Uglow, K. M., Jr.
Walker, H. R.
Ward, H. T., Jr.
Weinschel, B. O.
White, D. R. J.
Wibel, Donald
Wise, J. W.
Witte, J. J.
Young, H. D.
Young, H. M.

Region 4

Akron

Doran, T. F.
Mathis, H. F.
Pressel, P. I.
Strang, J. R.
Vaughan, T. J.
Welch, G. H.
Yarnall, W. M.

Cincinnati

Bereskin, A. B.
Dreyer, G. C.
Dutton, C. E.
Kelly, C. M.
Sang, W. W.
Saxe, R. E.
Zupansky, Milo

Cleveland

Ackerman, E. K.
Banshak, W. G.
Bird, J. R.
Cockerman, F. E.
Ehrman, J. R.
Elze, R. P.
Kessler, J. C.
Louis, J. R.
Peck, J. L.
Titterington, R. J.
Whipple, G. D.

Columbus

Baechle, J. R.
Boone, E. M.
Bulman, W. E.
Carter, C. J.
Clifton, J. K.
Damon, E. K.
Dawirs, H. N.
Falkenbach, G. J.
Hines, J. N.
Huffman, D. L.
Kirschbaum, H. S.
Levis, C. A.
Masters, R. W.
Mushiake, Yasuto
Nash, R. T.
Perry, R. C.
Peters, Leon, Jr.
Richmond, J. H.
Stoutenburg, D. V.
Tai, C. T.
Taylor, L. L.
Thurston, M. O.
Troyan, J. F.
Uenohara, Michiyuki
Ward, R. C.

Detroit

Batten, H. W.
Black, J. R.
Breymaier, R. W.
Dombrowski, G. E.
Frese, R. E.
Hok, Gunnar
Holland, L. N.
Hoop, R. E.
Miller, M. H.
Nace, P. E.
Nichols, A. D.
Rowe, J. E.
Settersten, R. A.
Warnick, Alan
Welch, H. W., Jr.
Wooster, A. F.

Emporium

Boden, E. H.
Golla, E. F.
Herman, E. B.
Lopez, A. F.
Snyder, Norman
Veley, H. N.

Pittsburgh

Clay, J. P.
Coles, D. K.
Courtney, J. E.
Curry, T. F.
Davis, J. M., Sr.
Flaherty, J. M.
Huet, F. R., Mrs.
Joller, C. R.
Josephs, D. C.
Kadak, Eugene
Klotzbaugh, G. A.
Martin, K. L.
McKinley, J. G.
Schatz, E. R.
Sinsel, P. W.
Totten, J. E.
Vogeley, C. E., Jr.

Toledo

Fujii, Takashi
Wott, H. W.

Region 5

Cedar Rapids

Coble, R. B.
Henrici, C. R.
Newell, D. E.

Chicago

Akerman, Steve
Anderson, C. J.
Anderson, J. M.
Arnow, C. L.
Beam, R. E.
Becker, R. C.
Brittain, G. H.
Brown, J. S.
Brunn, K. R.
Castor, R. W.
Clavier, P. A.
Cohn, G. I.
Coleman, P. D.
Cox, C. R.
Crampton, G. W.
Crotty, R. E., Jr.
Czeropski, W. P., Jr.
Damm, Fred
Damm, G. J.
Dervishian, Edward
Dougal, A. A.
Du Hamel, R. H.
Dyson, J. D.
Emery, W. L.
Ernst, E. W.
Fair, R. D.
Freymodsson, J. B.
Galejs, Janis
Gershon, J. J.
Gilden, Meyer
Graziano, Victor
Grimme, H. J.
Heathershaw, R. T.
Hedvig, T. I.
Hines, H. H.
Hupert, J. J.
Hyneman, R. F.
Kasai, Kiyoshi
Kaufman, Irving
Kowitz, A. E.
Krahe, L. R.
Kreer, J. B.
Kvitek, G. L.
MacAskill, R. B., Jr.
Maciszewski, A. H.
Magnuski, Henry
Maier, R. H.
Mayes, P. E.
McMullen, C. W.
Modesitt, M. B.
Moore, R. A.
Needle, J. S.
Oslake, J. J.
Pakan, J. J.
Pichler, R. H.
Raucher, W. L.
Rosselot, G. A.
Schaffner, Gerald
Shewan, William
Sirkis, M. D.
Skaperdas, D. O.
Spencer, R. L.
Stubner, J. W.
Swanson, B. E.
Trapp, R. R.
Wells, R. E.
Whitelaw, A. J.
Williams, J. T.
Woo, K. W.
Yahalom, Yair
Yang, R. F. H.

Dayton

Aulbach, C. E.
Birochak, Edward
Fried, W. R.
Gallagher, J. J.
Garman, D. F.
Gross, E. H.
Hilt, W. M.
Johnston, D. H., Jr.
Moyer, D. F.
Russell, J. D.
Sefton, H. B., Jr.
Vanderpool, H. D.
Von Tersch, L. W.
Waugh, R. E.
Weldon, J. C.

Des Moines-Ames

Loupee, B. J.

Evansville-Owensboro

Barrick, W. E.
Brannon, D. L.
Buchanan, H. R.

Fort Wayne

Artman, R. L.
Carrel, R. L.
Fisher, C. C.
Gough, L. E.
Hessler, John, Jr.
Johnson, D. L.
Killion, D. G.
Richards, G. A.
Wallace, C. E., Jr.
Zordell, J. W.

Indianapolis

Albon, Ralph, Jr.
Baker, George, Jr.
George, R. H.
Hayt, W. H., Jr.

Milwaukee

Ohms, D. V.
Scheibe, E. H.
Shenoy, R. P.
Swift, W. B.

Omaha-Lincoln

Beshore, P. S.
Borcher, E. J.
Rood, R. S.
Urschel, A. K.

Twin Cities

Froemke, D. J.
Jelatis, D. G.
Le Cocq, V. L.
O'Dea, O. B.
Rickett, R. J.
Taus, H. G.
Ulstad, M. S.
Walkup, L. A.

Region 6

Beaumont-Port Arthur

Ballard, B. J.
Collins, J. P.

Dallas-Fort Worth

Bains, R. W.
Blocker, R. E.
Bryan, K. W.
Bullock, M. W.
Clickner, G. M.
Coats, R. P.
Craig, W. H.
Dyke, Ed
Earhart, C. E.
Fisher, L. M.
Flowers, B. R.
Hallford, B. R.
Harman, D. G.
Hertel, Paul, Jr.
Johnson, G. D.
Logan, J. J.
Lowe, H. N.
Maxwell, J. W.
McKinney, R. C.
McMillin, J. M., Jr.
Miller, J. C., III
Petrasek, A. C.
Randolph, A. M.
Schafer, N. B.
Schwetman, E. D.
Schuffler, R. M.
Sivernell, R. B.
Spears, M. F.
Stanphill, J. R.
Stansch, H. C.
Stone, R. M.
Strom, L. D.
Sullivan, W. A., Jr.
Weedfall, W. W.
Weldon, J. F.

Denver

Beatty, R. W.
Daniels, W. H.
Estin, A. J.
Larson, R. E.
Robbins, C. M.

El Paso

Haas, H. W.
Kidwell, R. P.
Krivanich, M. A.
Lux, M. O.
Noda, T. T.
Smith, K. E.
Taylor, L. S.
Warnock, R. L.
Welch, C. M.

Houston

Barton, L. R.
Caplan, R. S.
Cooper, W. A.
Hulteen, C. K.
Rice, L. S.

Kansas City

Anderson, R. W.
Armstrong, D. A.
Balden, J. M.
Bennett, H. L.
Benton, W. J.
Hax, D. H.
Johnson, R. W.
Lane, C. A., Jr.
Pape, R. L.
Pyle, K. W.
Tierney, P. V.

Little Rock

Cannon, W. W.
Nider, M. E.

New Orleans

Dowe, R. J.
Rust, J. J.

Oklahoma City

Herriott, J. K., Jr.

St. Louis

Van Bladel, J. G.
Brooks, J. L.
Cummings, G. M.
Delong, W. A.
Hirsch, O. C.
Lechtreck, L. W.
Luedde, W. J.
McAllister, J. C.
Mitchum, M. M.
Mohrman, R. F.
Mosley, C. E.
Skitek, G. G.
Vandeven, D. W.

San Antonio

Bondy, M. A.
Herndon, R. A.
Lincoln, J. P.
McHugh, E. L.
Morris, C. R.
Weber, L. C.

Tulsa

Bolay, C. E.
Draheim, L. H.
Marshall, B. R.
Silverman, Daniel

Region 7

Albuquerque-Los Alamos

Arnot, G. A., Jr.
Bittner, B. J.
Boling, P. T.
Church, T. S.
Connell, J. C.
Dike, S. H.
Finch, H. D.
Fossum, D. E.
French, L. E.
Janza, F. J.
Jones, M. C.
Manigold, F. E.
Stearns, W. P.
Wilde, Ned
Williams, H. A.

Inyokern

Deyoe, D. C.
Wolf, J. E.

Los Angeles

Aaron, B. D.
Allen, R. J.
Anderson, A. T.
Anderson, D. B.
Anderson, G. R.
Andrew, V. J.
Bachman, C. G.
Barkson, J. A.
Becker, J. T.
Bedrosian, Edward
Begovich, N. A.
Benson, Stanley
Berry, D. C.
Bezera, Gebriel
Blackwell, M. B.

Blasberg, L. A.
Blatchford, Dean
Bonardi-Fondo, Giusto
Boyd, W. L.
Boyer, B. E.
Buchman, W. W.
Burnsweig, Joseph, Jr.
Butler, J. E.
Canfield, E. R.
Carr, J. W.
Chandler, C. W.
Clapp, R. W.
Clavin, Alvin
Cooper, P. V.
Corbin, G. C.
Cordray, R. E.
Cornell, J. R.
Creacy, J. N.
Cummings, C. I.
Curtis, C. W.
Davis, E. F.
Davis, J. I.
Deininger, C. F.
Dexter, G. W.
Dibos, R. A.
Dickerson, D. H.
Dobbertin, W. H.
Duvall, W. E.
Dvoracek, F. H.
Eatough, C. D.
Fahnestock, R. J.
Filman, N. J.
Fisher, M. K.
Futterman, Meyer
Gage, N. C.
Garrett, W. O.
Gibbons, T. J.
Giddis, A. R.
Gish, C. G.
Gleason, M. J.
Gola, A. S.
Gossland, J. K.
Gottier, R. L.
Graham, Walter
Gromer, R. D.
Gustafson, L. A.
Hajie, E. J.
Hansen, R. C.
Harris, L. M.
Hata, F. T.
Hickman, D. D.
Higa, W. H.
Hodson, W. G.
Holdsworth, D. M.
Hovda, R. E.
Hudspeth, Tom
Hughes, W. A.
Ittleson, J. S.
Jicha, A. J.
Joerger, J. C.
Jones, W. F.
Kasai, G. S.
Kaspin, Solomon
Keenan, O. B.
Kelly, P. M.
Kiesel, R. H.
King, G. J.
Kohlmeyer, R. B.
Koontz, D. E.
Kramer, A. G.
Krausz, Robert
Kreinheder, D. E.
Krill, C. K.
Krogh, R. A.
Kurtz, L. A.
Lambert, J. M.
Lance, H. W.
Landis, Vernon, Jr.
Lindewall, G. W.
Linnes, K. W.
Lockhart, E. H.
Loop, D. M.
Louie, William
Luchi, R. D.
Lulofs, J. R.
Lund, W. W., Jr.
Lundquist, C. R.
Lundstrom, O. C.
Macmillan, R. S.
Magid, Milton
Maguire, W. W.
Margerum, D. L.
McCann, J. G.
McCone, G. L.
McFarlane, M. D.
Metzger, H. W.
Meyer, D. R.
Milham, R. F., Jr.
Moore, J. A.
Mumma, J. W.
Munushian, Jack
Nealey, C. C.
Nelson, C. E.
Nelson, J. S., Jr.
Newton, W. P.
Noorland, Martinus
Notvest, R. A.
Oleesky, S. S.
Pamler, R. G.
Paulson, E. T.
Pincus, Leonard
Pischel, E. F.
Potter, P. D.
Poulson, W. A.
Rawlins, R. E.
Rees, W. L.
Reese, R. F.
Rumsey, W. E., Jr.
Samuelson, H. R.
Sassman, R. W.
Schaffer, Alvin, Jr.
Scharp, G. A.
Seaton, A. F.
Seltzer, L. J.
Sensiper, Samuel
Shahan, Onnig
Signer, R. M.
Silva, L. M.
Sisson, A. R.
Smith, R. G.
Snyder, W. A.
Starr, A. R.
Stegen, R. J.
Stevens, S. S.
Stone, R. E.
Strumwasser, Eric
Symonds, R. J.
Tampico, Joseph
Tasker, Raymond
Taylor, A. D.
Thorensen, Ragnar
Ullrich, W. J.
Vernon, F. L., Jr.
Vincent, B. T., Jr.
Votava, Yaro
Walters, A. W.
Wanselow, R. D.
Wayman, J. M.
Weglein, R. D.
Weil, F. M.
Wellsand, Rudolph, Jr.
Willis, M. R.
Wilson, H. G.
Wilson, T. A.
Wiseman, S. D.
Zeman, J. A.

Phoenix

Chittenden, W. R.
Dlouhy, F. W.
Echols, R. A.
Feist, W. E.
Fritz, C. B.
Hessemer, R. A., Jr.
Hickman, J. E.
Hoehn, A. J., Jr.
Lindsay, J. D. G.
Noon, J. R.
Samuelson, R. E.
Sloman, F. A.
Smith, D. A.
Sterns, W. G.
Streets, R. B., Jr.

Portland

Calnon, D. C., Jr.
Foster, J. H.
Ropiequet, R. L.
Surdam, E. L.
Torrance, J. W.

Salt Lake City

Grover, R. K.
Nicholes, G. H.

San Diego

Bostwick, W. E.
Dickstein, H. D.
Honer, R. E.
Keener, M. A.
Kluck, J. H.
Michael, F. J.
Mulvey, J. X., Jr.
Proctor, David
Ratkevich, A. E.
Scharrer, R. G.
Small, B. I.
Taylor, W. G.
Teeter, W. L.
Thomas, J. J.
Wolfe, G. W.
Wooley, G. J.

San Francisco

Abraham, W. G.
Adelson, M. B.
Allen, S. E., Jr.
Allison, J. E.
Anderson, S. E.
Angelakos, D. J.
Arfin, Bernard
Barnes, C. W., Jr.
Barquist, W. S., Jr.
Bert, J. E.
Birdsall, C. K.
Booth, R. E.
Borghi, R. P.
Bryant, N. H.
Caryotakis, George
Chang, Nein-Chih
Chodorow, Marvin
Christie, J. W.
Cohn, S. B.
Craig, R. A.
Crane, Milton
De Bell, J. M., Jr.
Derflinger, H. L., Jr.
Dinapoli, F. C.
Di Napoli, G. W.
Disman, Murray
Dodds, Wellesley
Dunbar, A. S.
Dunn, D. A.
Ellis, A. R.
Engler, C. G.
Feinstein, Lester
Feuchtwang, T. E.
Forrer, M. P.
Foster, C. P., Jr.
Gamara, N. J.
Geppert, D. V.
Gerling, J. E.
Goodman, D. H.
Grace, D. J.
Graf, E. A.
Hargrove, P. E.
Harman, W. A.
Heine, R. A.
Henschke, R. A.
Hiestand, N. P.
Honey, R. C.
Hurst, S. R.
Jaffe, J. S.
Jaynes, E. T.
Jones, E. M. T.
Kino, G. S.
Kohl, W. H.
Koontz, R. H.
La Bree, C. T.
Lagerstrom, R. P.
Lebacqz, J. V.
Leng, R. B.
Ling, J. N.
Ludovici, B. F.
Luebke, W. R.
Malter, R. H.
Maltzer, Irving
Mathers, G. C.
Maudens, L. C.
McIlwraith, Nicholas
McKee, L. H.
Menneken, C. E.
Misra, Harihar
Morita, Tetsu
Mueller, W. M.
Murphy, E. J.
Nalos, E. J.
Nevins, J. E., Jr.
Nikonenko, P. V.
Nitz, I. C.
Nordyke, C. J.
Oliver, B. M.
Olte, Andrejs
Pantell, R. H.
Parisky, R. N.
Peterson, C. J.
Proctor, E. K., Jr.
Rudee, Elliott
Ruetz, J. A.
Ryland, B. G.
Sarquis, R. H.
Schauers, C. J.
Schumacher, F. M.
Sherk, P. M.
Shimizu, J. K.
Siegman, A. E.
Sloan, D. H.
Smith, H. W., Jr.
Sonkin, Simon
Spangenberg, Karl
Stanbury, R. J.
St. Clair, M. W.
Stinson, D. C.
Stoddard, D. J., Jr.
Summers, J. W.
Thon, William
Tomiyasu, Kiyo
Utterback, W. J.

Vane, A. B.
Vehn, R. E.
Vinding, J. P.
Waldman, M. D.
Watkins, D. A.
Watson, W. H.
Wessel-Berg, Tore
Wharton, C. B.
Whinnery, J. R.
Wightman, B. A.
Winkler, R. H.
Wood, F. B.

Seattle

Bauman, E. J.
Belenski, J. D.
Dalby, T. G.
Decker, J. L.
Dorratcague, P. E.
Held, Gedalia
Klee, B. J.
Knight, W. H.
Loski, R. R.
McCarty, W. L.
Mead, W. H.
Morris, C. R.
Siddons, W. J.
Titefsky, E. J.
Wall, R. E., Jr.

Territory of Hawaii

Chang, Dai Chin
Higa, Yoken

Region 8

Alberta

Davis, A. P.

Hamilton

Evan-Jones, Walter

London

Dearle, R. C.
Greenwood, R. E.
Tull, E. H.

Montreal

Au, G. D.
Birman, Gerhard
Bricout, P. A.
Burridge, M. V.
Collin, R. E.
Dion, André
Fabiszewski, Henry
Galloway, N. D.
Glegg, K. C. M.
Haberl, J. F.
Hodge, N. H.
Hryhorijiw, Wolodymyr
Jamshedji, J. S.
Kassner, M. H.
Lavoie, Loic
McDonald, D. J.
Poznanski, Zdzislaw
Reeves, Rene
Sankey, Charles
Vaillancourt, R. M.
Weytze, D. W.

Ottawa

Beneteau, P. J.
Carroll, D. V.
Chambers, R. G.
Cheston, T. C.
Corbett, L. V.
Henderson, J. T.
Kalra, S. N.
McLeod, J. W.

Toronto

Baart, J. G.
Barclay, A. P. H.
Bergstad, P. A.
Blevis, B. C.
Bridgman, J. M.
Buckles, F. G.
Bull, T. R.
Byers, H. G.
Conquest, E. A.
Elliott, A. W. D.
Fischer, E. J.
Hackbusch, R. A.
Hodgson, A. D.
Hughes, J. K.
Kavadas, A. D.
Keeping, K. J.
Leonard, D. J.
Lyons, K. C.
Matthews, R. P.
Mittra, Rajjeshwar
Sengupta, D. L.
Sinclair, George
Stewart, A. C.
Stoddart, T. W. H.
Szekely, Zoltan
Toye, J. M.
Waller, M. J.
Yachimec, Peter
Yen, J. L.

Vancouver

Bohn, E. V.
Moore, A. D.
Noakes, Frank
Stephens, C. H.

Winnipeg

Bridges, Ernest
Wicks, A. A.

Foreign

Ackerman, E. G.
Adikaram, K. B.
Alma, G. H. P.
Arnaud, J. P.
Arreaza, R. G.
Ash, E. A.
Atassi, A. S.
Aurell, C. G. P.
Bar-Lev, Adir
Bartelme, R. R.
Bellis, V. L.
Berline, S. D.
Blassel, P. P.
Bode, M. C.
Bonanomi, J. A.
Bostad, J.
Caicoya, J. I.
Calon, A. E.
Chauvierre, M.
Chalekian, J. S.
Clark, J. E.
Dalzell, T. D.
De Andrade, P. E.
Desirant, M. C.
Egidi, Claudio
Elfving, A. L.
Fan, Sin-Pin
Floquet, Joel
Floriani, Virgilio
Garbrecht, F. S.
Gaumann, Tino
Girard, P. A.
Gloor, Bruno
Golde, H. P. O.
Granquist, C. E.
Grimsdale, R. L.
Gronlund, M. P. S.
Guanella, Gustave
Gudmandsen, P. E.
Guia-Monasterio, A. E.
Guiral, R. L.
Hagger, H. J.
Halberstein, J. H.
Hansen, G. K. F.
Harries, J. H. O.
Harris, K. E.
Hershberger, W. D.
Hessell, Alexander
Hian-Yao, Ong
Hoffman, J. D.
Hsu, Hsiung
Imai, Haruzo
Ito, Yoji
Jackson, W. R.
Jadisdha, Santa
Jenssen, Matz
Joaquin, D. S.
Kariambas, Nicolas
Kern, R. D.
Kulvik, Einar
Kumagai, Toshiro
Kuroiwa, Yutaka
Labin, Emile
Lang, G. J.
Lapostolle, P. M.
Lindstrom, Gunnar
Lofgren, E. O.
MacNee, D. H.
Mandel, Paul
Mita, Shigeru
Mizuma, Masaichiro
Montes, J. V.
Monti-Guarnieri, I. G.
Morita, Kiyoshi
Nag, D. S.
Nemoto, Tadao
Neu, Walter
Niguchi, Koichiro
Nijenhuis, Willem
Okamura, Sogo
Owaki, Kenichi
Parsons, A. N., Sr.
Pinasco, S. F.
Raman, S.
Rantzen, H. B.
Reynolds, D. K.
Rodriguez, Eugenio
Rouse, F. W. D.
Roy, K. M.
Rubenstein, Gerald
Sivers, C. H. V.
Tamir, Theodor
Tanimura, Isao
Tank, Franz
Tellegen, B. D. H.
Tiberghien, C. M. J., Jr.
Tomono, Masami
Tomota, Miyaji
Villadamigo, R. D.
Von Trentini, Giswalt
Wang, Chen-Chuan
Warnecke, R. R.
Yasuda, Ichiji
Yoshida, Shinichiro
Zakhaim, Moshe

Overseas Military

Cassidy, J. J.
Corte, R. L.
Decker, E. E.
Evfimenko, Andrew
Ferber, David
Hurlbut, G. N.
Madsen, J. F.
Phillips, R. A.
Tary, J. J.
Webb, T. E.

Contributors

W. Ayres was born on September 26, 1924 at Los Angeles, Calif. He served as an electronic technician aboard a destroyer during World War II. He returned to college in 1948 and received the B.S. degree in physics from Fresno State College in 1951. He then entered Stanford University where he received the M.S. degree in 1953 and the Ph.D. degree in 1954 in physics. In 1954 he joined the Applied Physics Section of the Electronic Defense Laboratory of Sylvania Electric Products Inc., Mountain View, Calif., where he has been engaged in ferrite research at microwave frequencies.

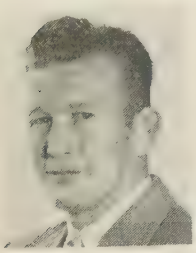

W. Ayres

❖

R. H. T. Bates was born in Sheffield, England, on July 8, 1929. He received the B.Sc. degree in engineering from University College in London in 1952.

From 1952 until the fall of 1955, Mr. Bates was in the radio frequency group of Vickers Armstrongs (Aircraft) Ltd. working in the guided weapons department. He is now in the antenna section of Decca Radar Ltd. in Surbiton, England.

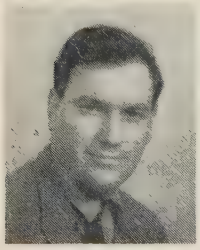

R. H. T. Bates

Mr. Bates is a graduate member of the Institution of Electrical Engineers.

❖

J. J. Bolus was born in Pittsfield, Mass., on December 15, 1929. In 1951 he received the B.S. degree in electrical engineering from the University of Connecticut, and subsequently has taken graduate courses at Brooklyn Polytechnic Institute. While employed by the Sperry Gyroscope Co. from 1951 to 1955, he specialized on waveguide components in their Microwave Components Engineering Department.

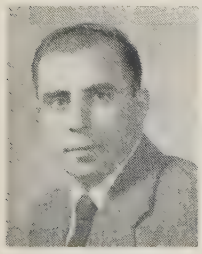

J. J. Bolus

He is presently serving in the U. S. Army and, under their program for the utilization of Scientific and Professional Personnel, is assigned to the Antenna and Microwave Circuitry Section of Evans Signal Laboratory, Belmar, N. J.

Mr. Bolus is a member of Eta Kappa Nu and Tau Beta Pi.

❖

R. E. Collin (M'54) was born at Donalda, Alberta, Can., on October 24, 1928. He received the B.Sc. degree in engineering physics from the University of Saskatchewan in 1951. From 1951 to 1953 he studied at Imperial College, London, England, on an Athlone Fellowship. From 1953 to 1954 he was on a Canadian Defence Research Board grant. He received the Diploma of Imperial College and the Ph.D. degree from the University of London in 1954. Since then, up to the present time, Dr. Collin has been a scientific officer at the Canadian Armament Research and Development Establishment, Valcartier, P.Q., where he is engaged in microwave work related to guided missiles.

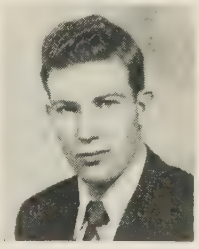

R. E. Collin

❖

J. I. Davis (S'48–A'49–M'55) was born in Detroit, Mich., on January 2, 1925. He received the B.S. degree in electrical engineering in 1945 from the University of Michigan and an M.S. degree in 1948. From 1948 to 1950 he was engaged in microwave antennas and circuit design for missile systems at Bendix Aviation Research and Development Laboratory.

J. I. Davis

From 1951 to 1955, while employed at Hycon Manufacturing Co., he was responsible for development of microwave components for automatic GO-NO-GO Missile Test Equipment. Subsequently he was in charge of field engineering and data analysis associated with missile test equipment. He is presently engaged by Litton Industries for development of microwave systems in the fields of dielectric heating, magnetron test, and microwave simulators.

For a photo and biography of J. W. Griemsmann, see p. 180 of TRANSACTIONS OF THE IRE, Vol. MTT-3, No. 2; March, 1955.

❖

R. A. Lebowitz (S'42–A'44–M'55) was born in Kingston, N. Y., on January 10, 1921. He received the B.E.E. degree from the Polytechnic Institute of Brooklyn in 1942. For three years he worked on high voltage, dielectric, and microwave measurements for the General Electric Co. From 1945 to 1948, he was employed on various vessels of the merchant marine as radio operator.

R. A. Lebowitz

Mr. Lebowitz is presently employed by the Polytechnic Research and Development Co., Inc. as head of microwave product engineering.

He is an associate member of Sigma Xi and the American Institute of Electrical Engineering.

❖

H. F. Mathis (M'47–SM'53) was born near Wichita Falls, Texas, on July 19, 1916. He received the B.S. in E.E. degree from the University of Oklahoma in 1939, the M.S. degree from Texas A. & M. College in 1941, and the Ph.D. degree from Northwestern University in 1953. He has also received the professional degree of Electrical Engineer from Texas A. & M. College and the University of Oklahoma.

H. F. Mathis

From 1942 to 1946 and from 1951 to 1953, Dr. Mathis served as a reserve officer on active duty in the Navy. He was a research electrical engineer at the Microwave Laboratory at Northwestern University from 1946 to 1949. From 1949 to 1954, he was an associate professor of electrical engineering at the University of Oklahoma. Since 1954, he has been a Research Engineer in the Aerophysics Department of Goodyear Aircraft Corp., Akron, Ohio.

Dr. Mathis is a member of Sigma Xi, the American Institute of Electrical Engineers, and the American Mathematical Society.

C. H. Mayer (M'47) was born on December 10, 1921, in Ossian, Iowa. He received the B.S. degree in electrical engineering from the State University of Iowa in 1943, and the M.S. degree in electrical engineering from the University of Maryland in 1951.

C. H. Mayer

In 1943 he joined the staff of the Naval Research Laboratory to work on the development of microwave components and antennas. Since 1948 he has been associated with the Radio Astronomy program at the Naval Research Laboratory.

He is a registered professional engineer in District of Columbia and a member of Scientific Research Society of America.

❖

J. L. Melchor was born on July 6, 1925 in Mooresville, N. C. He received the B.S. degree and the M.S. degree in physics from the University of North Carolina. His undergraduate studies were interrupted by military service in the U. S. Navy. In 1949 he worked as a civilian physicist with the U. S. Navy Mine Countermeasures Station. Attending the University of Notre Dame in 1950 he was a U. S. Rubber Co. Fellow in High Polymer Physics. In 1952 and 1953 he worked part time with the Missile Division of Bendix Aviation Corp, and was awarded the Ph.D. degree from Notre Dame in 1953.

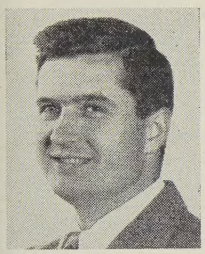

J. L. Melchor

Since 1953 he has been with the Electronic Defense Laboratory of Sylvania Electric Products Inc., and is currently engaged in ferrite research at microwave frequencies.

He is a member of Sigma Xi.

❖

P. A. Rizzi (S'50–A'54) was born in Providence, R. I., on December 10, 1930. He received the B.S. degree with high honors from the University of Rhode Island in 1951 and the M.Eng. and D.Eng. degrees in electrical engineering from Yale University in 1952 and 1955. During his graduate studies, he received the Yale University Scholarship and the Charles LeGeyt Fortescue Fellowship. Since August, 1954, Dr. Rizzi has been engaged in the development of ferrite components and microwave filters at the Missile and Radar Division of the Raytheon Manufacturing Co.

P. A. Rizzi

Dr. Rizzi is a member of Phi Kappa Phi, Sigma Xi, and Tau Beta Pi.

❖

Kiyo Tomiyasu (S'41–A'42–M'49–SM'52) was born in Las Vegas, Nev., on September 25, 1919. He received the B.S. degree in electrical engineering from the California Institute of Technology, in 1940, and the M.S. degree in communication engineering from Columbia University in 1941. With a Low Scholarship he studied at Stanford University and then entered Harvard University to continue graduate work on a Gordon McKay Scholarship. He served as a teaching fellow and research assistant at Harvard, and, after receiving the Ph.D. degree in 1948, he served as instructor.

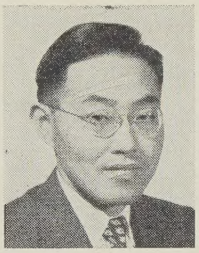

K. Tomiyasu

In September, 1949, Dr. Tomiyasu joined the Sperry Gyroscope Co., in Great Neck, N. Y., where he became engineering section head for microwave research in the microwave components department.

Since August, 1955, he has been employed at the General Electric Microwave Laboratory and has been engaged in research and advanced development of various microwave techniques and systems.

Dr. Tomiyasu is a member of Sigma Xi and the American Physical Society.

❖

P. H. Vartanian (S'55) was born in Rochester, N. Y., on June 14, 1931. He received the B.S. degree in electrical engineering in 1953 from the California Institute of Technology, and the M.S. degree from Stanford University in 1954. At Stanford he was a Tau Beta Pi Fellow and later a research assistant at the Electronics Research Laboratory. In 1951 and 1952 he worked part-time at the U. S. Naval Radiological Defense Laboratory on radiation detectors.

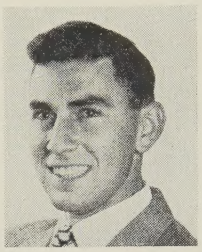

P. H. Vartanian

In 1954 he joined the Electronic Defense Laboratory of Sylvania Electric Products Inc., and is engaged in research in microwave applications of ferrites. He is also doing work at Stanford University under the Honors Cooperative Program leading to the Ph.D. degree in electrical engineering.

He is a member of Tau Beta Pi.

INSTITUTIONAL LISTINGS

The IRE Professional Group on Microwave Theory and Techniques is grateful for the assistance given by the firms listed below, and invites application for Institutional Listing from other firms interested in the Microwave field.

AIRCRAFT RADIO CORPORATION, Boonton, N. J.
Airborne Electronic Equipment, Associated Test Equipment

AIRTRON, INC., 1102 W. Elizabeth Ave., Linden, N. J.
Microwave Mixers, Duplexers, Ferrite Devices, Flexible Guides, Castings, Antenna Components; Design & Production

BOGART MANUFACTURING CORP., 315 Siegel Street, Brooklyn 6, N. Y.
Microwave Components and Radar Assemblies such as Mixers, Duplexers, Rotating Joints, Dummy Loads, etc.

COLLINS RADIO CO., Cedar Rapids, Iowa
Complete Industrial Microwave, Communication, Navigation and Flight Control Systems

ESPEY MFG. CO., INC., Congress and Ballston St., Saratoga Springs, N. Y.
Mfgrs. of X-Band and S-Band Wavemeters, Attenuators, Thermistor Mounts and Signal Generators

GENERAL PRECISION LABORATORY INCORPORATED, 63 Bedford Road, Pleasantville, N. Y.
A Subsidiary of General Precision Equipment Corporation
Research, Development and Production of Microwave, Radar, Computers, Airborne Electronic Systems

GORHAM MANUFACTURING CO., Bronze Div., Dept. 781, Providence, R.I.
Waveguide Components, Rotary Joints, Mixers, Antenna Feeds, Duplexers, Plaster Cast Waveguides

(Please see back cover for additional names.)

INSTITUTIONAL LISTINGS (Continued)

MARYLAND ELECTRONIC MANUFACTURING CORPORATION, College Park, Md.
Development and Production of Microwave Antennas and Waveguide Components

MEASUREMENTS CORPORATION, Box 180, Boonton, N. J.
Specialists in the Design and Development of Electronic Test Instruments

MICROWAVE DEVELOPMENT LABORATORIES, INC.
92 Broad St., Babson Park, Wellesley 54, Mass.
Design, Development and Production of Waveguide Components and Complete RF Assemblies

NATIONAL INSTRUMENT CO., 23 E. 26 St., New York, N. Y.
Wide-Band Microwave Equipment, Simulated Flight Instruments, Lobe Switches, Custom Built Precision Apparatus

RAYTHEON MANUFACTURING COMPANY, 148 California St., Newton 58, Mass.
Microwave Communications Systems, Radar, Missiles, Cooking Equipment, Tubes and Components

WEINSCHEL ENGINEERING CO. INC., Kensington, Md.
Attenuation Standards, Coaxial Attenuators and Insertion Loss Test Sets

WHEELER LABORATORIES, INC., 122 Cutter Mill Road, Great Neck, N.Y.
Consulting Services, Research and Development, Microwave Antennas and Waveguide Components

The charge for an Institutional Listing is $50.00 per issue or $140.00 for four consecutive issues. Applications for Institutional Listings and checks (made out to the Institute of Radio Engineers) should be sent to Mr. L. G. Cumming, Technical Secretary, Institute of Radio Engineers, 1 East 79th Street, New York 21, N. Y.